AD-A076 185 PENNSYLVANIA STATE UNIV UNIVERSITY PARK APPLIED RESE--ETC F/G 11/6
VIBRATION OF PLATES OF VARIOUS GEOMETRIES.(U)
JUN 79 E G WILLIAMS N00024-79-C-6043
UNCLASSIFIED ARL/PSU/TM-79-130 NL

1 OF 2
AD
A076185

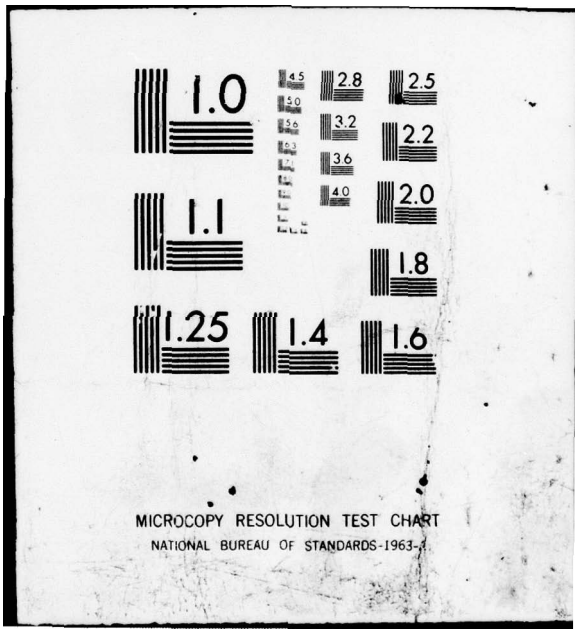
1.0
1.1
1.25
1.4
1.6
1.8
2.0
2.2
2.5
2.8
3.2
3.6
4.0
4.5
5.0
5.6
6.3
MICROCOPY RESOLUTION TEST CHART
NATIONAL BUREAU OF STANDARDS-1963-A

AD A076185

LEVEL II

12

VIBRATION OF PLATES OF VARIOUS GEOMETRIES

Earl G. Williams

DDC
RECEIVED
NOV 7 1979
E

Technical Memorandum
File No. 79-130
June 17, 1979
Contract No. N00024-79-C-6043

Copy No. 15

DDC FILE COPY

The Pennsylvania State University
Institute for Science and Engineering
APPLIED RESEARCH LABORATORY
Post Office Box 30
State College, PA 16801

APPROVED FOR PUBLIC RELEASE
DISTRIBUTION UNLIMITED

NAVY DEPARTMENT

NAVAL SEA SYSTEMS COMMAND

79 11 06 024

UNCLASSIFIED

SECURITY CLASSIFICATION OF THIS PAGE (When Data Entered)

REPORT DOCUMENTATION PAGE

READ INSTRUCTIONS BEFORE COMPLETING FORM

1. REPORT NUMBER: TM 79-130
2. GOVT ACCESSION NO.:
3. RECIPIENT'S CATALOG NUMBER:

4. TITLE (and Subtitle): VIBRATION OF PLATES OF VARIOUS GEOMETRIES
5. TYPE OF REPORT & PERIOD COVERED: PhD Thesis, July 1979
6. PERFORMING ORG. REPORT NUMBER: TM 79-130

7. AUTHOR(s): Earl G. Williams
8. CONTRACT OR GRANT NUMBER(s): N0024-79-C-6043

9. PERFORMING ORGANIZATION NAME AND ADDRESS:
The Pennsylvania State University
Applied Research Laboratory
P. O. Box 30, State College, PA 16801

10. PROGRAM ELEMENT, PROJECT, TASK AREA & WORK UNIT NUMBERS: 157

11. CONTROLLING OFFICE NAME AND ADDRESS:
Naval Sea Systems Command
Department of the Navy
Washington, DC 20362

12. REPORT DATE: June 17, 1979
13. NUMBER OF PAGES: 156 pages & figures

14. MONITORING AGENCY NAME & ADDRESS (if different from Controlling Office): Doctoral thesis

15. SECURITY CLASS. (of this report): Unclassified, Unlimited
15a. DECLASSIFICATION/DOWNGRADING SCHEDULE:

16. DISTRIBUTION STATEMENT (of this Report)

Approved for public release, distribution unlimited,
per NSSC (Naval Sea Systems Command), 7/24/79

17. DISTRIBUTION STATEMENT (of the abstract entered in Block 20, if different from Report)

ARL/PSU/TM-79-130

18. SUPPLEMENTARY NOTES

19. KEY WORDS (Continue on reverse side if necessary and identify by block number)

20. ABSTRACT (Continue on reverse side if necessary and identify by block number)

Point driven, flat, thin aluminum plates of various geometries with free boundaries are studied in this thesis. We have applied a theory which allows the mean of the driving point admittance to be predicted over a wide frequency range at any point on these plates. This prediction is compared to the experimentally determined admittance. Also, the expected minimum and maximum variations about this mean are predicted and compared to the experimental data over a broad frequency range. Measured loss factors for these free plates were used in the theoretical models. The actual admittance versus frequency

DD FORM 1 JAN 73 1473 EDITION OF 1 NOV 65 IS OBSOLETE

391 007

UNCLASSIFIED

SECURITY CLASSIFICATION OF THIS PAGE (When Data Entered)

20. ABSTRACT (CONTINUED)

for a center driven rectangular plate was predicted using a mode sum technique and compared to measured data. A simple algebraic formula was used to predict the resonance frequencies of the rectangular and square plates with free boundaries.

The transfer admittance of these point driven plates was also measured experimentally and compared to a theory which predicts the mean admittance versus frequency. The dependence of this mean on plate size and also on plate damping was demonstrated.

ABSTRACT

Point driven, flat, thin aluminum plates of various geometries with free boundaries are studied in this thesis. We have applied a theory which allows the mean of the driving point admittance to be predicted over a wide frequency range at any point on these plates. This prediction is compared to the experimentally determined admittance. Also, the expected minimum and maximum variations about this mean are predicted and compared to the experimental data over a broad frequency range. Measured loss factors for these free plates were used in the theoretical models. The actual admittance versus frequency for a center driven rectangular plate was predicted using a mode sum technique and compared to measured data. A simple algèbraic formula was used to predict the resonance frequencies of the rectangular and square plates with free boundaries.

The transfer admittance of these point driven plates was also measured experimentally and compared to a theory which predicts the mean admittance versus frequency. The dependence of this mean on plate size and also on plate damping was demonstrated.

Accession For
NTIS GRA&I
DDC TAB
Unannounced
Justification
By
Distribution/
Availability Codes
Dist | Avail and/or special

ACKNOWLEDGMENTS

The author's thesis advisor, Dr. Eugen Skudrzyk, has been a constant inspiration throughout this work with his fresh enthusiasm and particular interest in the subject matter. The author also wishes to thank the other members of his doctoral committee, Dr. John Snowdon, Dr. Sabih Hayek and Dr. Robert Farwell for their time and helpful discussions. The support of the Applied Research Laboratory was invaluable, providing materials, electronic equipment and shop facilities when needed. Also, thanks to Mr. Lynn Poole for his help with the design of the electronics for the mass cancellation system.

This research was funded by the Applied Research Laboratory at The Pennsylvania State University under contract with the Naval Sea Systems Command.

TABLE OF CONTENTS

Page

LIST OF TABLES

LIST OF FIGURES

CHAPTER I

INTRODUCTION

1.1 Objective of Study

It is the object of this work to further the understanding of plate vibrations by the use of a simplified theory to study experimental results. This theory encompasses the prediction of the mean level of vibration with respect to frequency of vibrators, specifically plates in this study, and expected deviations from this mean line (average levels of resonances and antiresonances). The details of the response of the vibrator are neglected and focus made of the average behavior of the system. However, this is not a statistical approach. Use is made of circuit theory to represent the vibrator, drawing upon solutions to predict aspects of the behavior of the vibrator. Much of the theory has been developed by Skudrzyk, and some of his theory has been extended here to deal with the vibrators encountered in this study.

This work is primarily an experimental study of flat aluminum plates of various geometries including square, rectangular, elliptical, circular, quadrilateral and others. The main thrust is the study of the driving point and transfer admittances (the ratio of acceleration or velocity to force) for point excited plates. Without exception all of the plates studied were with free-free boundary conditions, that is, zero shear and bending moment at the boundaries. The plates were studied over the full frequency range from 100 Hz to 10 kHz.

Important details relevant to the objective were studied. These include the loss factor of Young's modulus with respect to frequency for plates of different thicknesses; the resonance frequencies of square, rectangular and circular plates; the effects of the measuring system on the admittance which one desires to measure, along with mass cancellation schemes for the impedance head of the driver; effects of damping the surface of a plate; and finally, the display of the surface vibration of a plate.

1.2 Background

Work in plate vibration up to the year 1969 has been extensively reviewed by Leissa[1]. This reference is of great value as a research aid, providing much information and exhaustive references to other work in the field. Most of Leissa's summary deals with determination of the eigenvalues and eigenfunctions of various plate systems, however, little is said about the impedances of these plates. A great help to understanding plate vibrations is a book by Mary Waller[2] in which she summarizes a lifetime of her experimental work on the vibrations of free plates. (It is unfortunately out of print.) Many of her papers are instructive reading. Dealing more directly with impedances and point excited plates is a book, unusual in its integration of experimental and theoretical materials, by Cremer and Heckl translated and revised by E.E. Ungar.[3] Of direct importance to the author's work is the book by Eugen Skudrzyk[4] in which much of the detail of the theory used in this work are found, particularly the circuit theory approach to complex

vibrating systems. A very extensive paper[5] bringing up-to-date Skudrzyk's work in the field of vibrations contains many ideas and formulations which have been drawn upon and extended in the author's work.

Many papers have been published on point driven plates by John Snowdon.[6-10] These include experimental measurements (on simple supported plates) and comparative theoretical calculations for various boundary conditions. Contained are useful, exact solutions for rectangular and circular plates for various boundary conditions and source locations.

Experimental studies of plates with free boundaries appear to be few, probably due to the problem of plate support. The method used here, supporting the plate with a very compliant foam mat, was first developed and used at The Pennsylvania State University by Robert Hannon.[11] Hannon's thesis has served as a prelude to the present work.

CHAPTER II

EXPERIMENTAL SETUP

2.1 Introduction

The flat aluminum plates studied in this work are supported on a soft, compliant foam mat, which in turn is supported by six massive, slate-covered tables. This system filters out all but the lowest frequency background vibration from the floor, and prevents the plate vibrations from exciting any other resonant systems below the foam layer. A small area in the middle is left unsupported so that a vibration generator may be attached to the underside of the plate. A Wilcoxon Research Model F3 generator is used along with a Z602 impedance head mounted within the shaker. This unit was selected because of its excellent design: a low center of gravity which helps prevent any vibration outside of the axis of the shaker which could introduce bending moments and add rotational inertia. The shaker is capable of a nominal blocked force output of 0.75 pounds or 3.3 newtons. The impedance head measures the force between the plate, the driver and the acceleration of the stud mounted at the plate as a means of attachment. The mass between the force gauge and the plate is 21 grams. The Z602 is designed to measure, within its specified accuracy, a maximum impedance that would be the equivalent of a 114 kilogram mass or a compliance of 1.05×10^{8} newtons/meter. For larger impedances the measurement error is greater than 10%.

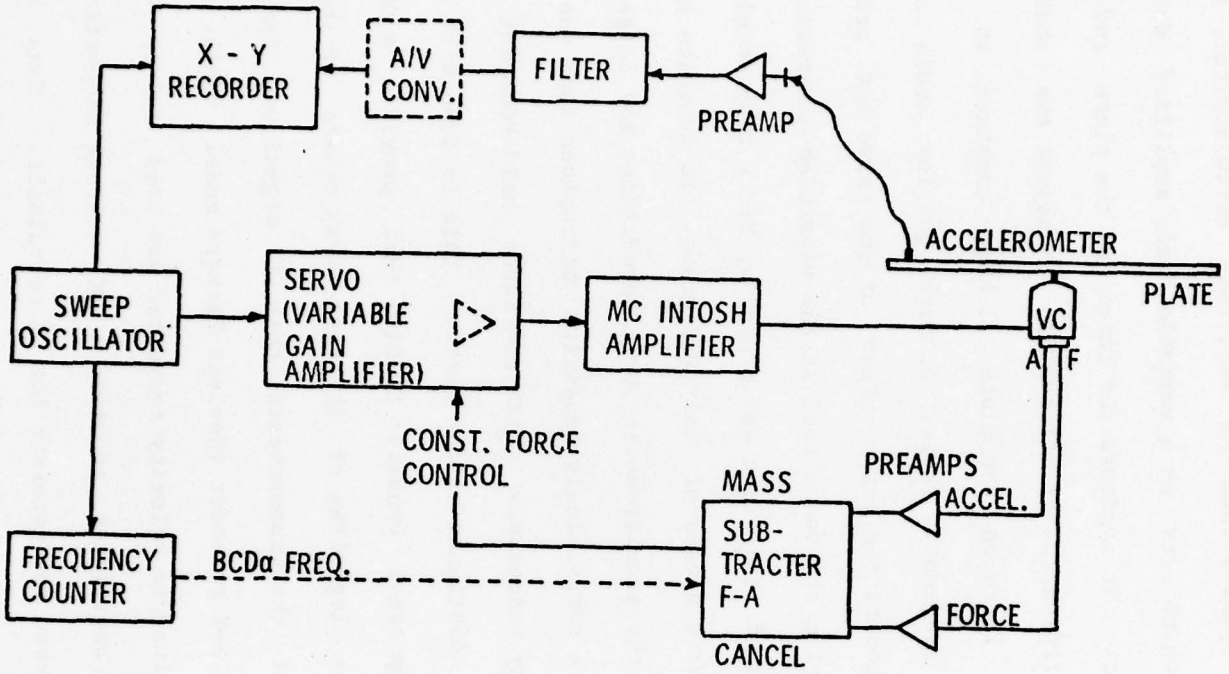

Figure 2.1 Block Diagram of Electronic Equipment

A block diagram of the electronic equipment is shown in Figure 2.1. The sweep oscillator (Spectral Dynamics SD104A) generates a harmonic driving signal for the shaker and is preset to sweep from 100 to 10000 Hz. This output passes into an amplitude servo/monitor (Spectral Dynamics SD105A) which acts as a variable gain amplifier driving the vibration generator. It monitors the force on the plate and provides the necessary amplification or attenuation to adjust the shaker input level so that the force on the plate is kept constant, at a preset level, over the frequency range. A high quality audio amplifier (McIntosh MC-30) boosts the power output of the servo and provides a low impedance to drive the voice coil in the vibration generator.

The vibrations of the plate are picked up by a tiny accelerometer (Endeco Model 22) with a mass of only 0.2 grams. It is quite necessary that the output of the accelerometer be filtered since the large area of the plate becomes a surprisingly sensitive microphone (and one with a very poor frequency response). With the force held constant the X-Y recorder plots the admittance of the plate. This is done with a 100 Hz bandwidth filter (Spectral Dynamics SD101B) that provides a DC output proportional to the logarithm of the root mean square of the input signal. In most of the measurements this DC signal was fed to the Y-axis input of an X-Y recorder (Hewlett Packard model 2FRA). In some cases the acceleration to velocity converter was used and is described below. The sweep oscillator provides a DC voltage proportional to frequency and is used to generate the X coordinate. Thus, the X-Y recorder graphs the frequency response of the plate. Further, a frequency counter (General Radio 1191-B) provides an accurate reading of the frequency when necessary.

The dynamic range of the measuring system is at best 60 dB, limited by the filter which has this range for any given setting of the dials. Thus, a continuous, uninterrupted sweep can be made over the whole frequency region as long as the measured signal does not vary more than 60 dB. By changing front panel switches to follow the signal, one can increase the sensitivity of the system to 110 dB, but this is troublesome since it requires continual attention with each frequency curve generated.

2.2 Mass Cancellation

A system for mass cancellation consisting of two preamps (Ithaco Model 453) with adjustable gain and an operational amplifier that subtracts their outputs is shown also in Figure 2.1. It provides an adjusted value of the force which is necessary due to the following. Because of the design of the impedance head, there exists a mass of 21 grams (including the mounting stud) between the plate and force gauge. Thus, the actual force on the plate is reduced by the inertial loss in this 21 gram mass. Further, the impedance measured is that of the plate in series with this mass. As long as the plate impedance is much greater than 21 grams, the effect of this mass can be ignored. However, this is generally not the case. The thin plate in fact is very soft, especially at a resonance, and can easily exhibit a dynamic mass of only a few grams. (This is simply demonstrated by touching very lightly the driving point of a plate when it is in resonance and noting the resultant strong damping of the vibration.) Thus, we are essentially

limited to measuring a minimum impedance of 21 grams. (It should also be evident that any external accelerometer placed at the driving point should be very light, preferably less than a gram.) Standard techniques exist, however, for cancelling the effect of this mass which can be understood with the aid of Figure 2.2 below.

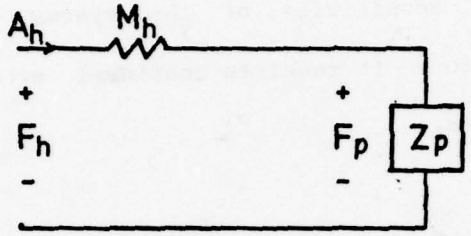

FIGURE 2.2: The effect of the mass below the force gauge.

Here F_h is the force measured by the impedance head, F_p the actual force on the plate, Z_p the impedance of the plate and a resistor, M_h, represents the mass below the impedance head. A_h is the acceleration measured by the impedance head, here represented as a current flowing into the circuit. Thus,

$$F_p = F_h - (M_h \times A_h) \qquad (2.1)$$

Viewing F_H and A_h as the signals into the preamps shown in Figure 2.1, one can adjust the gains such that the difference between the outputs represents the right side of Equation (2.1). The differencing is produced in an operational amplifier with a potentiometer in the acceleration input so that a fine tuning of the cancellation can be made. The standard technique for adjusting the cancellation is to drive

the shaker with only the stud loading the impedance head and adjust the gains until the output of the operational amplifier is at a minimum. Generally, at a single frequency, one can get from 40 to 50 dB of cancellation, that is, an impedance of 100 times less than M_h can be measured (0.21 grams).

A more realistic picture, however, is obtained by referring to Figure 2.3. This strong null soon disappears when the frequency is changed, and the figure shows the effects of nulling the output of the operational amplifier at different frequencies. The result is a reduction of the cancellation to as little as 23 dB. The cause of this is simple to understand. The sensitivity of the accelerometer in the impedance head increases with frequency (about 1.5 dB from 100 to 10000 Hz). Thus, the current A_h in the circuit above is larger than it should be as the frequency increases. This can be viewed instead as an apparent increase in the mass below the force gauge. (If we set the mass to 21 grams at 100 Hz, then it appears to be 25 grams at 10,000 Hz.) With only 23 dB of cancellation we are limited to measuring an impedance minimum of about 2 grams.

In the course of this work it became apparent that a system was needed which provided more cancellation over the frequency range. Thus, a more sophisticated mass cancellation was developed. Better cancellation can be obtained if we equalize the gain in the accelerometer over the whole frequency range. This can be done with an attenuator at the output of the acceleration preamp programmed to equalize the increase in sensitivity. A digital technique was used to provide the necessary attenuation values and the resulting circuit is shown in Figure 2.4.

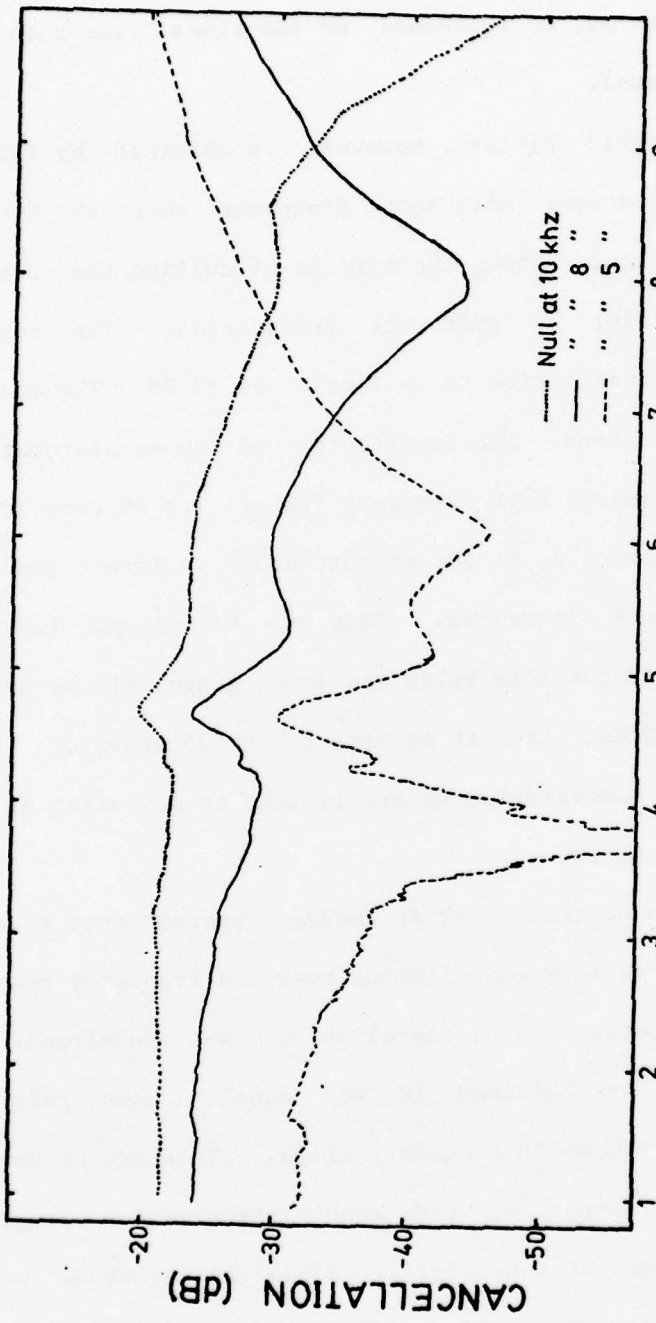

Figure 2.3 Amount of Cancellation versus Frequency for Simple Mass Canceller

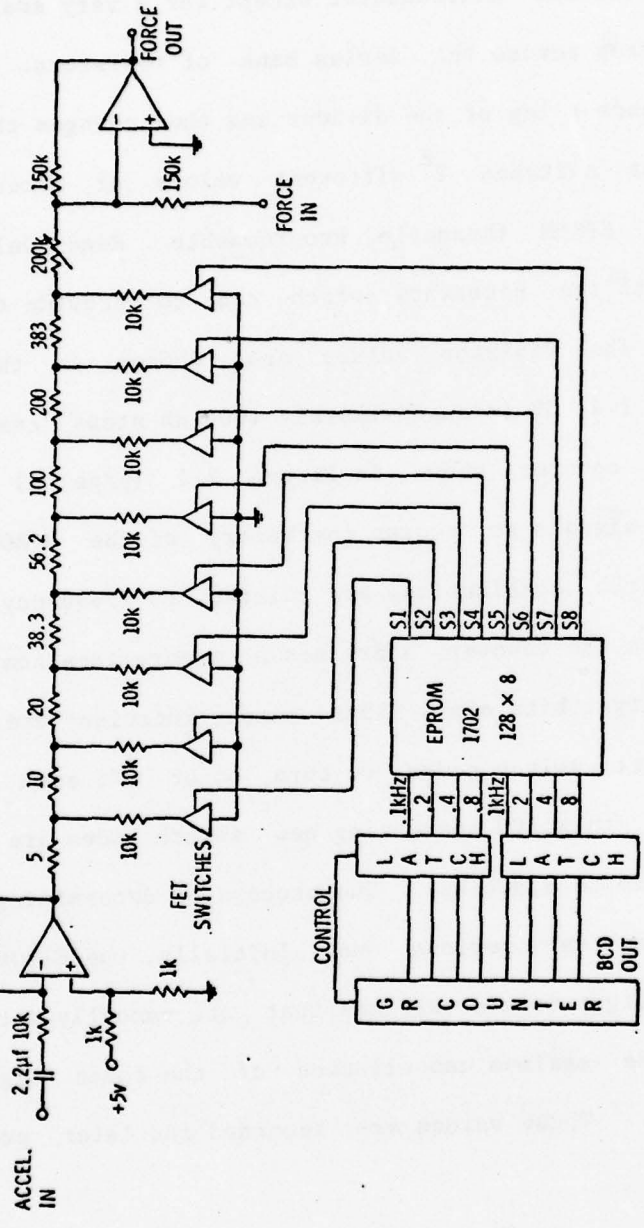

Figure 2.4 Circuit for the ROM Cancellation Device

Figure 2.4 is a ladder attenuator with FET switches selecting the appropriate attenuation. The resistors represent a high class voltage divider. When all the switches are open the signal passes straight through undivided and unattenuated except for a very small loss due to the voltage drop across the series bank of resistors. When a switch closes it grounds a leg of the divider and thus changes the attenuation. With all eight switches 2^8 different values of attenuation can be selected. An EPROM (Erasable Programmable Read Only Memory) is programmed with the necessary switch code to provide the equalizing attenuation. The resistor values are chosen so that a maximum attenuation of 1.4 dB in approximately .006 dB steps can be generated. The frequency counter shown in Figure 2.1 (page 5) provides the necessary BCD signals to access the memory of the EPROM so that the appropriate switch combinations are related to frequency. Each eight bit signal from the counter addresses a memory location in the EPROM consisting of eight bits also. These memory locations are preprogrammed with the correct switch codes to turn on or off each of the eight switches. With this BCD addressing new switch codes are output every 100 Hz from zero to 9,900 Hz. The process of determining the correct switch codes is a very tedious one. Initially, the EPROM is replaced with a bank of eight toggle switches that are manually set by trial and error to provide maximum cancellation of the force signal over the frequency range. These values are recorded and later programmed into the EPROM.

The resultant cancellation with the EPROM circuit is shown in Figure 2.5. The cancellation is at worst 30 dB. But even more

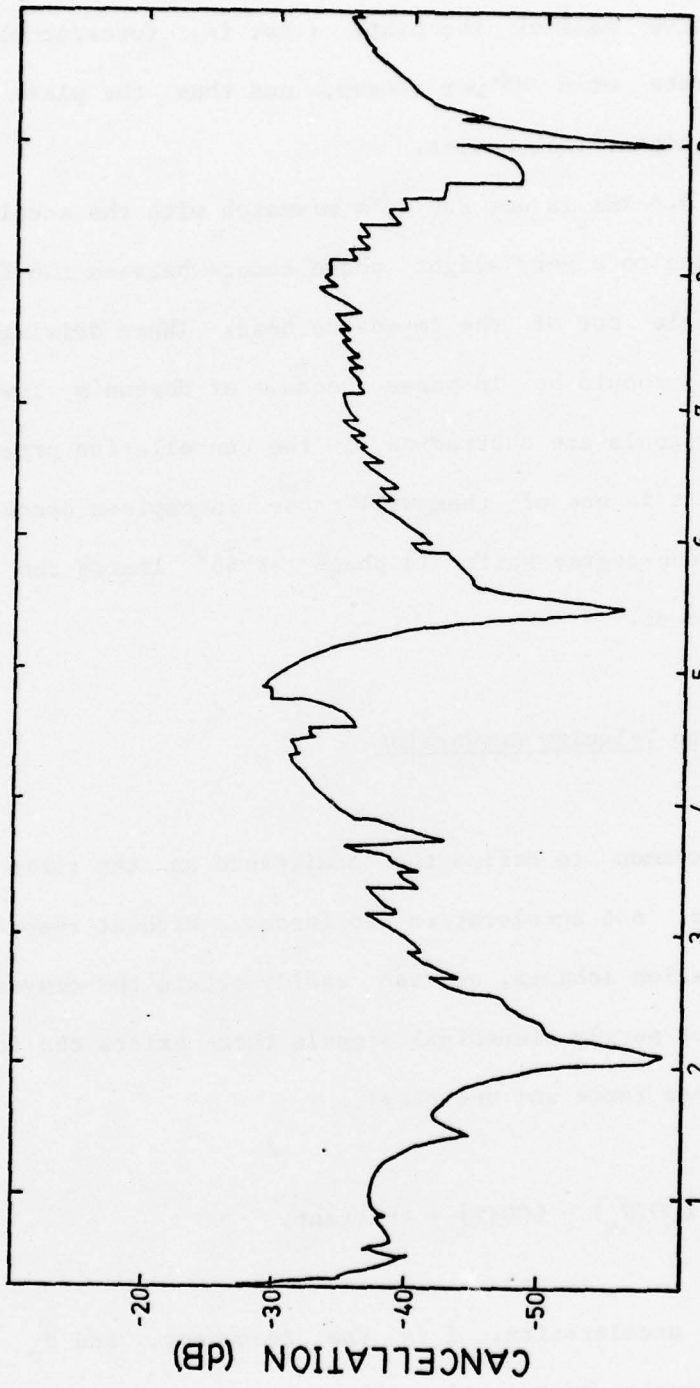

Figure 2.5 Amount of Cancellation versus Frequency for ROM Cancellation Circuit

important is the fact that the cancellation from 7 to 10 kHz is at worst 36 dB. The cancellation at these frequencies is especially critical since the effective mass of the plate (that is, force/acceleration) decreases at a rate of 6 dB per octave, and thus the plate is much "lighter" at the higher frequencies.

The peak at 4.8 kHz is not due to a mismatch with the accelerometer sensitivity but due to a very slight phase change between the force and acceleration signals out of the impedance head. (When driving a mass these two signals should be in phase because of Newton's law, f=ma.) Since these two signals are subtracted in the cancellation process, any slight phase shift in one of them will cause incomplete cancellation. For example, a one-degree shift in phase at 45^{o} limits the maximum cancellation to 38 dB.

2.3 Acceleration to Velocity Conversion

It is more common to define the admittance as the ratio of the velocity to force, not acceleration to force. Without resorting to electronic integration schemes, one can easily obtain the conversion by the following: For purely sinusoidal signals there exists the following relationship between force and velocity:

$$\mathrm{LOG}(V_v) = \mathrm{LOG}(V_a) - \mathrm{LOG}(f) + \text{constant}, \qquad (2.2)$$

where V_a is the acceleration, f is the frequency, and V_v is the velocity. The signals representing the terms on the right side of

Equation (2.2) are output from the filter and sweep oscillator, respectively. The simple circuit which provides the acceleration to velocity conversion is shown in Figure 2.6. The variable resistor is adjusted so that the output drops at exactly 6 dB per octave as the frequency is increased. The position of the converter is shown in the block diagram in Figure 2.1 on page 5.

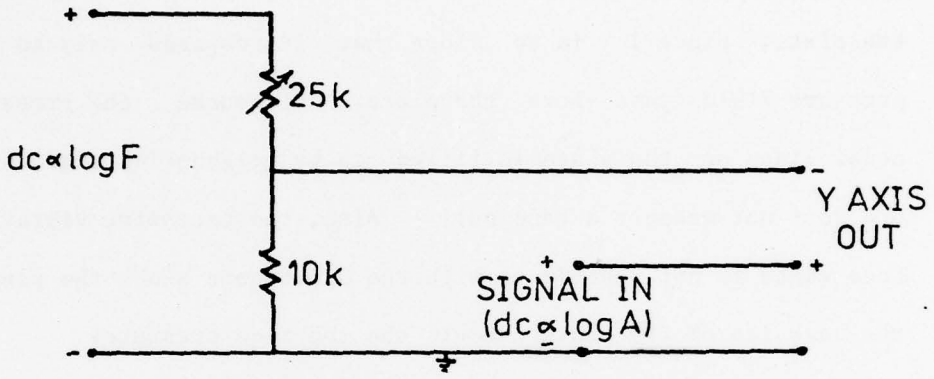

Figure 2.6: Acceleration to Velocity Converter

2.4 Effect of the Foam Support

The technique of resting the plates on a foam mat support was developed by Hannon and is presented in his PhD thesis.[11] The foam provides an ideal free-free plate condition and eliminates the difficult task of supporting the plate boundaries with an experimentally difficult boundary condition. The foam does not distort the vibration pattern of the free plate in any way, as will be seen later, and reduces the Q of the plate to under 1000 at high frequencies. This reduced Q is a saving grace since the dynamic range of the measuring system is at best 60 dB continuous, and very high Q's would easily exceed this limit.

2.5 Microphone Scanner

Some of the measurements in this work were made using a mechanical microphone scanner built by Hannon and used in his thesis work. It is described there in detail. The nearfield pressure field (at a distance of 1/5 of an inch) is measured and recorded over the entire surface of the plate. The microphone records essentially the vibration pattern of the plate, since it is so close that it responds only to the local pressure field just above the plate. Of course, the pressure above nodal lines on the plate is filled in by neighboring regions and thus one does not measure a true null. Also, the excessive vibration of the free edges is not reproduced with the microphone since the pressure from the backside of the plate cancels the top side pressure.

2.6 Attachment of the Driver to the Plate

The seemingly simple problem of the attachment of the driver to the plate must be done with caution and foresight. The vibration generator is attached to the plate by means of a flat mounting stud which is glued to the plate and screwed into the impedance head of the shaker. Problems with this type of attachment are known.[12] Reference 12 states that due to the low elastic modulus of the glue, the layer between the stud and the plate should be as thin as possible, preferably less than .005 of an inch thick. Since a piece of paper is typically .002 of an inch thick, it is evident that care must be taken when attaching the stud to the plate. Ideal for this is the fast drying glue, Aron Alpha,

which flows on easily and forms a layer about .002 of an inch thick. However, even with this very thin layer troubles are encountered.

Tests were made to investigate the effects of this layer by gluing a small lumped mass of 195 grams to the shaker. The shaker was supported by a foam cushion surrounding its base with the mass vertically above. This mounting prevents any spurious resonances from entering the system. The frequency curve for this test is shown in Figure 2.7. The vertical axis represents the force divided by the acceleration at the impedance head, and thus represents a dynamic mass. The force is held constant throughout the frequency range and the mass cancellation unit has been removed so that the force from the impedance head is fed directly to the servo, see Figure 2.1 (page 5). Due to Newton's law we would expect this measured curve to be a horizontal line. Clearly it is not. The culprit here is the glue layer. It produces a small compliance between the stud and the mass to which it is glued. One can model this system with an equivalent circuit as shown in Figure 2.7. When K and M are in resonance this branch becomes open circuited and the system has an antiresonance, that is, the acceleration goes to zero and the dynamic mass (F/A) becomes infinite. This antiresonance occurs at 3500 Hz. Since we know the value of M we can calculate the value of K, which turns out to be 1.05×10^{-8} meters/newton. From this value the rest of the curve can be calculated and is shown in the figure. At higher frequencies the impedance of M becomes large compared to K and a resonance occurs when K resonates with M_a. The resonance occurs at about 11 kHz and agrees with the theory. When the lumped mass is removed and the shaker driven with just the stud

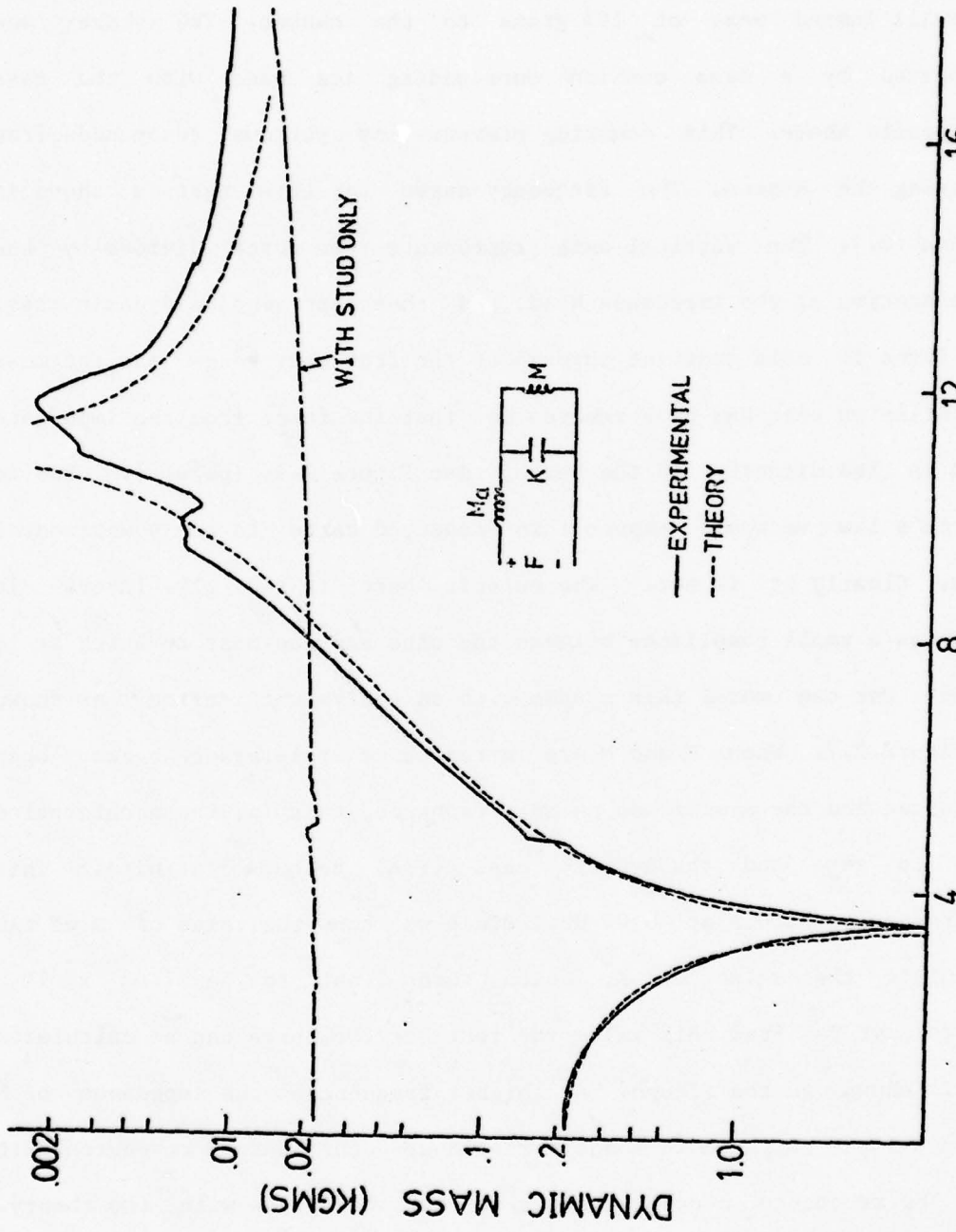

Figure 2.7 Measured Dynamic Mass of a 195 Gram Mass Glued to Shaker (Insert represents equivalent circuit for this system.)

loading it, the broken line shown in Figure 2.7 is measured. It is interesting to note that this line slopes upward due to the increase in sensitivity of the accelerometer (which is designed to operate up to 10 kHz), and at low frequencies the dynamic mass is about 21.6 grams. This is just the mass below the force gauge plus the stud which weighs about a gram. (See Section 2.2.) Another similar experiment with a 100 gram mass gave a value of K to within one percent of 1.05×10^{-8}.

An interesting result occurs when the above experiment is repeated with the 195 gram mass just resting, unglued, on top of the shaker. A similar curve results (as long as the acceleration stays below one g so that the mass stays in contact with the driver) but the compliance increases tenfold to 1.06×10^{-7} meters/newton. Clearly, the body contact between the stud and the lumped mass offers a compliance to the system. If, in fact, one removes the stud and rests the mass directly on the impedance head of the shaker, this value is about the same. Furthermore, and more surprising, even when the mass is bolted down to the impedance head, the compliance is reduced only to 0.75×10^{-8}. Apparently, unevenness between the mating of the two surfaces introduces an appreciable (for our purposes) amount of compliance. Further reduction would necessitate careful machining of the mating surface to assure a large area of contact.

Of main interest here is the effect of the compliant glue layer on the impedance measurements on thin plates. In the case of a plate measurement the mass M in Figure 2.7 will be replaced by the plate impedance, Z_p. First, one can see that this compliance K does not alter the force on the plate if it is kept in mind that the force out of the

mass cancellation unit is the force across K which is equal to $F-M_a A$. Second, the actual acceleration of the plate is not the acceleration measured on the head, since part of this is drawn through the compliance K. In fact, if the impedance of the plate is large, this compliance will, especially at high frequencies, tend to short out the plate. In order to make an accurate driving point impedance measurement on the plate it is necessary to attach a very light accelerometer on the opposite side of the plate in line with the impedance head.

Actually, what we attribute to just the glue compliance is the sum of this plus the compliance in the impedance head itself. The latter, as given in Bulletin Number 4 of Reference 12, is 1.14×10^{-9} meters/newton. Thus, the actual compliance of the glue layer is our experimental value minus this value or 0.94×10^{-8}.

2.7 Attachment of Receiving Accelerometer

Transfer impedance measurements require the use of an external accelerometer attached by some means to the plate. For this purpose the Endeco model 22 accelerometer was used. It has a mass of only 0.2 grams and a frequency response up to 10 kHz. Since the accelerometer was constantly being moved to different locations on the plate it was necessary to have a convenient means of attachment. For this a green, sticky putty, Duxseal, was used. To determine the compliance of this mounting a 100 gram mass was attached by it to the vibration generator and the response curve recorded. The results are shown in Figure 2.8. Again, the equivalent circuit shown in Figure 2.7, page 18, can be used

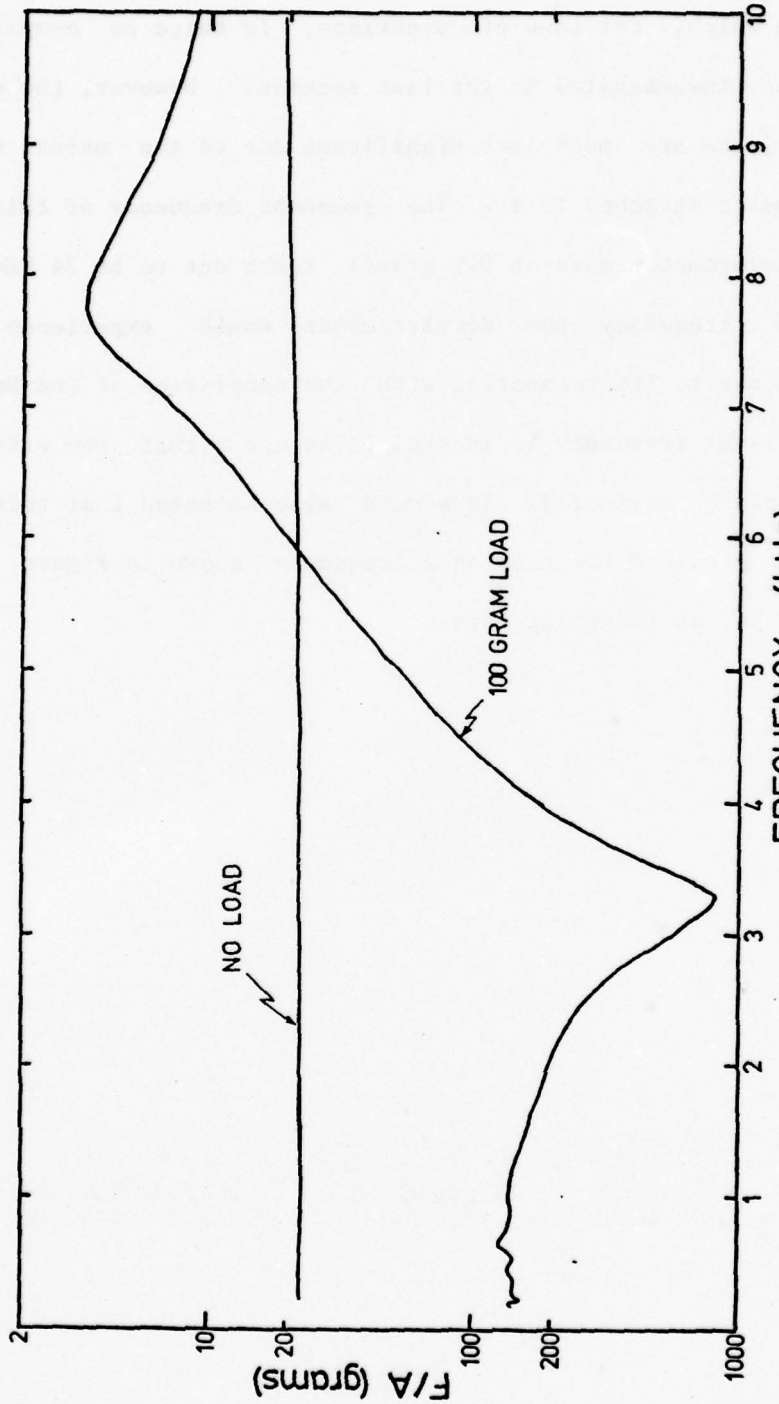

Figure 2.8 Experimental Resonance Curve Indicating the Effects of Duxseal Mounting for the Accelerometer

to calculate the compliance of the Duxseal. Here the antiresonance occurs at 3300 Hz and provides us with a compliance of 2.3×10^{-8} meters/newton which, for sake of comparison, is twice as compliant as the glue layer investigated in the last section. However, the effects of this compliance are much less significant due to the actual mass of the accelerometer attached to it. The resonant frequency of this sytem (with the accelerometer mass at 0.2 grams) turns out to be 74 kHz; that is, at this frequency the accelerometer would experience large accelerations due to its resonating with the compliance of the Duxseal. Since our maximum frequency is 10 kHz it is clear that the effects of the mounting can be neglected. It should also be noted that this value of compliance predicts the resonance frequency shown in Figure 2.8 to occur at 7920 Hz, as indeed it does.

CHAPTER III

PRELIMINARY INVESTIGATIONS

3.1 Comparison of Experimental Eigenfrequencies with Theory

Warburton[13] applied the Rayleigh-Ritz method to determine the eigenfrequencies of rectangular and square thin plates for all of the possible combinations of boundary conditions. His results are exceedingly simple to use since the eigenvalues are determined by an algebraic expression and can be calculated with the aid of a programmable hand calculator. They were applied to calculate the resonance frequencies for various rectangular and square plates. The results for a 2′ x 4′ x 3/16" aluminum plate (plate I of Appendix I) are shown in Figure 3.1. Table 3.1 lists the results for a similar plate, in this case of dimensions 24" x 42" x 3/16", and includes measured loss factors which will be discussed in Section 3.3. The theoretical frequencies were determined by using an average value for the stiffness parameter of the plate, alpha [see Equation (4.2)], calculated so that the errors over the tabulated frequency range were minimized. This led to a value for alpha of 2.708 meters/sec$^{1/2}$. It is clear that the agreement with Warburton's theoretical values is excellent and in most cases is within 1%. In fact, all of the resonances which are measured (the modes of the plate) are accounted for in the theory. It should be noted that the plates used in the reported results here were driven at the center so that only the even modes were excited; those modes with

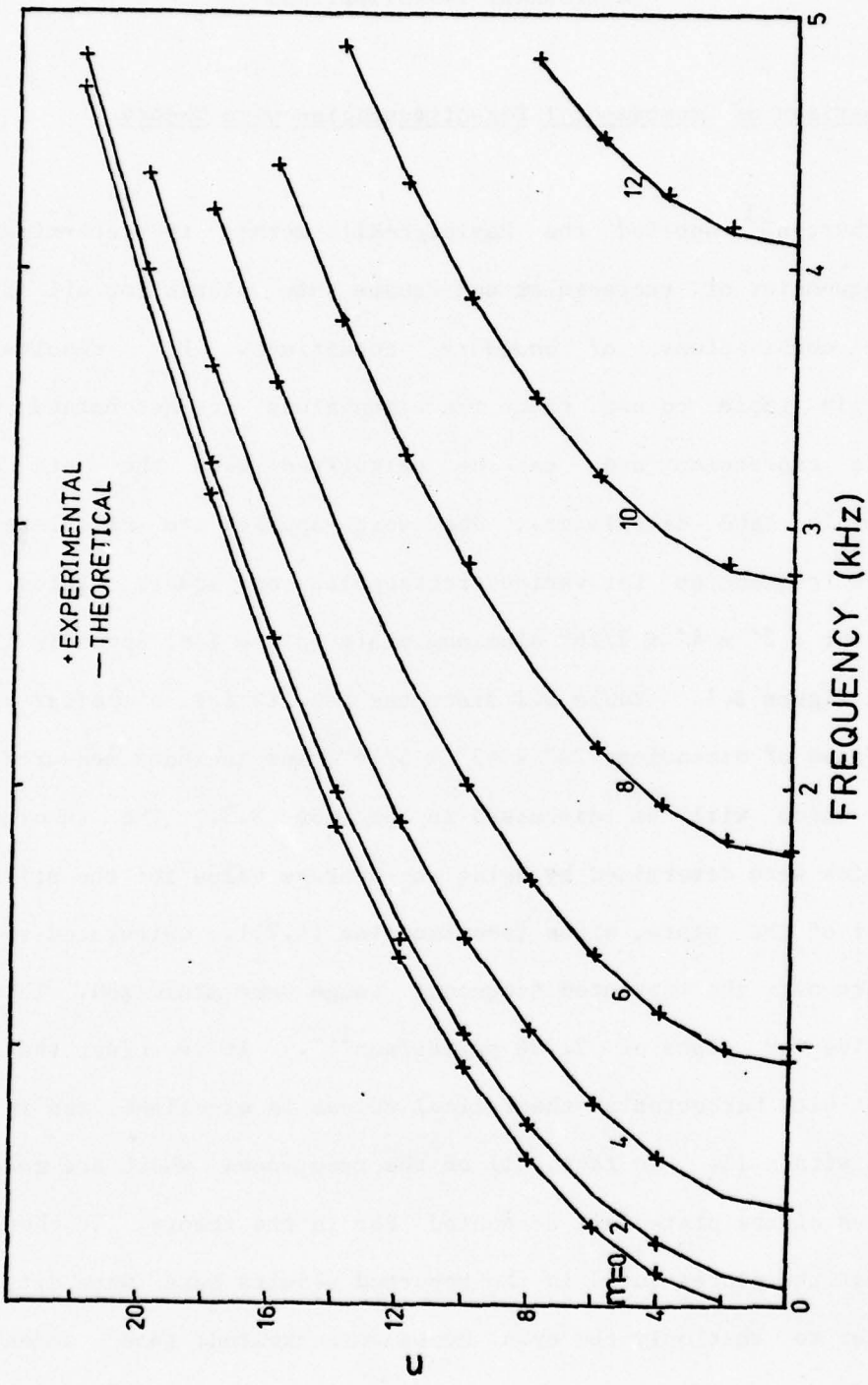

Figure 3.1 Experimental versus Theoretical Eigenvalues for a Rectangular Plate

TABLE 3.1

EIGENFREQUENCIES AND LOSS FACTORS FOR A CENTER DRIVEN RECTANGULAR PLATE (42" x 24" x 3/16")

MODE (n,m)	FREQUENCY (THEORY) (Hz)	FREQUENCY (MEASURED) (Hz)	% ERROR	3 DB BANDWIDTH (Hz)	LOSS FACTOR
(2,4)	251	248	1.0	6	.024
(0,6)	307	310	1.0	8	.026
(2,8)	701	703	.3	11	.016
(4,6)	787	782	.6	14	.018
(6,8)	1643	1649	.3	18	.011
(2,12)	1468	1482	1.0	18	.012
(8,6)	2152	2165	.6	22	.011
(4,14)	2360	2366	.3	23	.0097
(0,18)	3100	3137	1.1	25	.0080
(4,18)	3617	3635	.5	25	.0069
(2,20)	3974	4007	.7	22	.0055
(12,6)	4499	4526	.6	24	.0053
(0,22)	4679	4709	.6	22	.0047
(6,20)	4990	4992	.04	22	.0044
(8,18)	5089	5087	.04	21	.0041
(10,16)	5485	5474	.2	25	.0046
(14,8)	6347	6343	.06	20	.0031
(10,20)	6937	6899	.9	20	.0029
(4,26)	7096	7072	.3	20	.0028
(14,12)	7192	7160	.4	21	.0029
(16,6)	7840	7818	.2	23	.0029
(14,16)	8352	8281	.9	20	.0024
(10,24)	8701	8609	1.1	20	.0023
(4,30)	9322	9233	1.0	20	.0022

nodal lines at the driver were not excited. This agreement is reassuring because it demonstrates that indeed a free plate condition is being obtained with the foam support, except, of course, for the reduction in the Q of the plate. It is also clear that we are dealing with a homogeneous material, a basic assumption in Warburton's calculations. It is interesting to note that the resonance frequencies above 8000 Hz in Table 3.1 begin to diverge from the theoretical values. Here the effects of the neglected shear and rotary inertia are beginning to be felt. It is known that the addition of shear and rotary inertia is such as to "soften" the plate and thus lower the eigenfrequencies. (See, for example, Reference 14, Chapter 11.) This effect increases the mode density at the higher frequencies. Because their effects are as yet minimal, the analysis throughout the rest of this work neglects the effect of shear and rotary inertia.

3.2 Square Plate Eigenfrequencies and Modes

The square plate offers some interesting results. Whereas in the rectangular plate nodal lines are always parallel to the edges, this is not the case in the square plate. For example, see Waller's book, Reference 2, for a clear discussion of this. The microphone scanner described in Section 2.5 was used to record a few of these nodal patterns for a square plate of dimensions 2′ x 2′ x 3/16" (plate VII of Appendix I). A microphone was placed a fraction of a wavelength from the surface of the plate and moved over the entire area to record the pressure field. At such a close distance the pressure measured is

proportional to the velocity of the surface at all points, except near the edges where radiation from the back side of the plate cancels the front radiation in a dipole effect. Figures 3.2, 3.3 and 3.4 show three such recordings of distinct modes of a square plate, (2/4 + 4/2), (2/6 + 6/2) and (4/6 + 6/4), respectively. The nulls in the recording represent the nodal lines of the plate. Whereas in the rectangular plate the modes 2/4 and 4/2 (representing modes with two nodal lines in the short dimension and four in the long dimension and vice versa) are distinct and occur at different frequencies, the symmetry of the square plate allows these two modes to occur at the same frequency, causing the well known degenerate mode condition. Now two new modes are formed, represented by m/n+n/m and m/n-n/m, at two new eigenfrequencies. The latter have a node at the center and the former an antinode at the center. Warburton develops a slightly different formulation to deal with this. (See Appendix III.)

The resonance frequencies of the square plate were determined experimentally, and compared to Warburton's predictions. The results are shown in Table 3.2.

The smallest magnitude of errors occur with a calculated value for alpha of 2.68 meters/sec$^{1/2}$; however, the errors are generally larger than for the rectangular plate as shown in Table 3.2. Measurements were made only up to 5000 Hz in this experiment.

SQUARE PLATE MODE

2/4 + 4/2

523 Hz

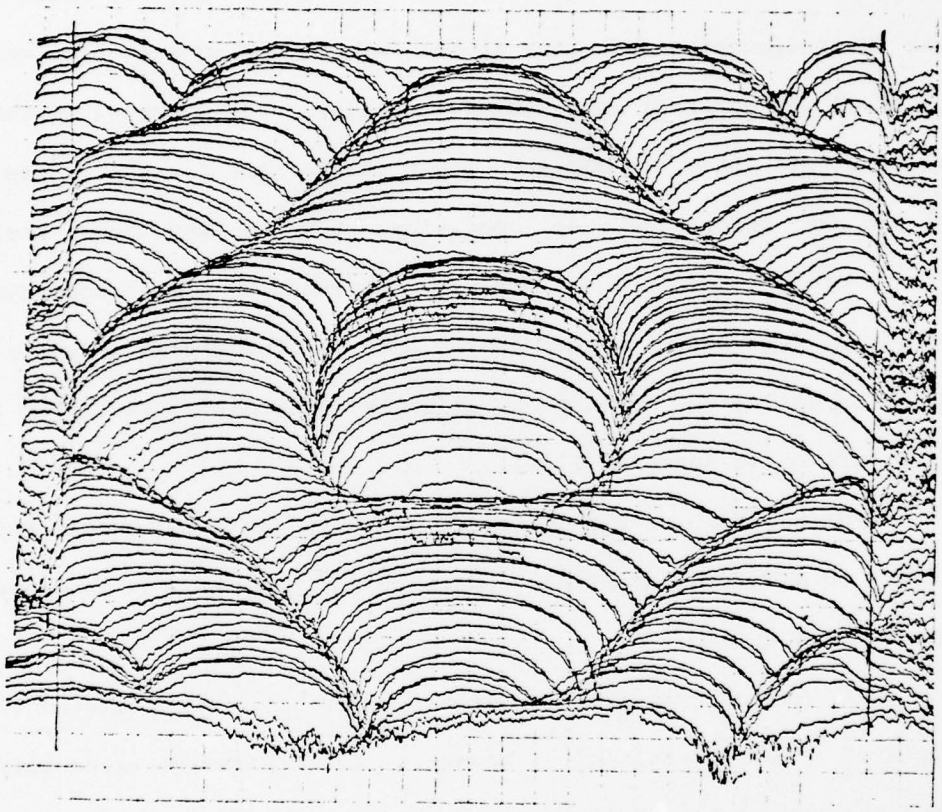

Figure 3.2 Degenerate Eigenfunction for a Square Plate

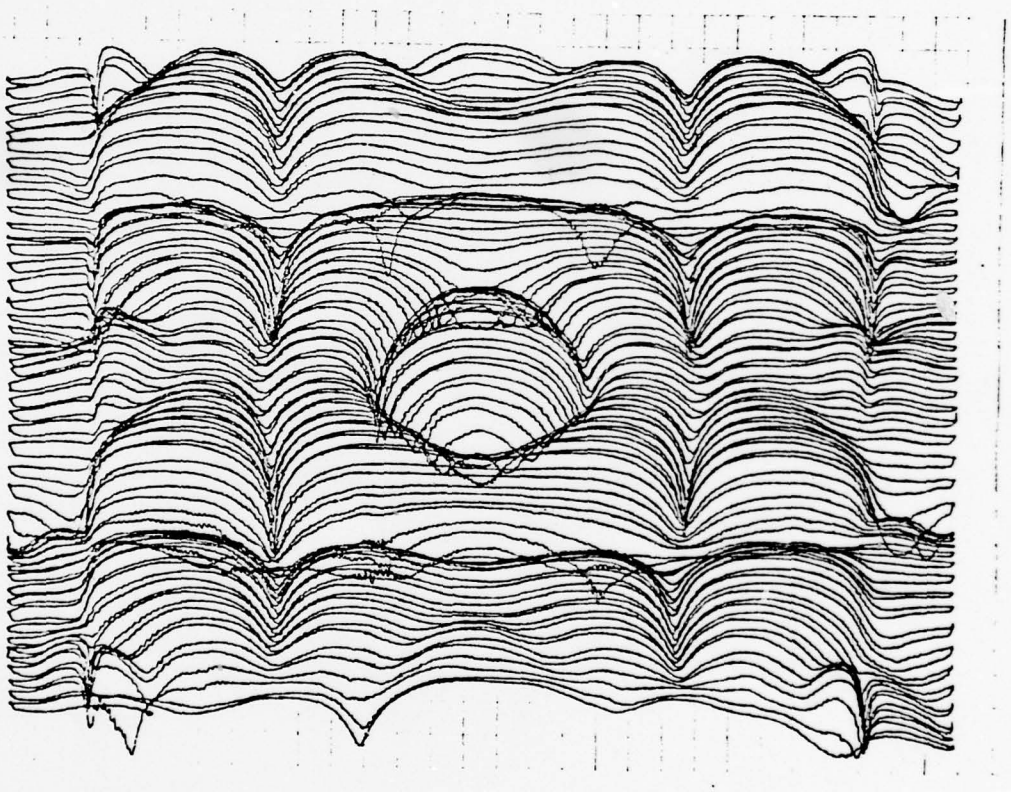

Figure 3.3 Degenerate Eigenfunction for a Square Plate

SQUARE PLATE MODE

4/6+6/4

1444 Hz

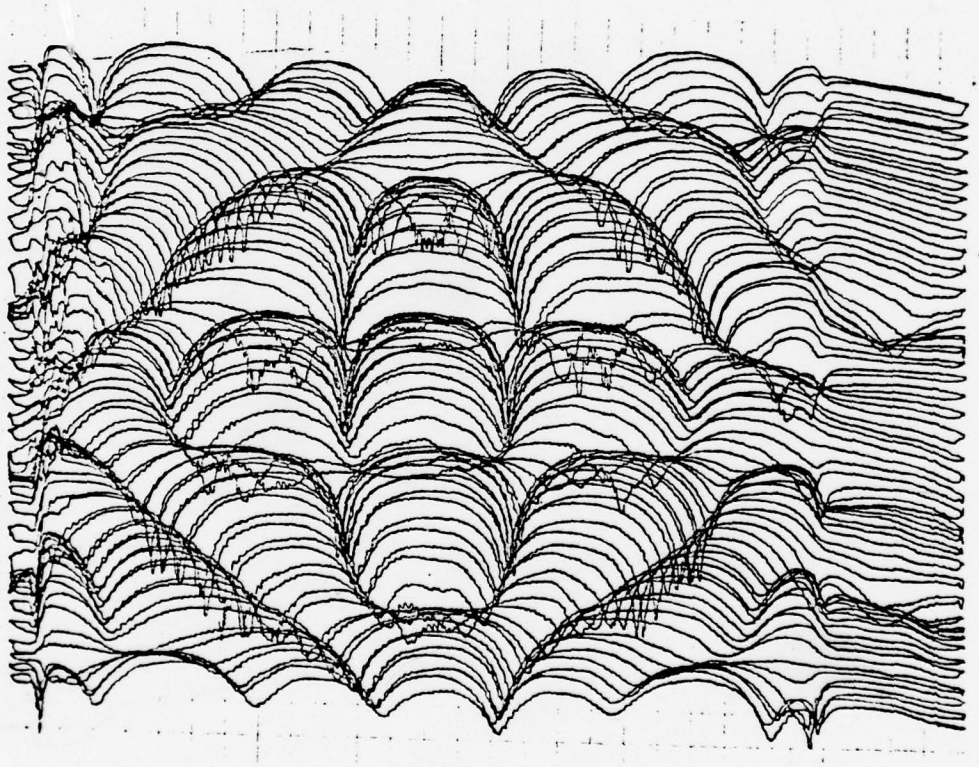

Figure 3.4 Degenerate Eigenfunction for a Square Plate

TABLE 3.2

EIGENFREQUENCIES FOR A CENTER DRIVEN SQUARE PLATE

(24" x 24" x 3/16")

MODE n/m+m/n	FREQUENCY (THEORY) Hz	FREQUENCY (EXPERIMENT) Hz	% ERROR
2/0+0/2	76	82	7.3
2/2	202	200	1.0
4/0+0/4	380	384	1.0
4/2+2/4	542	523	1.7
4/4	881	870	1.2
6/0+0/6	925	937	1.2
6/2+2/6	1082	1073	.8
6/4+4/6	1476	1449	1.9
8/0+0/8	1713	1735	1.2
8/2+2/8	1867	1864	.2
6/6	2039	2035	.2
8/4+4/8	2263	2244	.8
10/0+0/10	2744	2766	.8
8/6+6/8	2882	2849	1.1
10/2+2/10	2894	2913	.7
10/4+4/10	3290	3281	.3
8/8	3681	3676	.1
10/6+6/10	3919	3892	.7
12/0+0/12	4015	4055	1.0
12/2+2/12	4166	4175	.2
12/4+4/12	4559	4552	.2

3.3 Loss Factors

With the frequencies of the resonances of the plate well defined, one is able to proceed with the measurement of the loss factors for the plates. The method used here is to measure manually the 3 dB bandwidths by slowly changing the driving frequency, vibrating the plate and noting when the response at the driving point drops 3 dB from the peak, resonance value. It is important to realize that one must have well defined, well separated resonance peaks of single modes to use this technique. Often, however, modes overlap and these are excluded from our measurements. Table 3.1 (page 25) shows the measured bandwidths for a plate of thickness 3/16". The loss factor is calculated using the relation, loss factor = 3 dB bandwidth/center frequency. Well separated resonance peaks are easily identified by use of Warburton's formulation. A summary of the loss factors for this plate along with those for a plate of thickness 3/8" (plates I and X of Appendix I) are shown in Figure 3.5. The hyperbolic nature of the data is evident, which indicates that the bandwidths are nearly constant with respect to frequency. (See for instance Table 3.1, page 25.) In fact, the average bandwidth for the 3/16" plate was 20.7 Hz, and that for the 3/8" plate was 10.2 Hz over the frequency range 500 to 10,000 Hz.

To understand more fully what is going on here it is necessary to note a few facts about loss factors for aluminum plates. Both Young's modulus and the shear modulus have damping (loss) factors associated with them, and this is usually expressed by representing these moduli as complex numbers. That is:

$$E_f^* = E_f(1 + j\eta_{ef})$$

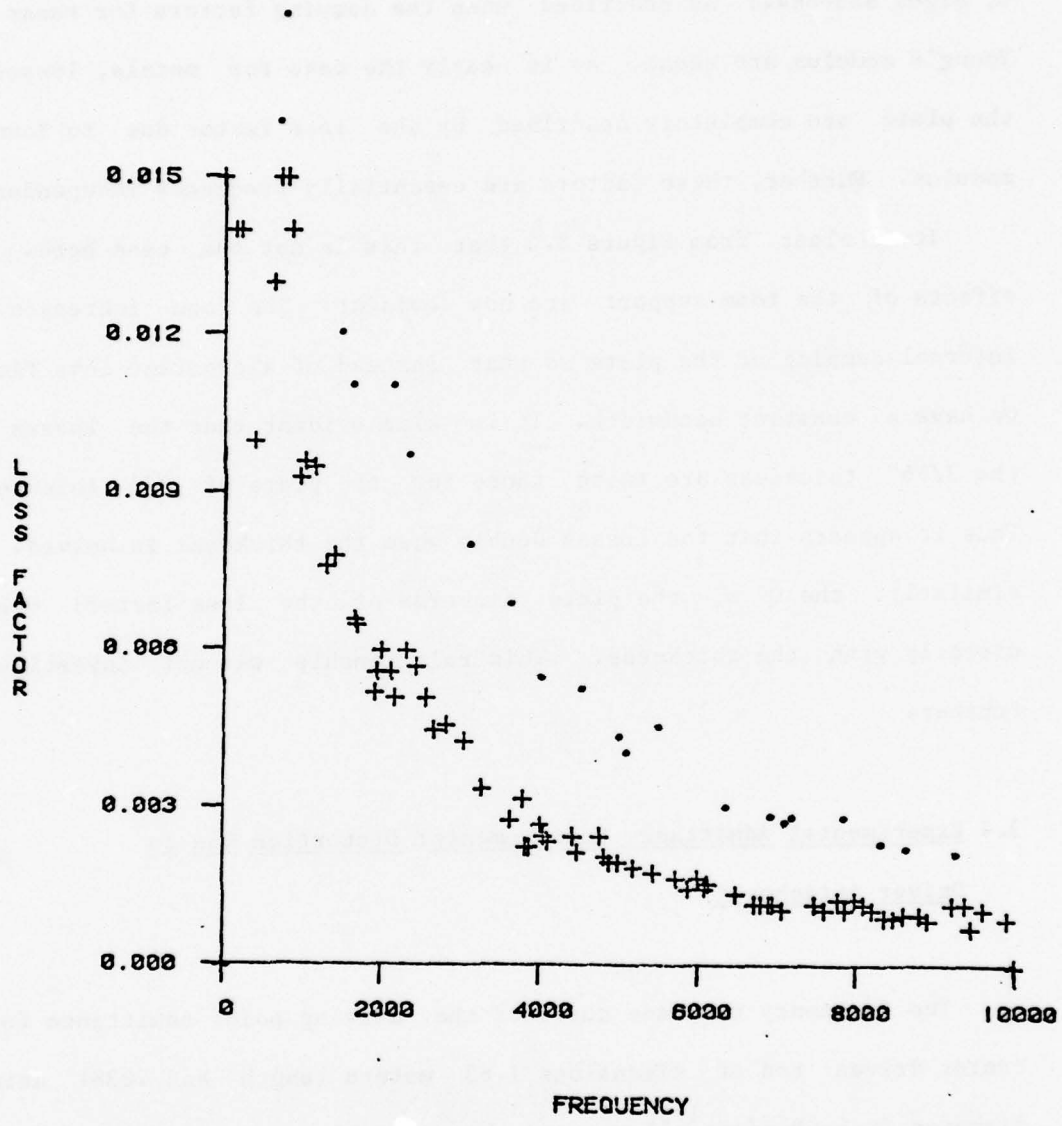

Figure 3.5 Loss Factors for Plates of Different Thicknesses

and

$$G_f^* = G_f(1 + j\eta_{gf}) \ .$$

where the subscript f denotes dependence on frequency. (See Reference 6, pages 883-884.) As described[6] when the damping factors for shear and Young's modulus are equal, as is nearly the case for metals, losses in the plate are completely described by the loss factor due to Young's modulus. Further, these factors are essentially frequency independent.

It is clear from Figure 3.5 that this is not the case here. The effects of the foam support are now evident. The foam increases the internal damping of the plate so that instead of a constant loss factor we have a constant bandwidth. It is also evident that the losses for the 3/16" thickness are twice those for the plate of 3/8" thickness. Thus it appears that the losses double when the thickness is halved. Or similarly, the Q of the plate (inverse of the loss factor) varies directly with the thickness. This relationship was not investigated further.

3.4 Experimental Admittance Measurements: Distortion Due to Driver Attachment

The frequency response curve of the driving point admittance for a center driven rod of dimensions 1.83 meters length and .0381 meters diameter (α=6.99 m/sec$^{1/2}$) was made by attaching the shaker via a glued stud, as described in Chapter II, and recording the acceleration from the impedance head instead of with an external accelerometer. The results are shown in Figure 3.6. As the circuit diagram in Figure 2.7

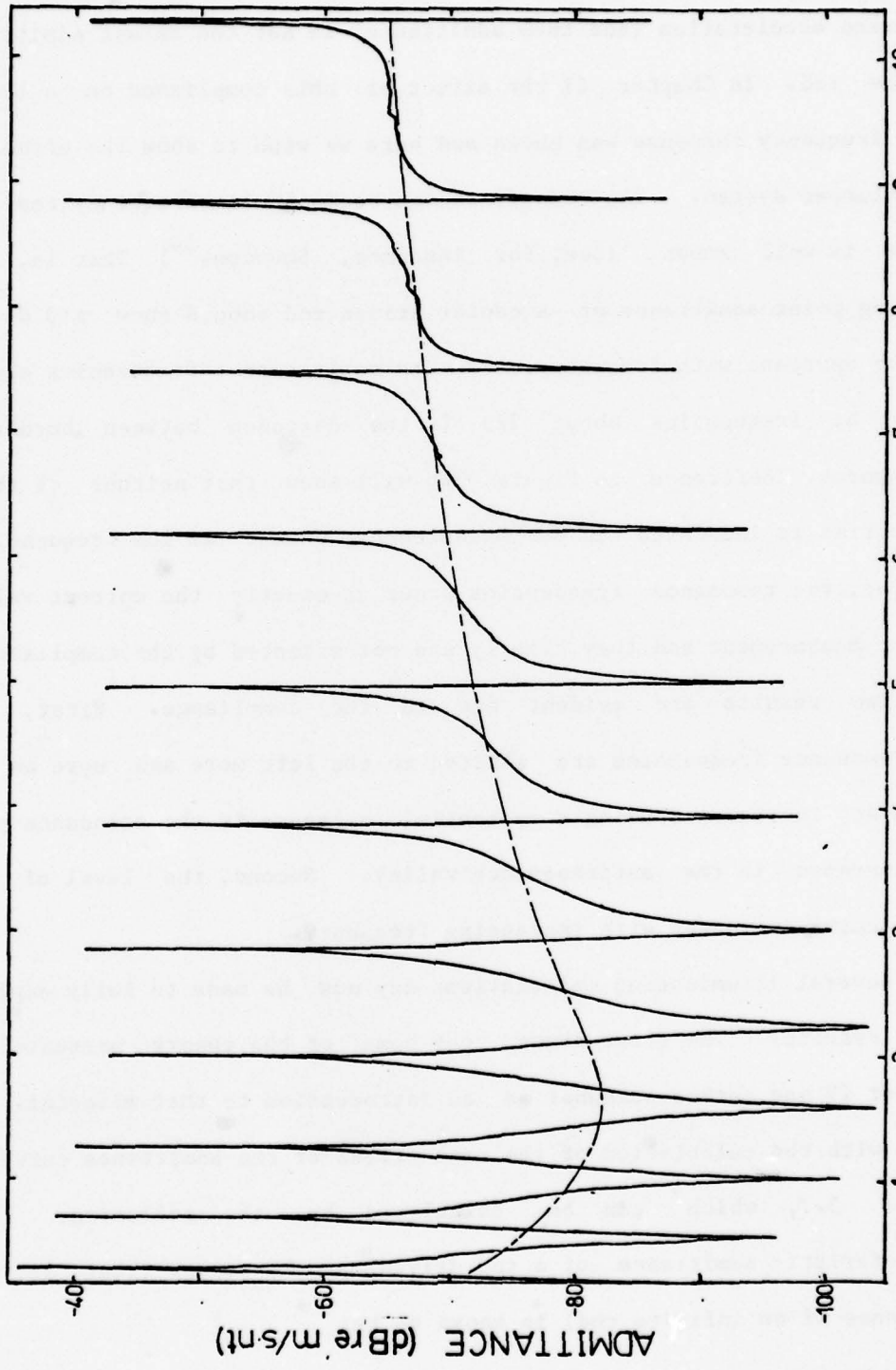

Figure 3.6 Acceleration of a Rod Measured in the Impedance Head

(page 18) indicates, due to the acceleration which branches into the shunt compliance (the glue layer and impedance head compliance), the measured acceleration (and thus admittance) is not the actual admittance of the rod. In Chapter II the effect of this compliance on a lumped mass frequency response was shown and here we wish to show the effect on a nonlumped system. The rod was chosen because its frequency response curve is well known. (See, for instance, Snowdon.[14]) That is, the driving point admittance of a center driven rod should show a 3 dB per octave decrease with frequency, and its antiresonant frequencies should occur at frequencies about 2/3 of the distance between bordering resonances. Reference to Figure 3.6 will show that neither of these properties is indicated in our measurement, except at low frequencies. However, the resonance frequencies occur at exactly the correct values in our measurement and they clearly are not affected by the compliance.

Two results are evident due to the compliance. First, the antiresonance frequencies are shifted to the left more and more as the frequency increases causing a sustantial decrease in the resonance peak and increase in the antiresonance valley. Second, the level of the whole curve increases with increasing frequency.

Several illuminating calculations may now be made to fully explain these results. The first draws upon some of the theory presented in Chapter IV and serves somewhat as an introduction to that material. It deals with the calculation of the mean trend of the admittance curve of Figure 3.7, which can be calculated by the following. The characteristic admittance of a rod driven at the center (that is, the impedance of an infinite rod) is known to be:

$$Y_c = (1 - j)/2^{3/2}mc \ , \qquad (3.1)$$

where m is the mass per unit length (3.06 kg/m) and c the bending wave speed ($c = a\sqrt{\omega}$). Y_c decreases 3 dB per octave with frequency due to the frequency dependence of c. Now this admittance appears in parallel with the compliance of the mounting system K as described before. Using the circuit theory approach the mean line of this combination is simply the sum of two parallel branches or

$$Y = j\omega K + Y_c \ . \qquad (3.2)$$

The absolute value of Equation (3.2) is the dashed line plotted in Figure 3.6. The value for K is that measured in Chapter II, 1.05×10^{-8} meters/newton. The agreement could not be better, and the success of the circuit approach is clear.

The other effect of the compliance K, the shift of the antiresonance frequencies, is explained by the circuit model shown below in Figure 3.7. The two parallel branches represent two modes of the rod and the third the compliance K of the mounting system. We want to determine the effect of K on the antiresonance that occurs between two resonances f_1 and f_2 of each M-K branch, respectively. With a little algebra one arrives at the following expression for the antiresonance frequency:

$$f_a^2 = f_1^2 + f_0^2 + 2f_0^2/(f_1^2 - f_2^2) \ , \qquad (3.3)$$

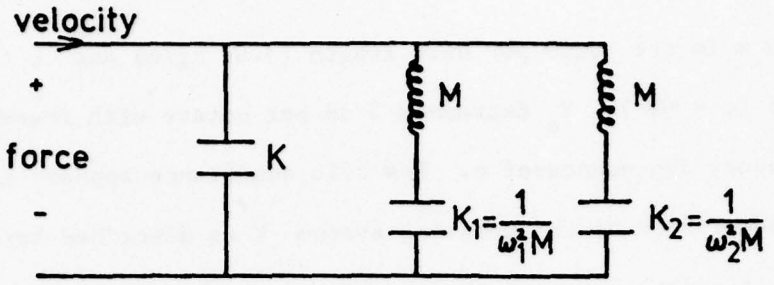

Figure 3.7: Circuit Model for Demonstrating Antiresonance Shift

where f_0 is the resonance frequency of K with M. Using the following values for the rod, M=2.8 kgms, K=1.05 x 10^{-8}, f_1=7500 Hz, f_2=8850 Hz, f_0 is calculated to be 923 Hz. The last term in Equation (3.3) is equal to .07 and thus can be neglected. Thus f_a is nearly equal to f_1 and, in fact, if we were to increase K, f_0 would become smaller and the antiresonance would shift even closer to the bordering resonance below. [Equation (3.3) was derived assuming that f_0 is less than f_1.] Also at lower resonance frequencies the quantity f_1 is smaller but f_0 does not decrease in value and thus the antiresonance is more separated from the resonance below.

Similar measurements on thin plates showed little discrepancy between the impedance head accelerometer and an external one attached at the same position. The following list should help to indicate when problems would occur. Listed are the average admittance $(kg/sec)^{-1}$ at 10 kHz for various mechancial elements.

Y of plate (1/8" thick) .... -50.6 dB

Y of plate (3/16" thick).... -57.8 dB

Y of compliant mount .... -63.6 dB

Y of plate (3/8" thick) .... -69.8 dB

Y of rod .... -80.6 dB

Thus, the first two elements would be relatively unaffected by K whereas the last two would be affected, especially the rod.

In summary, when there is compliance between the measuring accelerometer and the system to be measured the effect is (1) to drastically change the mean level of the admittance curve, and (2) to shift the antiresonances of the system to lower frequencies (as far as the resonance below) with no corresponding effect on the resonance frequencies. It is also interesting to note that the reverse effect is true if this compliance is replaced by a mass, so that the system is driven through this added mass. In this case the antiresonance frequencies remain unchanged, but now the resonance frequencies are shifted to a lower frequency. (See Snowdon,[14] page 231.) Thus, measurements taken from the impedance head accelerometer must be used with caution and they may be altogether incorrect for admittance determination. With these important effects in mind one is armed with a stronger insight for interpreting the measurements of more complicated systems.

CHAPTER IV

THE CHARACTERISTIC ADMITTANCE OF PLATES

4.1 Mean Value Theory: Prediction of Mean Vibration Levels

The mean value theory drawn from Skudrzyk[5] is presented here and extended to deal with cases where the driving point is close to the boundary of a vibrator. The mean value can best be represented by the line which passes through the inflection points of the frequency response curve of a vibrator. In this case the admittance is plotted on a dB scale and it will be seen that this mean line effectively bisects this plot. The mean value or mean line is calculated using the simple expression:

$$Y_{ca} = j\omega/8m\alpha^2 , \tag{4.1}$$

where Y_{ca} is the magnitude of the characteristic admittance (acceleration/force), ω the radian frequency, m the mass per unit area, and α the plate stiffness constant given by:

$$\alpha^4 = Eh^2/12(1-\nu^2)\rho, \tag{4.2}$$

where E is Young's modulus, h the thickness of the plate, ν is Poisson's contraction, and ρ is the density. The units of α are meters/second$^{1/2}$. Note that the admittance here is defined as the ratio of acceleration to force and thus the ca subscript on Y. Throughout the work we will also

use the admittance as the ratio of velocity to force which will be represented as Y_c. Thus,

$$Y_c = 1/8ma^2 \ . \tag{4.3}$$

Y_c is exactly the solution for the admittance of an infinite plate. In order for this to describe the mean line for a finite vibrator one is forced to the conclusion that the reflections from the boundaries of that vibrator do not contribute to the mean level. We can model this effect by picturing a characteristic wave[5] that propagates out from the driver and does not return and is unaffected by the boundaries. This characteristic wave is given by the solution for the point excited infinite plate and can be written as:

$$Y_c(k_o r) = [H_o^{(2)}(k_o r) - H_o^{(2)}(-ik_o r)]/8a^2 m \ , \tag{4.4}$$

where $H_0^{(2)}$ is the zero order Hankel function of the second kind, $k_o = \omega/c$, and r is the distance away from the driving point. At the driving point r=0, and this expression simplifies to Equation (4.3). Equation (4.4) can be simplified by noting that for all but the lowest frequencies (usually the first few modes of a finite plate) for small r (less than a few inches), the Hankel function of imaginary argument can be ignored since it represents a decaying exponential in $k_o r$ and is soon negligible compared to the oscillating first term in Equation (4.4). This second term corresponds to a distortion field near the driver, a "wattless field"[5] that does not propagate any appreciable distance.

4.2 Source in Plate Interior Not Near an Edge

Figure 4.1 is the experimentally determined admittance (a/f) of a rectangular plate (2′ x 4′ x 3/16") driven at the center, as indicated by the dot in the inserted rectangle in the figure. This was recorded as described in Chapter III. The mean value, Equation (4.1), is the dotted line on this curve; it is seen to bisect the experimental curve and thus is an excellent prediction of the mean trend of the data. Note that since the vertical scale is in decibels, the mean is essentially a geometric mean. The significance of the mean line is brought out further by damping the surface of the plate. To do this two coats of GP-1 damping compound were applied to the top surface of the plate. The driving point admittance (again at the center of the plate) was measured. The measured results, after adjusting them for damping effects as explained in Appendix II, are shown also in Figure 4.1 (the heavy, less undulated curve). This is an important result for it shows that as the plate is damped its response curve tends to the mean line prediction, and again reflections from the boundaries are unimportant.

To further prove that the boundary of the plate has no influence on the mean line one can look at the results of studies on plates of different geometries. Figure 4.2 shows the frequency response for a plate with nonparallel boundaries with the driving point at the center of mass of the plate. The largeness of this plate is reflected in its increased density of resonances. The thickness of the plate is 1/8" and its calculated mean line is plotted in the figure. The agreement is excellent and the mean line passes directly through the center of the data.

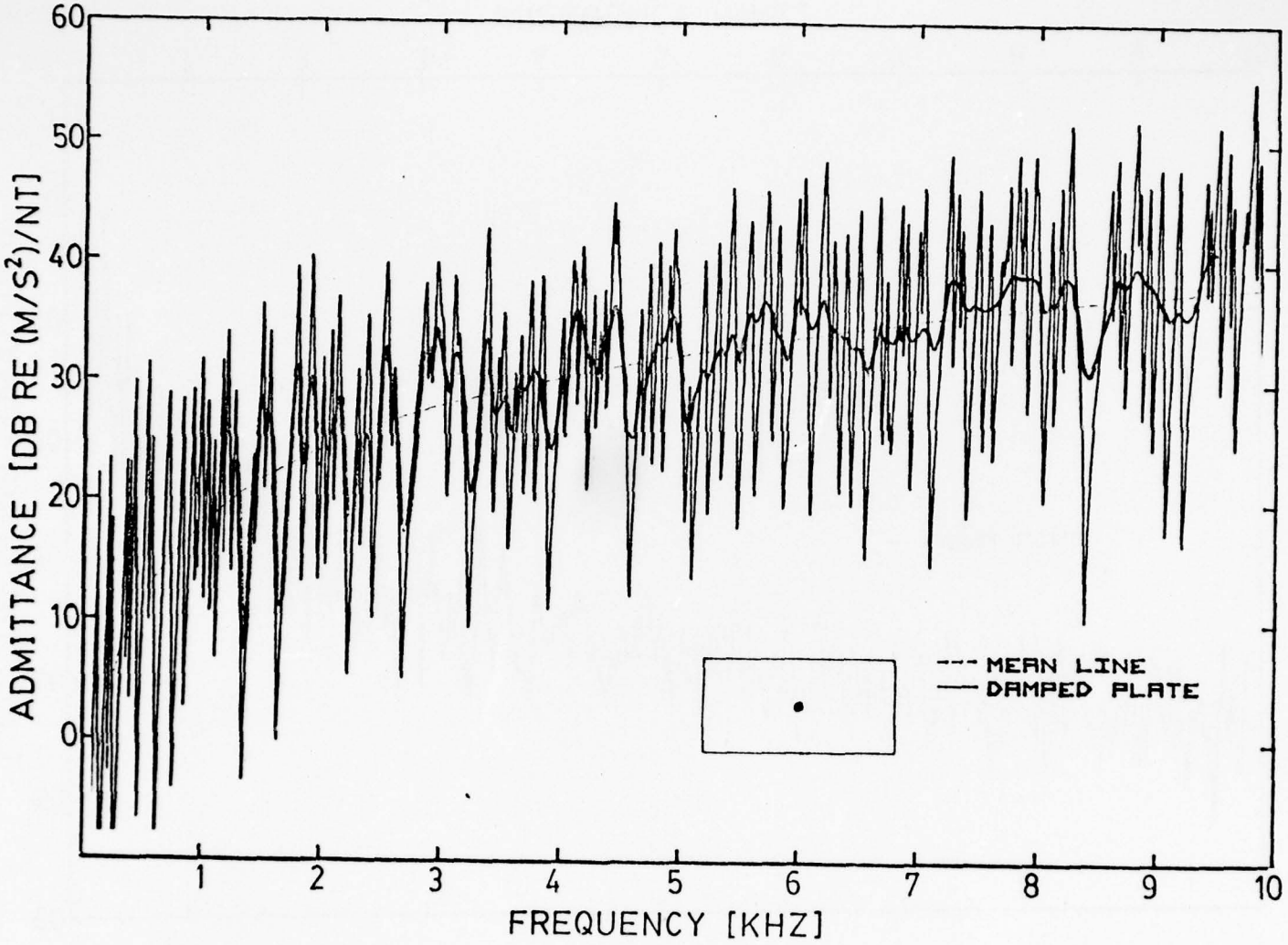

Figure 4.1 Driving Point Admittance of a Rectangular Plate Driven at the Center, Undamped and Damped

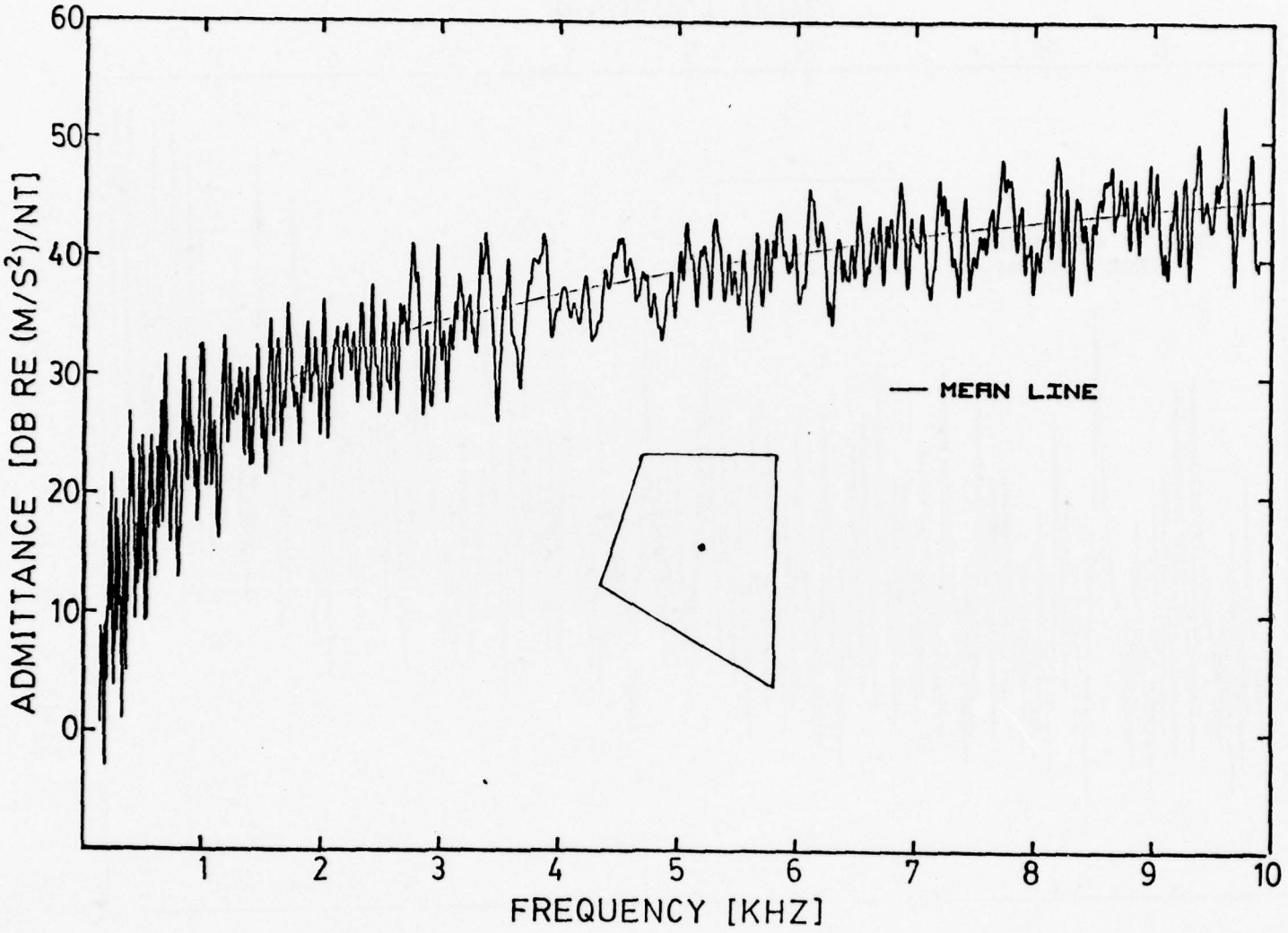

Figure 4.2 Frequency Response with Mean Line for a Quadrilateral Plate

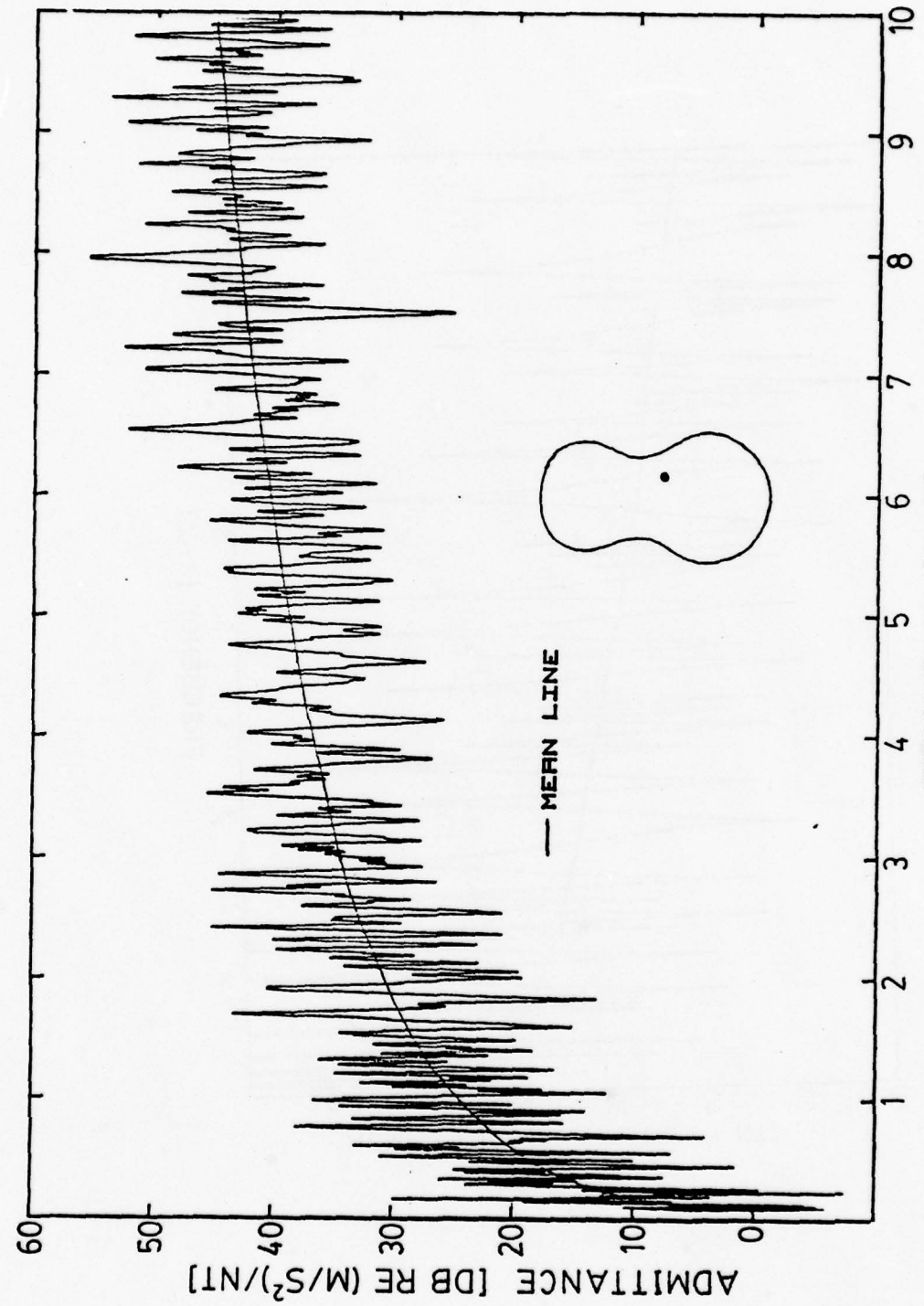

Figure 4.3 Frequency Response with Mean Line for a Figure Eight Plate

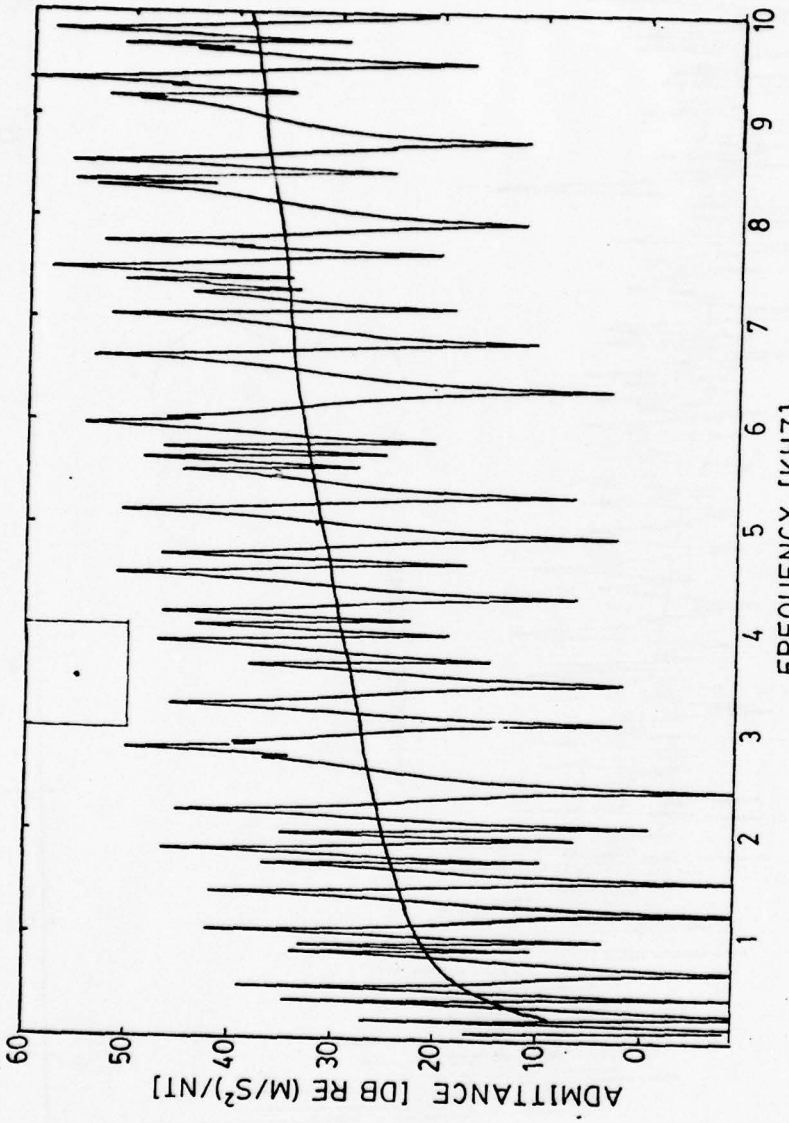

Figure 4.4 Frequency Response with Mean Line for a Square Plate

Figure 4.3 shows the frequency response curve for a plate with curved boundaries (figure eight shape) with the driver and receiver in the position indicated by the dot in the insert in the figure. The mean line is plotted as shown and again passes through the center of the data. The mean of the data drops somewhat low in the frequency region 4 to 6 kHz, an effect that will be accounted for later using image theory. Again this plate has a thickness of 1/8".

Figure 4.4 shows the frequency response curve for a square with the mean line indicated (plate VII of Appendix I).

4.3 Source on the Boundary of the Plate

The effect of placing the driver on the boundary is shown in Figure 4.5 for the rectangular plate (compare to Figure 4.1). Note the absolute level of the mean line for these two cases. With the driver on an edge the level of the response curve increases by 6 dB. This result appears surprising at first but can easily be attributed to the "edge distortion" present at the free boundaries of a plate vibrator. To understand this effect it will be helpful to consider the simpler case of a beam vibrating with free edges.

Since the boundary condition at a free edge requires that the bending moment there vanish, the region near the edge vibrates with a constant slope which, like a lever effect, amplifies the extent of the motion at the edge. In the mathematical solution, Equation (4.5), for the displacement amplitude of a center driven beam of length 1 this "edge distortion" effect appears as a term proportional to $e^{-k(1-x)/2^{1/2}}$.

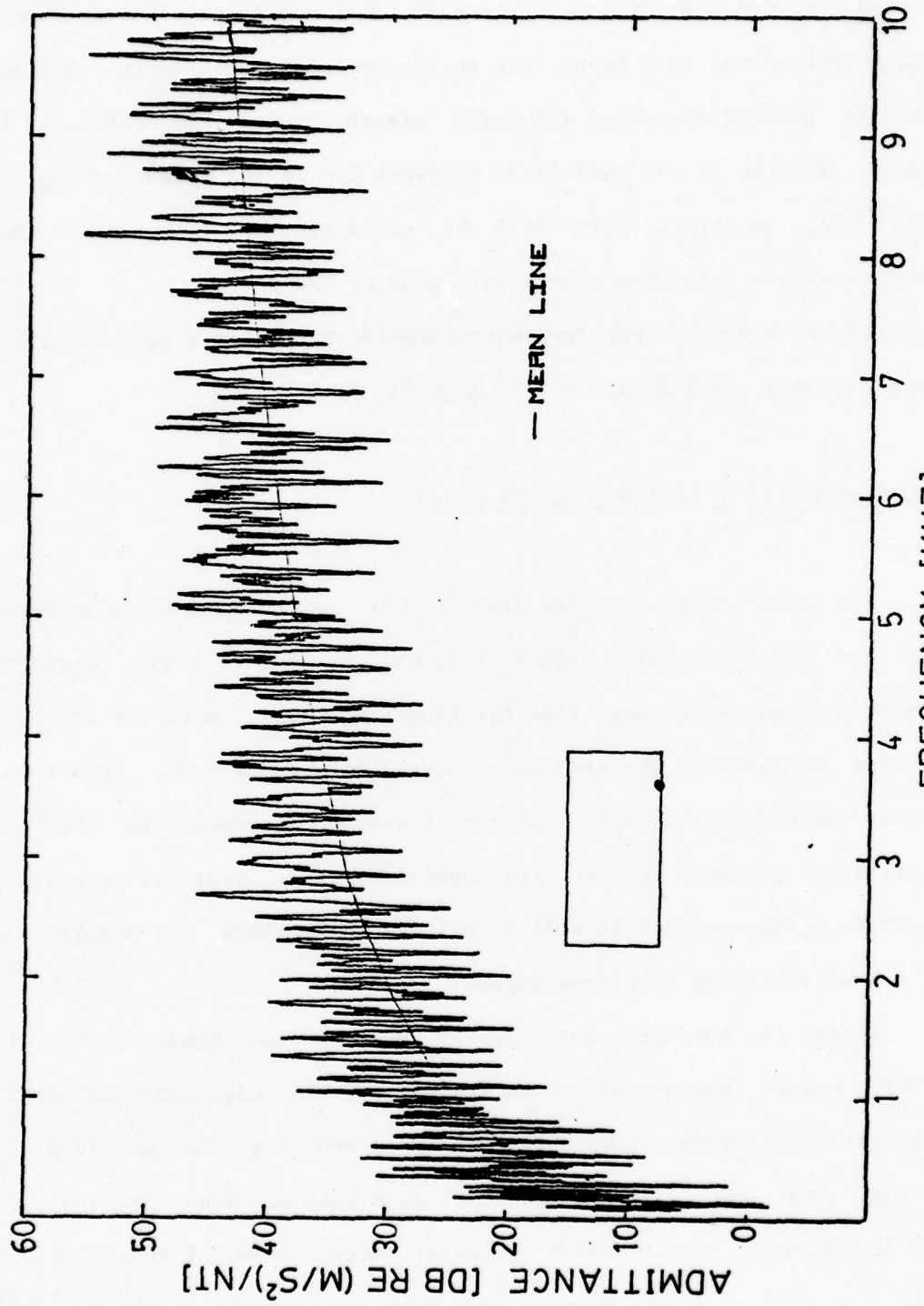

Figure 4.5 Driving Point Admittance on the Edge of a Plate

$$y(x)=F\frac{[\cos(k(1-x)+\pi/4)+e^{-kx}\sin(kl+\pi/4)+e^{-k(1-x)}/\sqrt{2}]}{2\cdot mc\cdot\sin(kl+\pi/4)} \quad \text{for } x\geq 0 \; . \qquad (4.5)$$

The driver is placed at x=0; the above solution neglects the edge distortion at the left end and is valid in the right half of the beam. At x=l this solution reduces to:

$$y(1)=\frac{F[1/\sqrt{2}+1/\sqrt{2}]}{2\cdot mc\cdot\sin(kl+\pi/4)} \; . \qquad (4.6)$$

This is equivalent to saying that the admittance at the edge is twice that at the center. The response at the center has the same form except that the second factor, $1/\sqrt{2}$, is missing. Thus it can be concluded that this edge distortion term actually doubles the amplitude of the motion at the edge of the beam. This doubling of amplitude is reflected in the admittance, which correspondingly must also increase by the same factor. Note that $kl=(n\pi-\pi/4)$.

In the next figure, 4.6, the driver and receiver are placed at the corner of the plate. Now the admittance increases another 6 dB, a total of 12 dB above that shown in Figure 4.1. The effects of the two free edges combine to quadruple the amplitude of the corner versus an interior point.

4.4 Source Near the Boundary: Effect on Mean for a Beam

The driving point admittance for the case where the driver is near a boundary of the plate is best understood by again looking at the similar case for the beam. The characteristic wave for a beam is

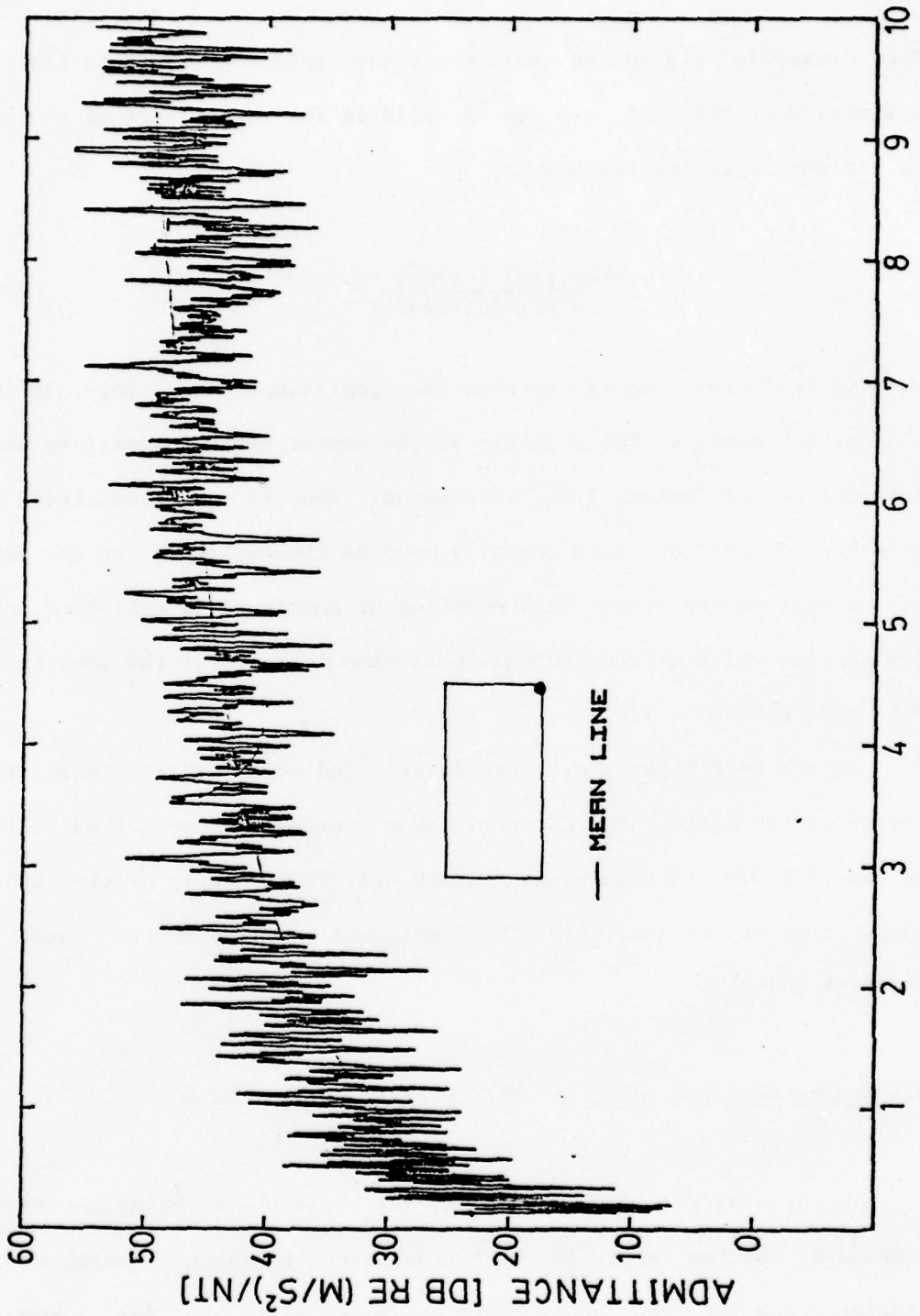

Figure 4.6 Driving Point Admittance at the Corner of a Plate

determined by considering the infinite case of a point excited beam. The analytic solution is conveniently represented with the Green's function for the problem and can easily be shown to be:

$$g(x|a) = [e^{-ik|x-a|} - ie^{-k|x-a|}] /4ik^3 , \qquad (4.7)$$

where a is the coordinate of the driver, x is the field point and k the wave number (ω/c_b). From this the characteristic velocity for a point force of strength F per unit length is easily found to be:

$$V_c = [e^{-ik|x-a|} - ie^{-k|x-a|}] F/4mc_b , \qquad (4.8)$$

where m is the mass per unit length, and c_b the bending wave velocity. In this development we have used the important relationship

$$c_b = a\sqrt{\omega} . \qquad (4.9)$$

The characteristic admittance is given by the ratio V_c/F.

Now we can deal with the situation of the finite beam and the driver close to the end. We make the very important assumption here that the mean line response will be given by the characteristic wave added to its reflection from the near boundary, an assumption which we will see is valid for plates as well as beams. This is merely an image source technique with one important consideration. The characteristic wave undergoes a perfect reflection from the end of the beam, but experiences a phase change which we will show is equal to $-\pi/2$ radians or -90^o. Setting a=0 for convenience and considering only the right

part of the beam, the right going wave can be represented as e^{-ikx} and the reflected wave traveling to the left as $e^{+ik(x-2l)+i\phi}$, where ϕ is the phase change upon reflection. The sum of these two waves can be shown to give

$$2\, e^{-i(kl+\phi/2)}[\cos(kl-kx)-\phi/2)] \cdot \tag{4.10}$$

The final solution for the characteristic wave and its reflection is:

$$V_c = e^{-i(kl+\phi/2)}[\cos(kl-kx)-\phi/2)]\ F/2mc_b \cdot \tag{4.11}$$

Figure 4.7 shows this result plotted against the exact solution for a beam driven at the center, with the receiver at a distance of 2/10 of the length l from the end of the beam. The normalized frequency Ω is the ratio ω/ω_1 where $\omega_1 = \pi c/l$, the approximate frequency of the lowest mode (the total length of the beam is 2l). Thus, it can be seen how the characteristic wave plus its reflection describes the mean trend of the real admittance of the beam. It is also interesting to note that the deep antiresonances are correctly predicted by this mean line. With the identification of $\phi = -\pi/2$, the cosine term in Equation (4.5) is the same as the one in Equation (4.11). Since kl is much greater than k(l-x) (when the receiver is close to the end) the denominator is a rapidly varying function of frequency and the numerator a slowly varying function. It is the former that shows up as the higher frequency oscillations in the figure and the latter is represented by the deep nulls. Unless k(l-x) is small (for instance at the very low

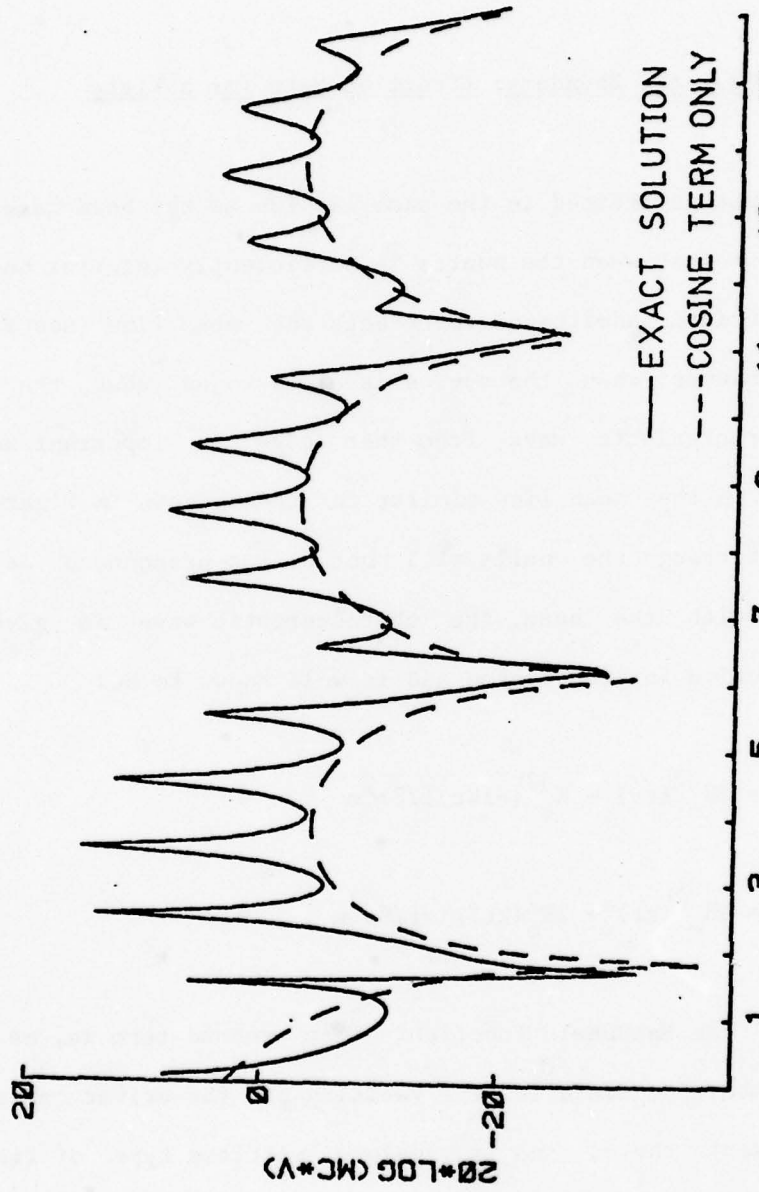

Figure 4.7 Theoretical Calculation for a Beam of Length 2L Driven at the Center and Received at .1L from End with Mean Line

frequencies) the second and third terms in Equation (4.5) are negligible. We will find that there is a perfectly analogous situation in the case of a plate, although here due to the spreading of the characteristic wave the nulls will not be as pronounced.

4.5 Source Near the Boundary: Effect on Mean for a Plate

This case is treated in the same fashion as the beam case. We have already shown that when the source is sufficiently interior in the plate the characteristic admittance represents the mean line (see Figures 4.1 to 4.3). However, when the source is close to an edge, the reflection of the characteristic wave from that edge is important and causes undulations in the mean line similar to those shown in Figure 4.7 for the beam, although the nulls will not be as pronounced as indicated above. As with the beam, the characteristic wave is given by the Green's function for the system and is well known to be:

$$Y_c = [H_o^{(2)}(kr) - H_o^{(2)}(-ikr)]/8\alpha^2 m$$

or

$$Y_c = [H_o^{(2)}(kr) + 2K_o(kr)/i\pi]/8\alpha^2 m \ , \qquad (4.12)$$

where K_o is the MacDonald function. This second term is, as with the beam, a distortion field in the vacinity of the driver caused by the bending moments there, and is again a wattless type of field. The MacDonald function, or the Hankel function of imaginary argument, decays essentially exponentially away from the driver and in almost all cases

can be neglected. Although each of the terms in Equation (4.12) is singular at r=0, their singularities cancel and the terms within the brackets reduce to unity. Thus, we have the important expression for the driving point admittance of the infinite plate:

$$Y_c = 1/8\alpha^2 m \ , \tag{4.13}$$

where m is the mass per unit area, α is the stiffness parameter given in Equation (4.2) and Y_c is the velocity/force.

When the source is close to the boundary of the plate, the boundary's local effect can be expressed by introducing an image source on the other side of the boundary at the same distance away as the original source. The reflected characteristic wave behaves as if the plate were semi-infinite in character; thus, one could obtain some mathematical rigor by looking at the semi-infinite plate with a point source near the boundary. The solution for this problem can be expressed in the form of an image solution, and the standard technique would be to express the functional form of the image so that the boundary conditions on the edge between the source and its image are satisfied. These boundary conditions are no moment and no shear force at the boundary. We back away from this rigorous type of solution since a simpler approach can be found. It is reasonable to expect that the functional form of the image source will be the same as that of the source, that is, a Hankel function, although the phase of its argument will be different due to the phase change which occurs when the wave travels across the boundary (actually reflected), as was the case with the beam.

We will assume that the source is far enough from the boundary that the distortion term will be negligible, an assumption that has proven to be valid if the source is at least a few inches from the edge. To determine the correct phase for the image source we can use the following technique.

4.5.1 Reflection of a Plane Wave from a Semi-infinite Free Boundary. Skudrzyk[5] considers the reflection of a plane wave from this free boundary by formulating the wavefield in the plate to be:

$$w(x,y) = e^{-k_y y}[\cos(k_x x+\phi) + Ce^{-\beta x}] , \qquad (4.14)$$

where C is a constant which represents the amplitude of the edge distortion due to the free boundary, and ϕ is the phase change due to the free boundary. This satisfies the wave equation if $k_x=k\cdot\cos\theta$, $k_y=k\sin\theta$, $\beta^2=k^2(1+\sin^2\theta)$, where $k=\omega/c_b=\sqrt{\omega}/\alpha$ and θ is the angle of incidence (from the normal) of the plane wave incident upon the boundary.[5] It is easily shown that the reflection coefficient is given by $e^{-2i\phi}$. When Equation (4.14) is plugged into the equations for the boundary conditions at the free edge we are able to determine $\phi(\theta)$ and $C(\theta)$. The algebraic solution is complex and is not repeated here; however, the solution is plotted in Figure 4.8. Part (a) shows the negative of the actual phase change for a plane wave hitting the boundary at an angle θ. It is seen that at normal incidence the phase change is -90^o as is the case in the beam where all the waves are at normal incidence to the free end. This should be contrasted with the

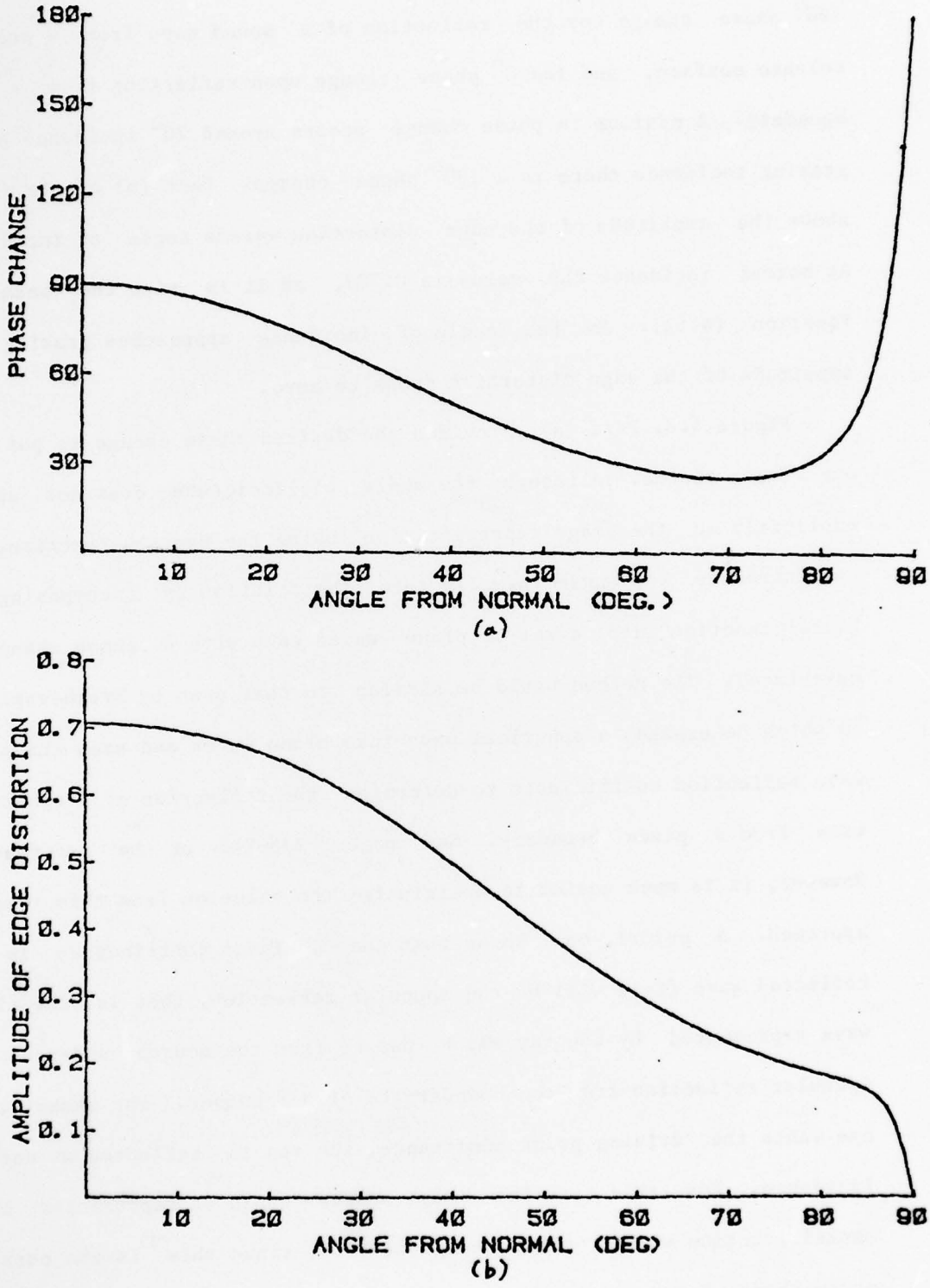

Figure 4.8 Phase Change (a) and Edge Distortion (b) for a Plane Wave Reflected from a Free Boundary

180° phase change for the reflection of a sound wave from a pressure release surface, and the 0° phase change upon reflection from a rigid boundary. A minimum in phase change occurs around 70° incidence and at grazing incidence there is a 180° phase change. Part (b) of the figure shows the amplitude of the edge distortion versus angle of incidence. At normal incidence the value is 0.707, as it is with the beam [see Equation (4.6)]. As the angle of incidence approaches grazing the amplitude of the edge distortion drops to zero.

Figure 4.8, Part (a), provides the desired phase change to put into our image source. Although the angle of incidence does not appear explicitly in the image representation using the Hankel function, one can introduce the angle formally into the solution by decomposing the Hankel function into a set of plane waves each with a phase change as calculated. The method would be similar to that used by Brekhovskikh[15] in which he expands a spherical wave into plane waves and uses the plane wave reflection coefficients to determine the reflection of a spherical wave from a plane boundary. (See pages 238-245 of the reference.) However, it is much easier to anticipate the solution from this type of approach. A priori, one knows that the dominant contribution in the reflected wave field will be the specular reflection, that is, the plane wave represented by the ray which passes from the source undergoing a specular reflection from the boundary to the receiver. For example, if one wants the driving point admittance, the ray is reflected at normal incidence. For this case the image source would be represented by a Hankel function with a phase change of -90°, since this is the correct phase change for a plane wave normally reflected.

4.5.2 Driving Point Admittance with an Image Source. To account for the image, a term representing the Hankel wave with appropriate phase change must be added to the characteristic admittance of a plate in Equation (4.3). This gives

$$Y_c = [1 + H_o^{(2)}(kr_i)e^{-i\phi}]/8\alpha^2 m \ , \qquad (4.15)$$

where r_i is the distance from the source to the image source, and is the phase change given in Figure 4.8, part (a). As was stated before we have neglected the distortion term for the image since it will be assumed that the source is far enough from the boundary to allow this. In fact, we generally will have the condition that kr>4, so that we can use the asymptotic expansion for the Hankel function and thus make use of a simpler formulation for the mean line including the image, which turns out to be

$$|Y_{ci}| = [1 + \cos(kr_i - \pi/4 + \phi)\sqrt{8/\pi kr_i} + 2/\pi kr_i]/8\alpha^2 m \ , \qquad (4.16)$$

where Y_{ci} is the characteristic admittance for a source close to the edge of a plate, r_i is the image distance and ϕ is the phase change. Now due to the cosine term in Equation (4.16), $|Y_{ci}|$ is an undulating function and no longer constant as it was for the source in the interior of the plate.

To bear out the above assumptions experiments were made with the source close to the edge of a rectangular plate. Figure 4.9 is a

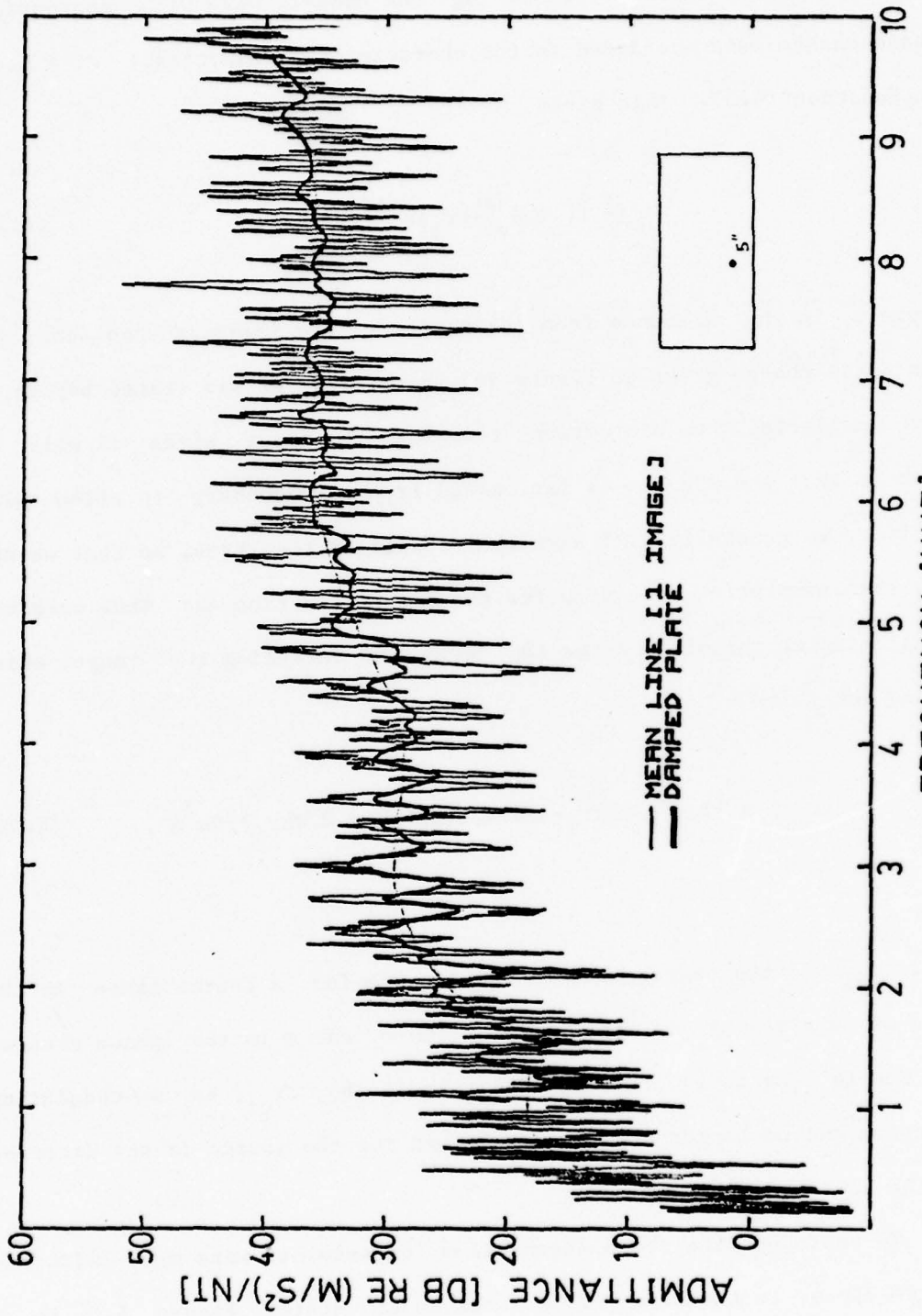

Figure 4.9 Driving Point Admittance Near the Edge of a Rectangular Plate - Mean Line with One Image

display of the experimental results with the source 5" from the edge of a plate of dimensions 24" x 48" and thickness 3/16". The mean line calculated by the above approach is shown and it can be seen to accurately predict the trend of the mean of the experimental data. Also included in this figure is the same measurement on this plate when it was damped, as described in Appendix II. Again, the very significant result is obtained: the damped plate response coalesces to the mean line prediction, in this case with a single image source added to the solution.

4.5.3 Driving Point Admittance-Source Near a Corner. Next this theory can easily be extended so that we can predict the driving point admittance when the source is close to two boundaries. In this case we need three images to account for the reflections from the corner, two being the mirror images across the two real edges of the plate, and the third lying such that the line from the source to it passes through the corner of the plate. This last image represents a wave which is reflected at an angle of 45^{o} from each adjacent edge, assuming that the source is placed equidistant from the two edges. Referring back to Figure 4.8, part (a), this corresponds to a phase change of 46^{o} upon each reflection or a total of 92^{o}. With these phase changes added to the three images a mean line prediction is made for the case of a source within 5" of the corner, and the results are shown in Figure 4.10. The agreement is excellent. It should be noted that if one does not add the phase changes in the reflected waves, the resulting mean line has minima at 4.8 and 9.1 kHz instead of 3.9 and 7.5 kHz as shown in Figure 4.10.

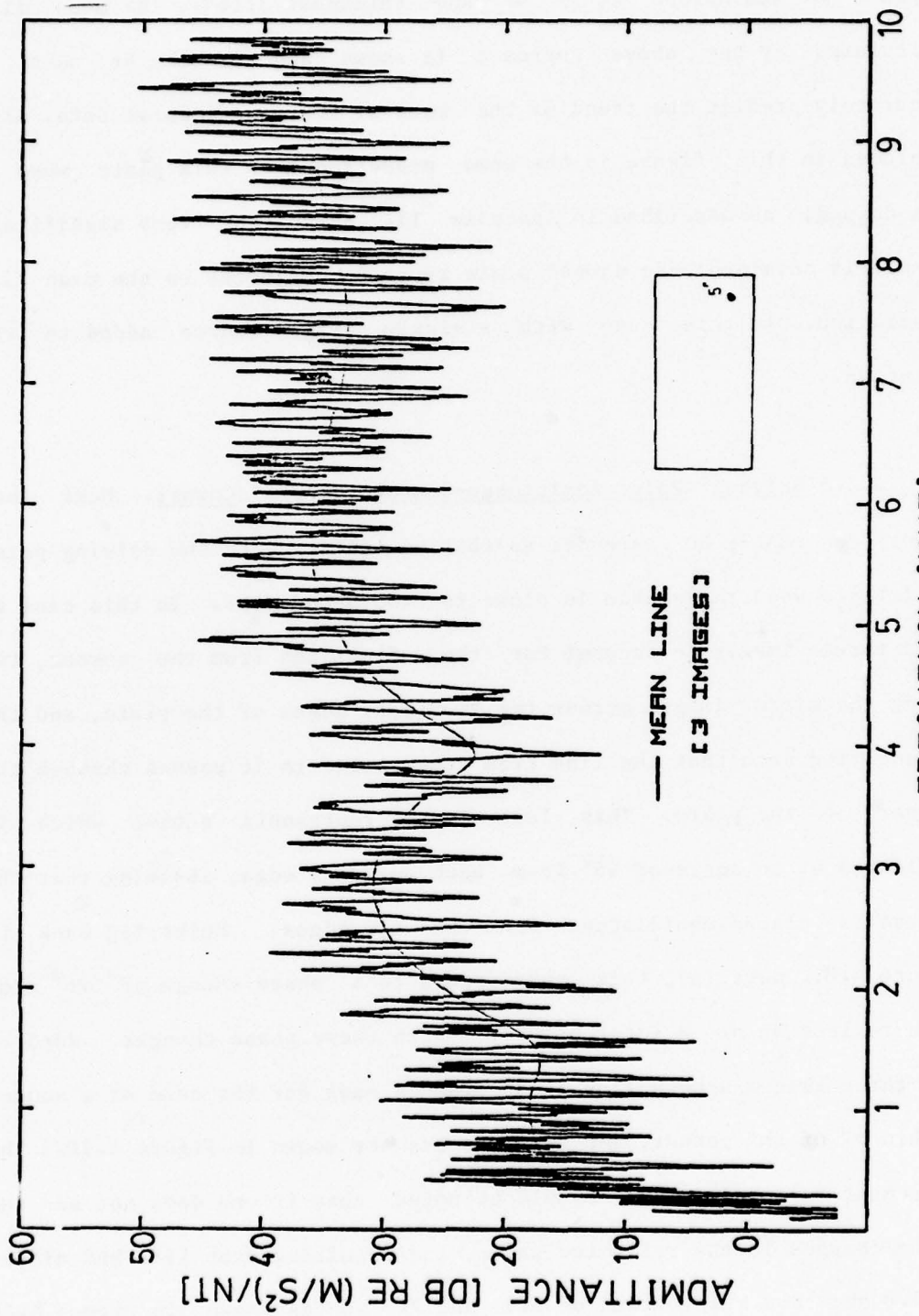

Figure 4.10 Driving Point Admittance Near Corner of a Rectangular Plate - Mean Line with Three Images

Figure 4.11 shows the similar case but with the source only 3.5" from the corner.

The frequency response curve was also obtained for the case of the driving point in the corner at a distance of 5" from the edges when the plate is damped (see Appendix II for a discussion of damping). The results are shown in Figure 4.12, and again the results are in excellent agreement with the theory. Again we have important verification of the fact that as the plate is damped the measured results converge to the mean line with images.

To further the understanding of this image method Figure 4.13 is included. This is a theoretical calculation of the effects of including more and more images in the mean line calculation. Source and receiver are separated by 4" and the driver is closer to the boundary at a distance of 5" as shown in the insert in the figure. The images are selected so that those with the smallest path lengths are the ones included. One can see that as more images are added the effect is to create an oscillation about the one image line, but not a shift in the actual level of the curve. As we progress past five images the oscillation becomes more rapid; however, the one image line will still serve as the mean of that oscillation.

4.5.4 Driving Point Admittance Near a Convex Boundary: The Elliptical Plate. In this section we extend the image method to deal with the reflection from a curved boundary, in this case the curve about the ends of the major axis of an ellipse. The plate used was of the following dimensions: major axis=0.93 m, minor axis=0.606 m, interfocal

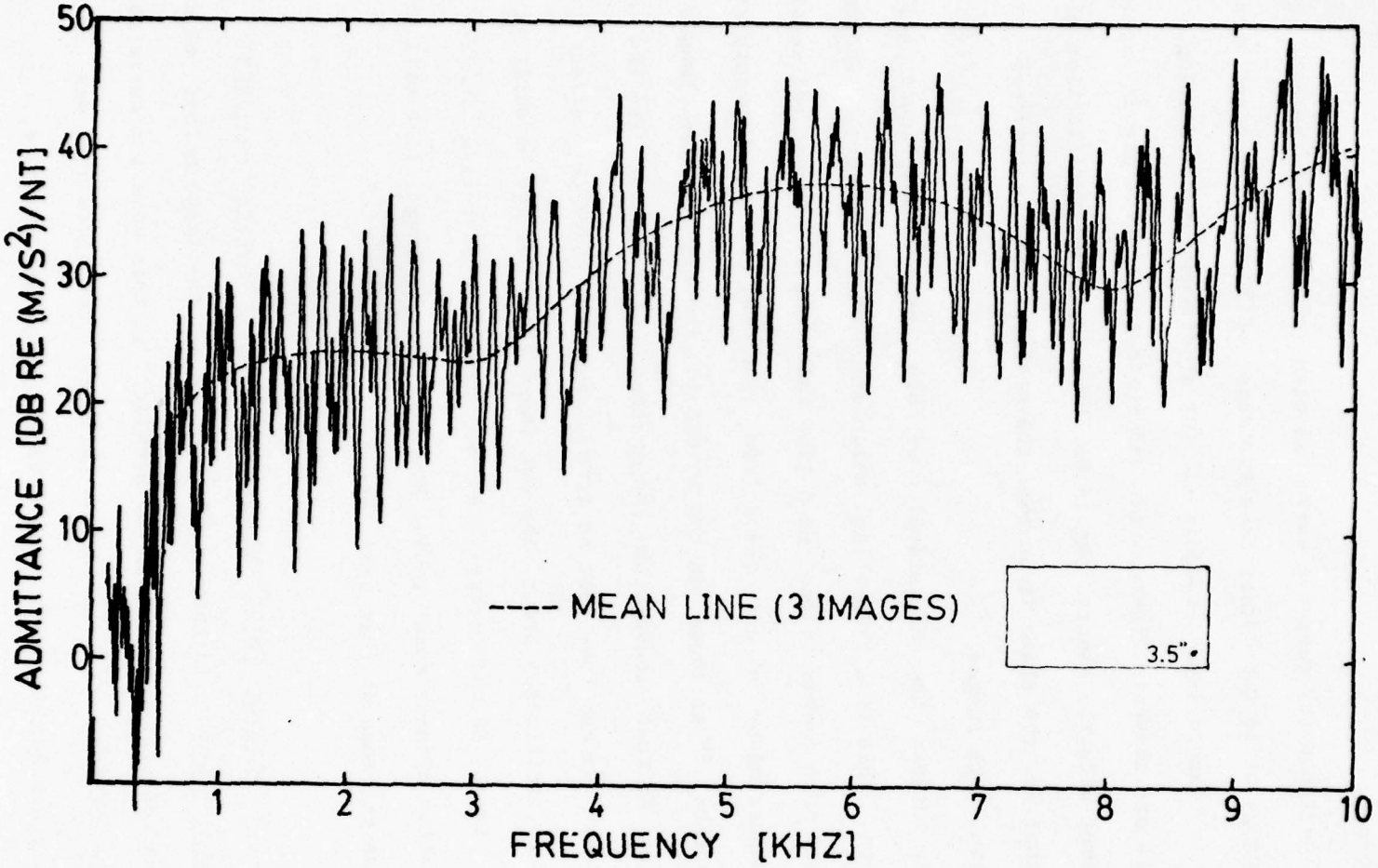

Figure 4.11 Driving Point Admittance Near Corner (3.5") - Mean Line with Three Images

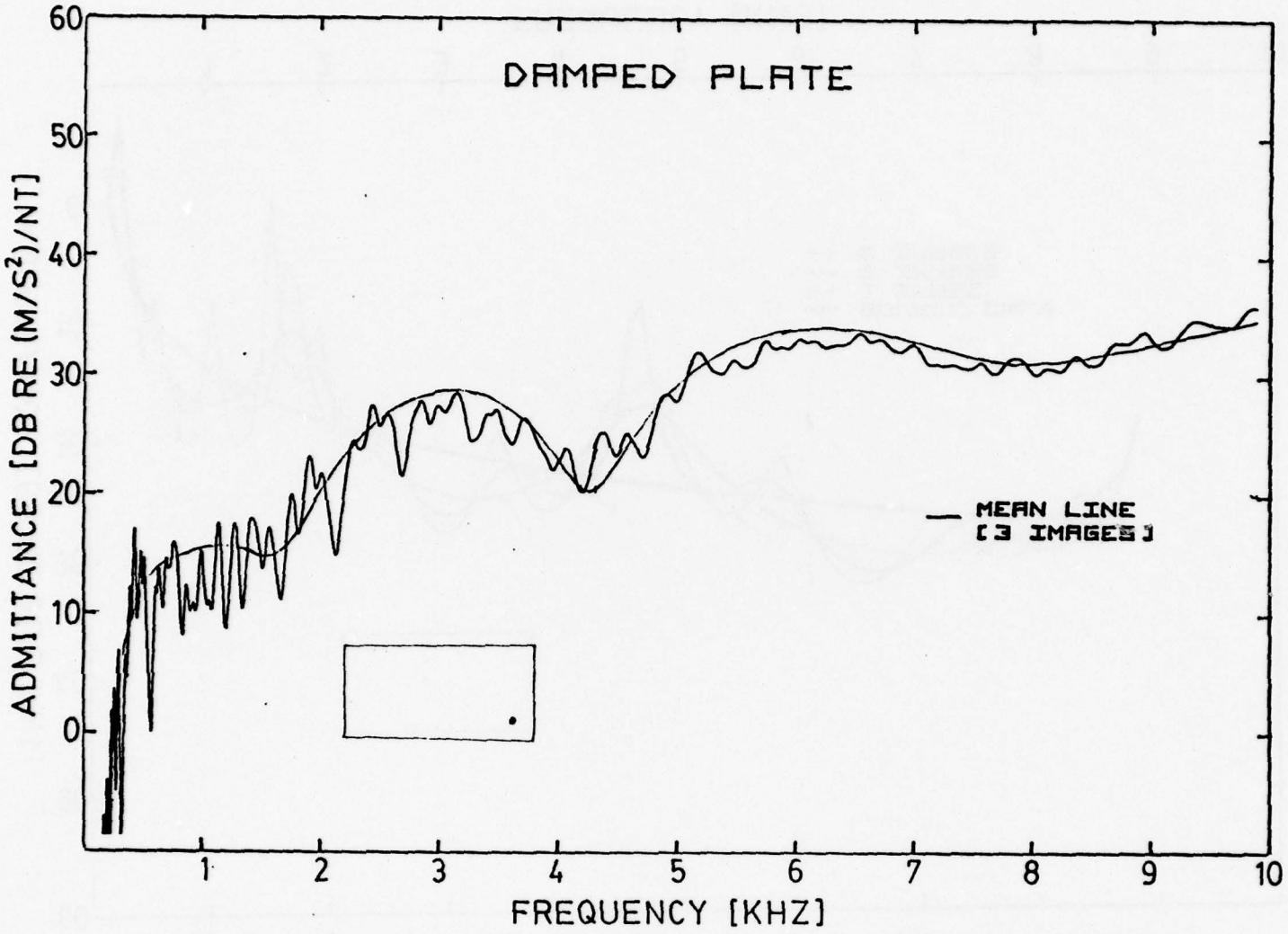

Figure 4.12 Driving Point Admittance Near Corner (5") for a Damped Plate - Mean Line with Three Images

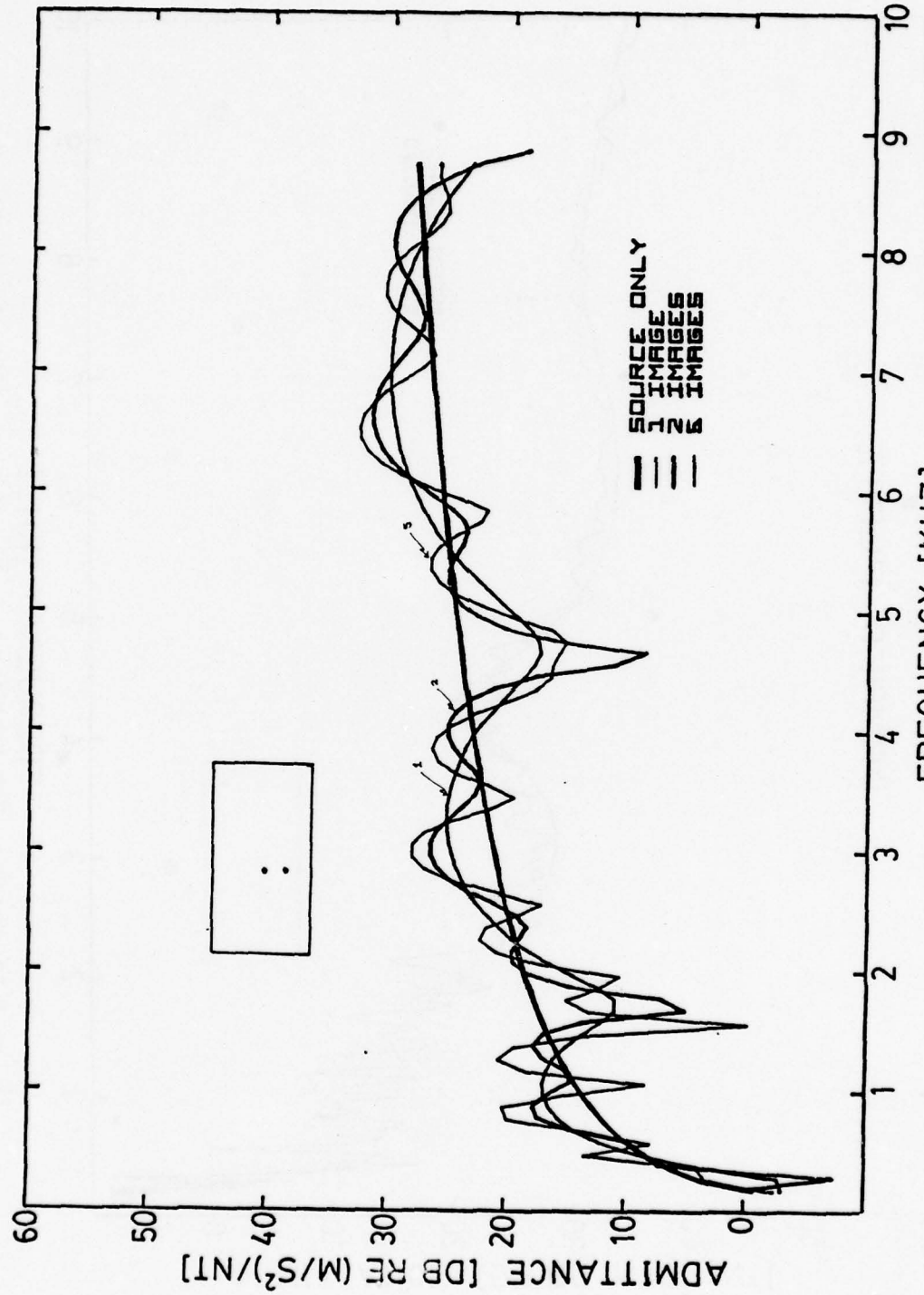

Figure 4.13 Theoretical Calculation Illustrating the Effect of Adding More Images

length=0.706 m. The aluminum plate had a thickness of 1/8" and an α=2.23 m/sec$^{1/2}$ cut from the standard stock alloy 6061-T6.

The driver was placed at the focus of the ellipse and a driving point frequency response curve was made as shown in Figure 4.14. This figure demonstrates the remarkable regularity of the resonances and is unlike any of the other plate frequency response curves, except the circular plate driven at the center (see Figure 5.2 in Chapter V) where only the one-dimensional ring modes were excited. This regularity indicates the special geometric role that the focus plays in which any ray emitted from a focus will return to that focus with the same path length independent of the angle of emission. This same effect occurs in the center driven circular plate.

The mean line prediction for this case shown in Figure 4.14 was obtained by using one image in the solution. The image was placed as shown in the insert in the figure and is located at an equal distance from the end of the ellipse as the source. It represents the wave which is specularly reflected off the highly curved bowl of the ellipse and, thus, returns to the driver. It is especially interesting and somewhat significant that the image technique that treats this bowl as though it were a straight edge works so well, and even more surprising is its success at the low frequencies (below 2.5 kHz). The wave length at these low frequencies of the bending waves in the plate is actually larger than the distance from the focus to the near end of the major axis. In fact, in the calculation of the effect of the image no attempt was made to include the effect of the curvature of the boundary at the point of reflection. It would appear that the ray theory approximation

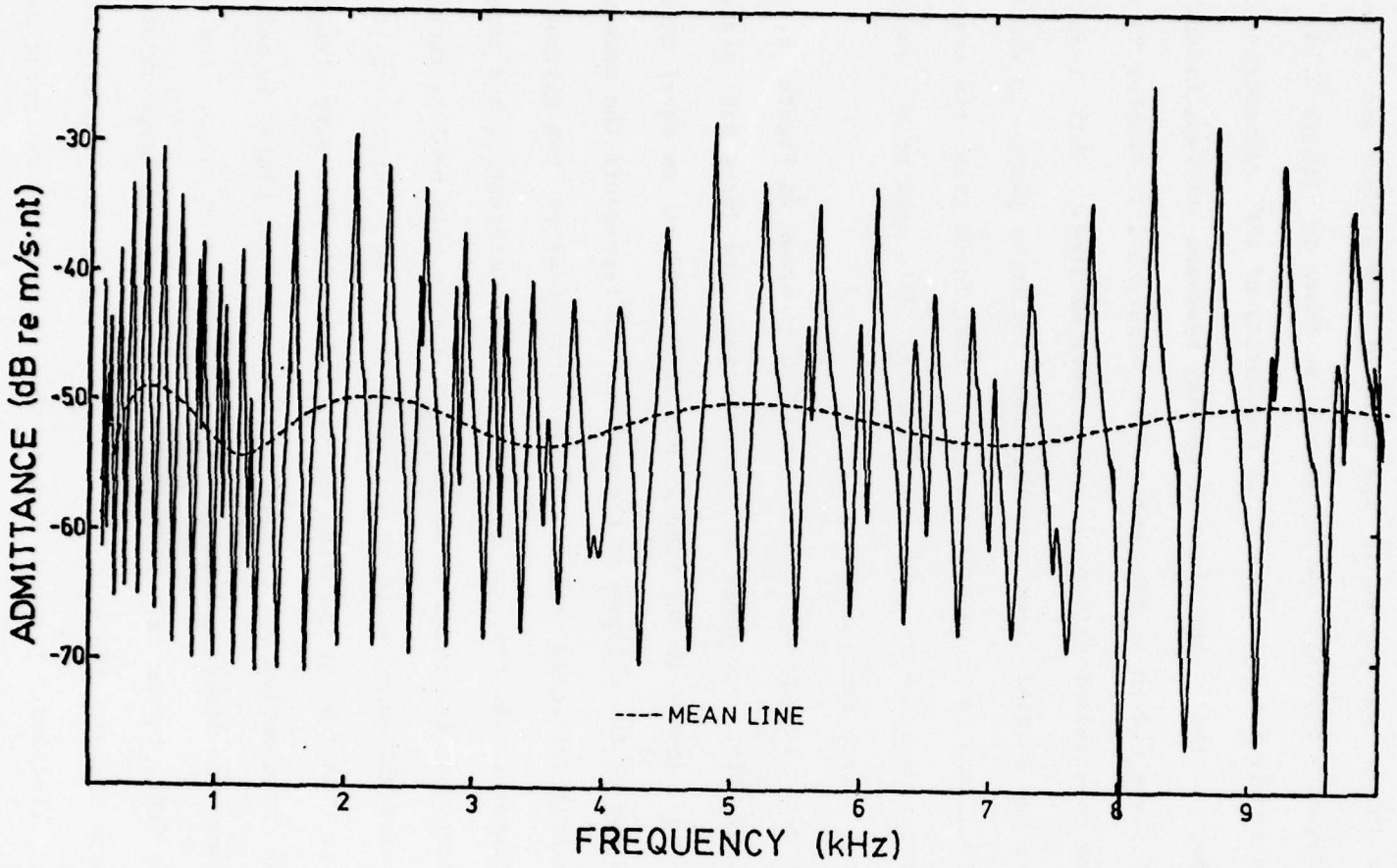

Figure 4.14 Frequency Response and Mean Line (1 Image) of an Elliptical Plate Driven and Received at a Focus

was working well in a region (distances of the order of a wavelength) where one would expect problems.

The next figure, Figure 4.15, is a frequency response curve for the case where the source is at one focus and the receiver at the other. This is an extremely interesting curve for it displays the symmetry present at the foci. Compared to Figure 4.14 with driver and receiver at the same point, we can see that the half of the curve above the mean line is identical in both these cases. The height of the resonances does not change. Indeed, all of the energy from the one focus is reflected into the second one without any loss at the resonances. One can understand this in another way. Since the source and receiver are at symmetrical locations with respect to the boundaries, one would expect that the magnitude of each mode shape would be the same at these two points. In other words the mode shapes for an elliptical plate are always symmetrical (or antisymmetrical) across the minor axis.[16] If the mode is antisymmetrical across the minor axis then the phase of the vibration is 180^{o} compared to the driver. Generally, at the second focus succeeding modes (with respect to frequency) are alternately in phase and out of phase with the driver. This alternation of phase explains the disappearance of the antiresonances in Figure 4.15. That is, an antiresonance is caused when the mass reactance of the mode below just cancels the upper mode's compliant reactance. But if the phase of one of these modes is in 180^{o} opposition to the other, then both of the modes are either compliant or masslike at the antiresonance frequency and this cancellation does not occur. Instead a shallow trough occurs which is tangent to the mean line prediction. It can be

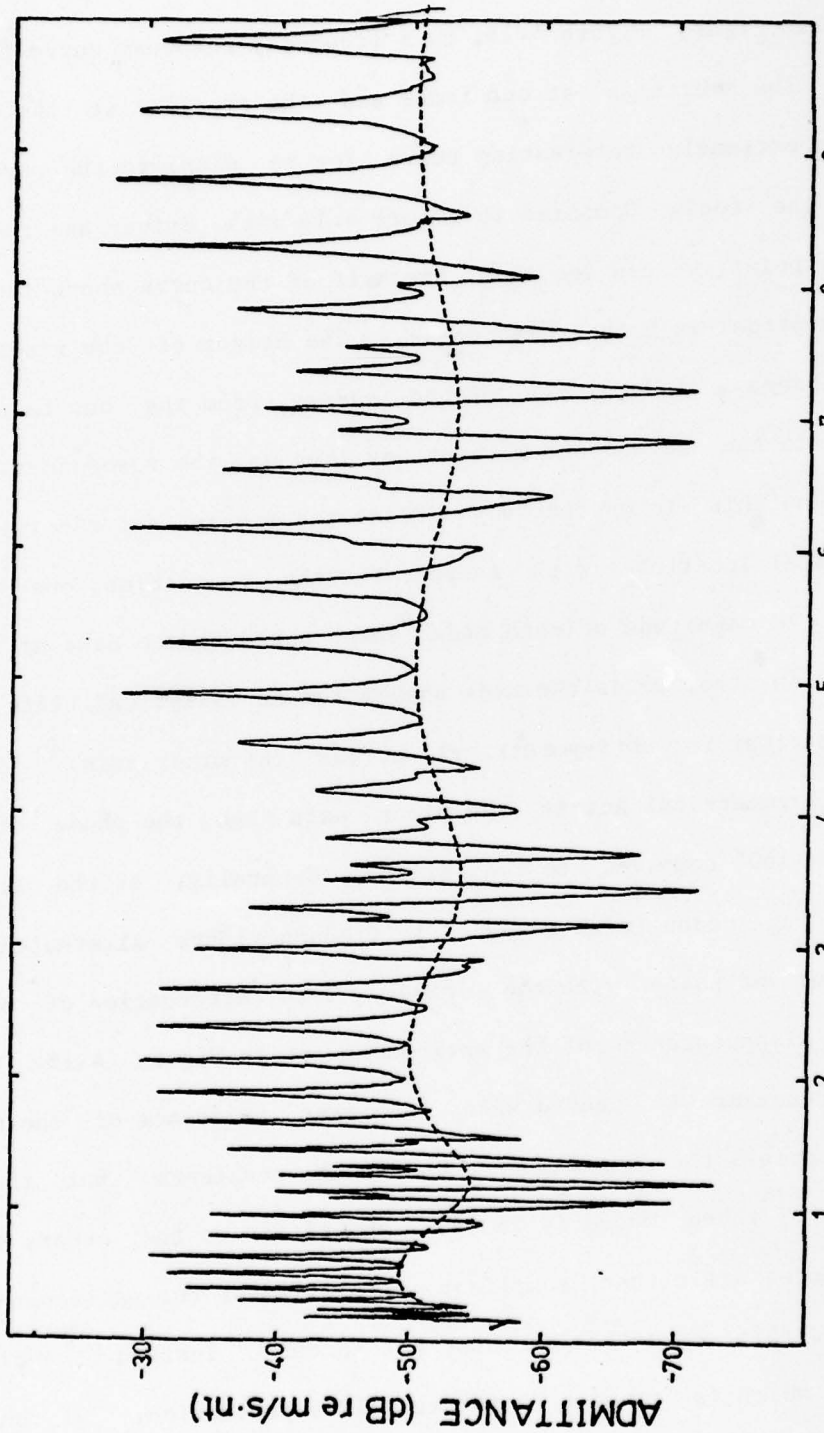

Figure 4.15 Transfer Admittance and Mean Line (1 Image) Between One Focus and the Other

easily verified that the regions where the antiresonances do occur in Figure 4.15 are regions in which two succeeding modes occur with the same phase. (See for instance Waller,[2] page 25.)

This case should be contrasted with the end driven beam shown in Figure 4.16. Here without exception the modes alternate in sign at the end opposite to the driven end, and all of the antiresonances are turned into shallow troughs which are tangent to the mean line.

The final figure, 4.17, on the elliptical plate shows a case in which the receiver is at the very end on the major axis opposite to the driver (still at the focus). It is included because of its interesting response curve. It is similar to the others only at the very low frequencies and in the occurrence of the shallow troughs.

4.5.5 Driving Point Admittance Near a Concave Boundary: The Figure Eight. The final example of the use of this image theory is the figure-eight plate with the driver situated near a convex boundary. To find the image the specular reflection is calculated for a ray emitted from the source, and thus the image source is located directly across the boundary along the line of this ray at an equal distance from the boundary as the source. The distance between source and image is 19 cm, or 7.5 inches. Again the phase change upon reflection is taken to be -90^{o} as before. The mean line prediction with one image is shown along with the experimental results in Figure 4.18 and agrees remarkably with the data. As before geometric optics seems to apply and to find the correct image one need only find a tangent to the closest boundary that is perpendicular to the line connecting the source with its image.

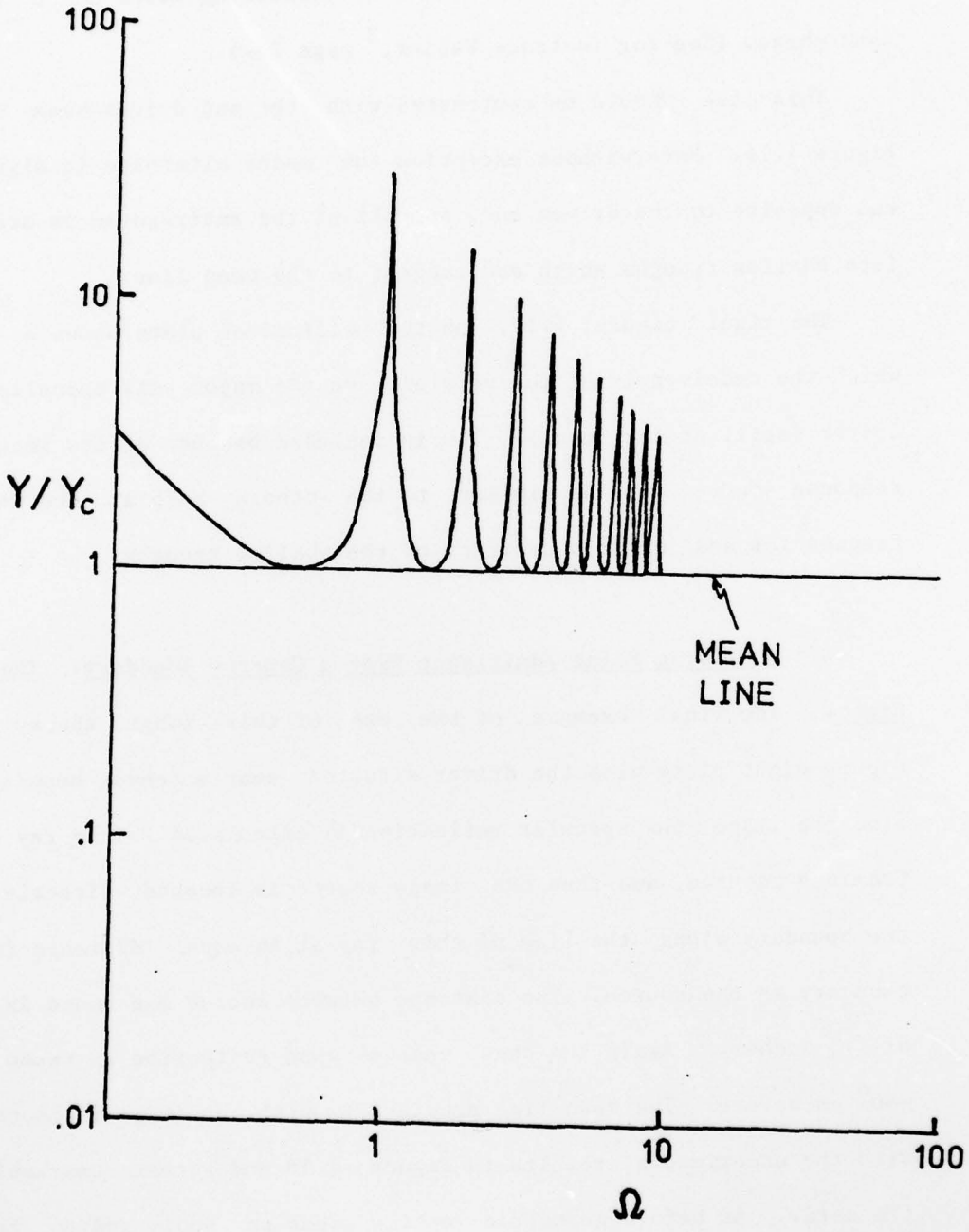

Figure 4.16 Admittance at the End of a Beam Driven at the Opposite End with the Mean Line

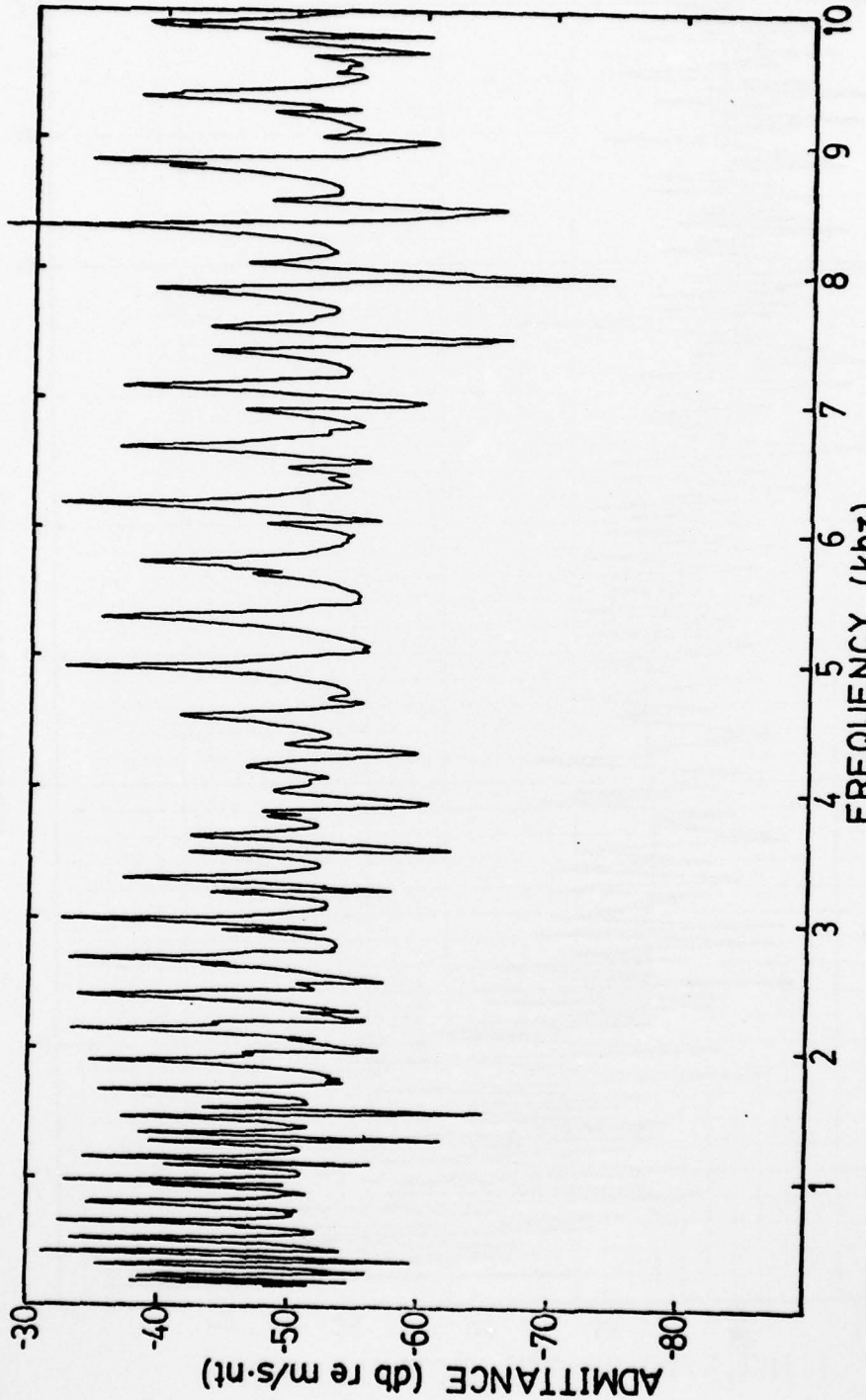

Figure 4.17 Transfer Admittance of an Elliptical Plate from the Focus to the End of the Major Axis Opposite

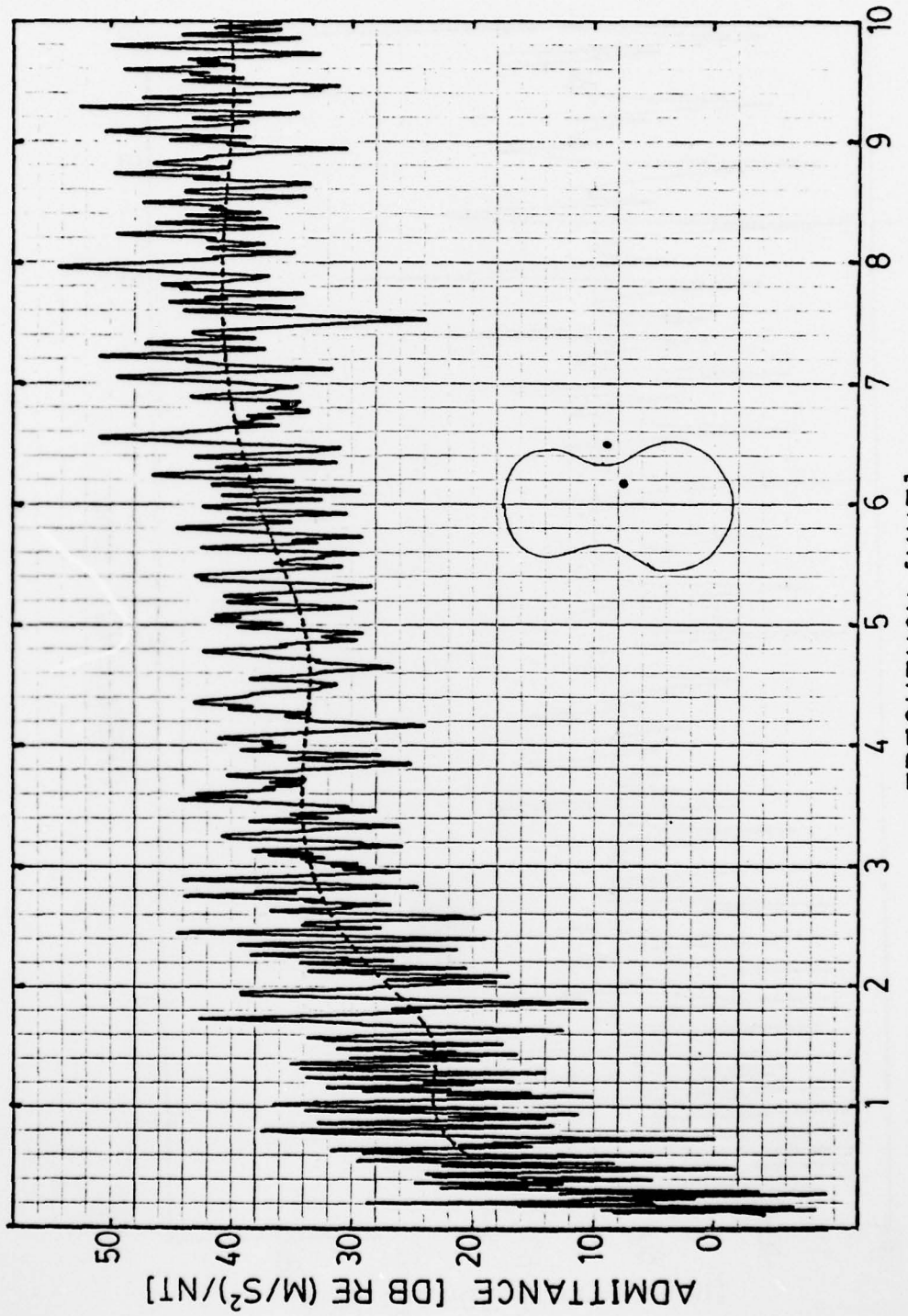

Figure 4.18 Driving Point Admittance and Mean Line (1 Image) - Figure Eight Plate, Driven Near the Concave Boundary

4.6 Transfer Admittance (Source and Receiver Separated): Theory and Experiment.

The mean value theory accounts[5] for the case where the source and receiver are separated using the same considerations as we saw in Section 4.1. Equation (4.4) represents the admittance of a plate which is infinite in extent, and it will be used here to predict the characteristic admittance of finite plates. Now r represents the distance between the driver and receiver. Again, unless the receiver is located within a bending wavelength of the driver, the second term in Equation (4.4) is negligible. In this case we generally are in the region of the asymptotic expansion of the Hankel function; then Equation (4.4) reduces simply to:

$$|Y_c| = (2/\pi kr)^{1/2}\ 1/8\alpha^2 m\ , \qquad (4.17)$$

and the characteristic admittance has a cylindrical divergence with distance. Thus, the mean line decreases 3 dB for every doubling of the separation between driver and receiver. When kr is at least 4 the difference between 4.18 and 4.4 is negligible and is at worst about one dB difference when kr>0.8. Since $k=\omega^{1/2}/\alpha$, if r = 1" and $\alpha=2.23$ (1/8" thick plate), then kr>0.8 as long as the frequency is at least 775 Hz or 1.1 kHz if $\alpha=2.72$ (3/16" thick plate). Figure 4.19 is a plot of the loss as the source and receiver are separated at two frequencies (5 and 10 kHz) for a plate of thickness 3/16"; it is calculated by taking the magnitude of Equation (4.4) and it will be useful in interpreting the curves that follow.

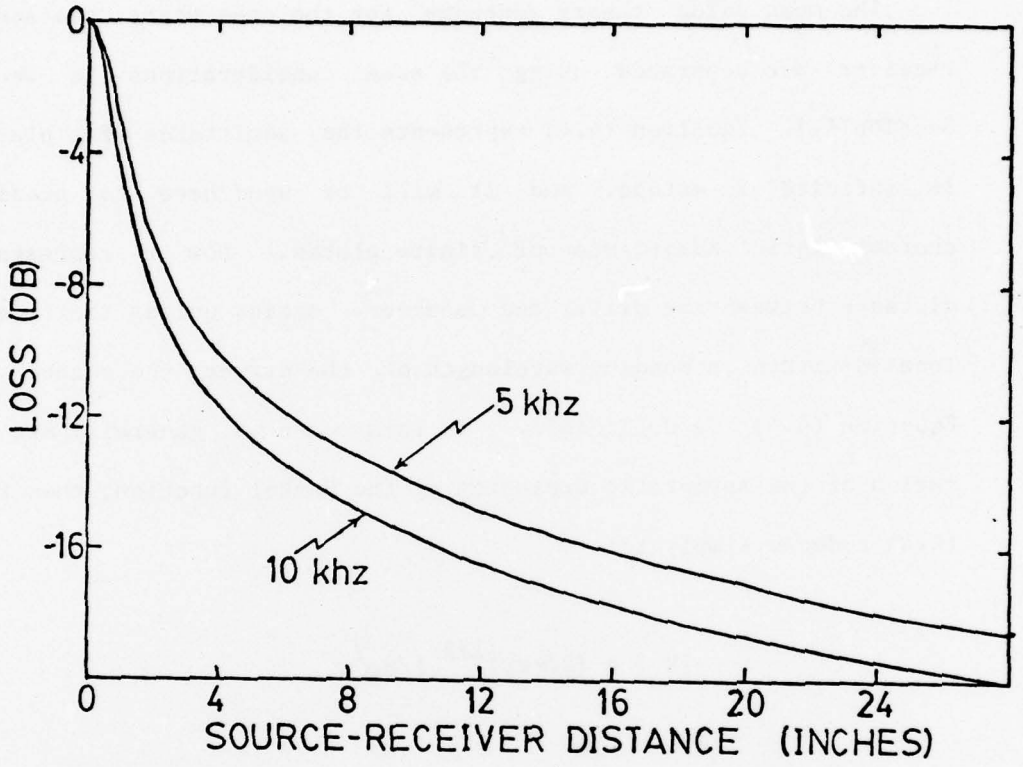

Figure 4.19 Decrease of Transfer Admittance as the Receiver and Driver Are Separated for 3/16" Thick Plate at 5 and 10 kHz

4.6.1 Experimental Results: Damped Rectangular Plate. Plate I (see Appendix I) with damping compound applied to its top surface was measured in the following set of figures. The source was placed off center so that the full set of modes were excited and frequency response curves were made at source to receiver separations of 0,1,2,3,5 and 10 inches. The results are shown in Figures 4.20 through 4.26; the inserts in each figure describe the placement of the driver and receiver. Figure 4.20 is the driving point admittance included for comparison. The dotted lines on the figures represent the mean line calculated using Equation (4.4). They indicate that the mean line offers an excellent prediction of the mean trend of the experimental results over the entire frequency range. The drop off in level at 10 khz should be noted in these figures, and as can be seen from reference to Figure 4.19, the level is down by about 16 dB from that at the driving point at a 10" separation. The next figure, 4.27, represents the case where the source is at the center of the plate and the receiver at a corner so that their separation is 26.8". In this case 12 dB is added to the mean line response to account for the corner effect, as described in Section 4.3. At the lower frequencies the mean line prediction appears to be somewhat low.

When the source or receiver is close to a boundary, the method of images can be used as before with the driving point admittance in Section 4.5. Figures 4.28 and 4.29 are made by imaging the source across the longer edge of the plate located a distance of 5" from that boundary. The solid line represents the mean line prediction with one image, and it is seen to represent the mean of the data fairly well. In

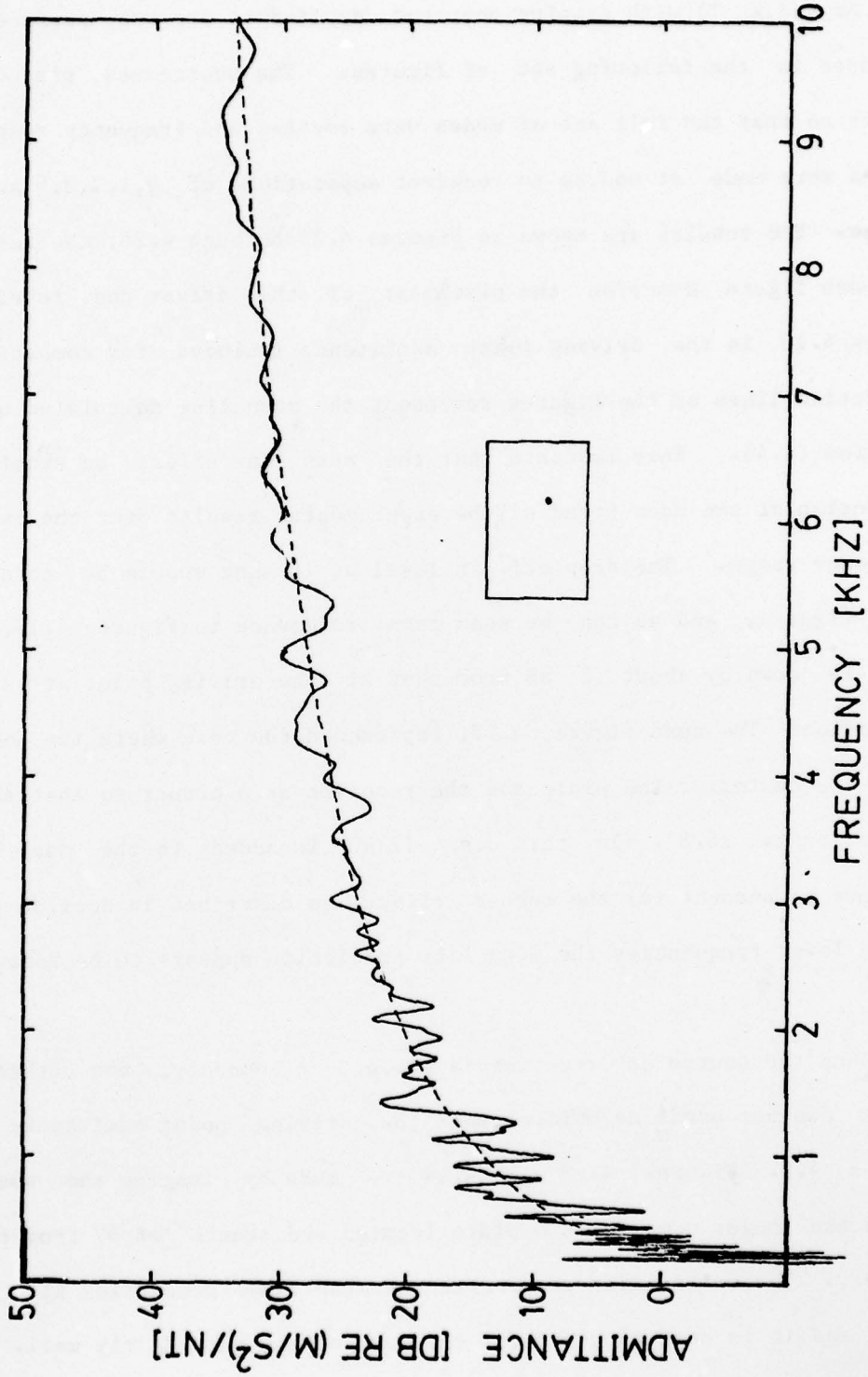

Figure 4.20 Driving Point Admittance - Damped Plate

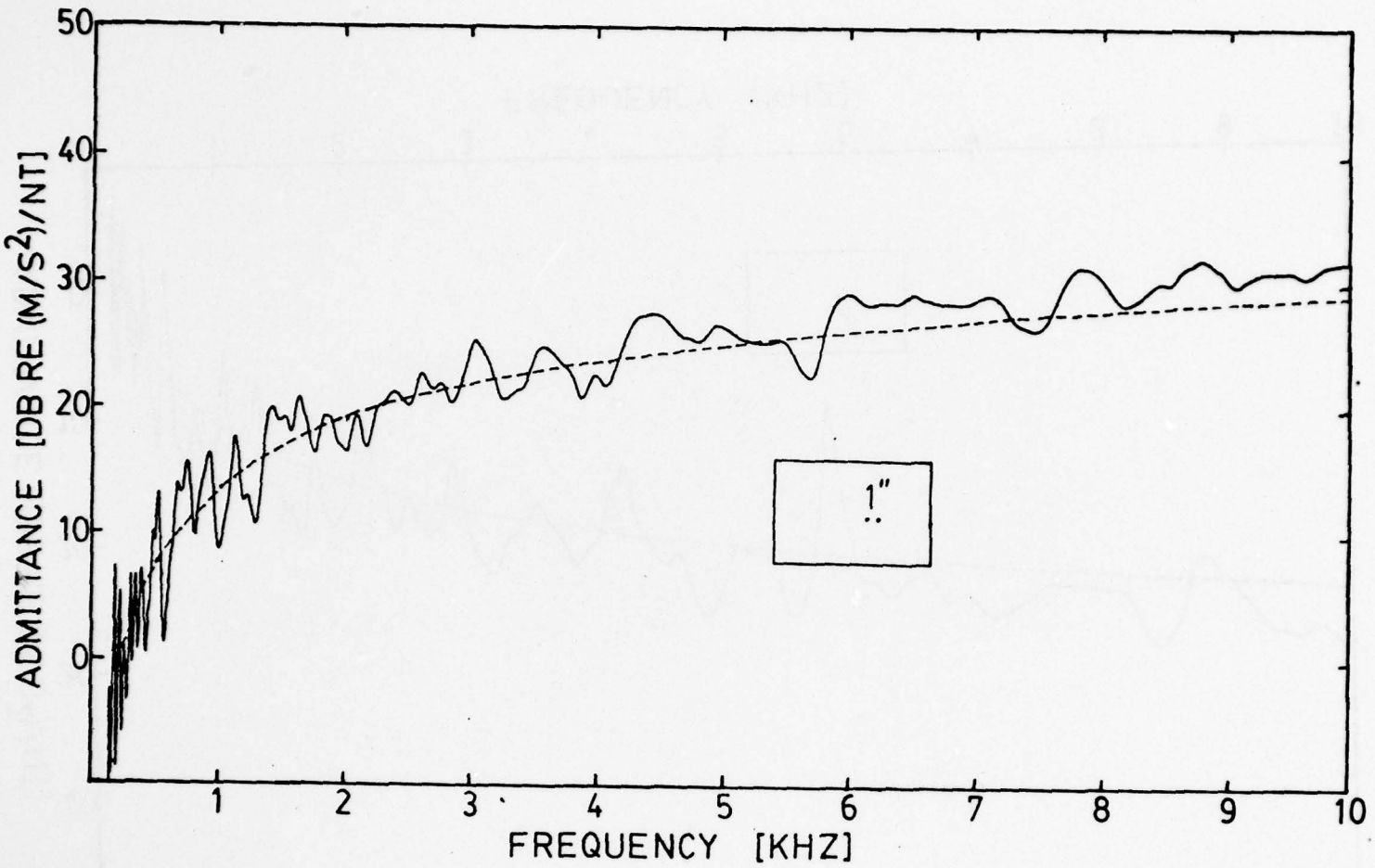

Figure 4.21 Transfer Admittance - Damped Plate

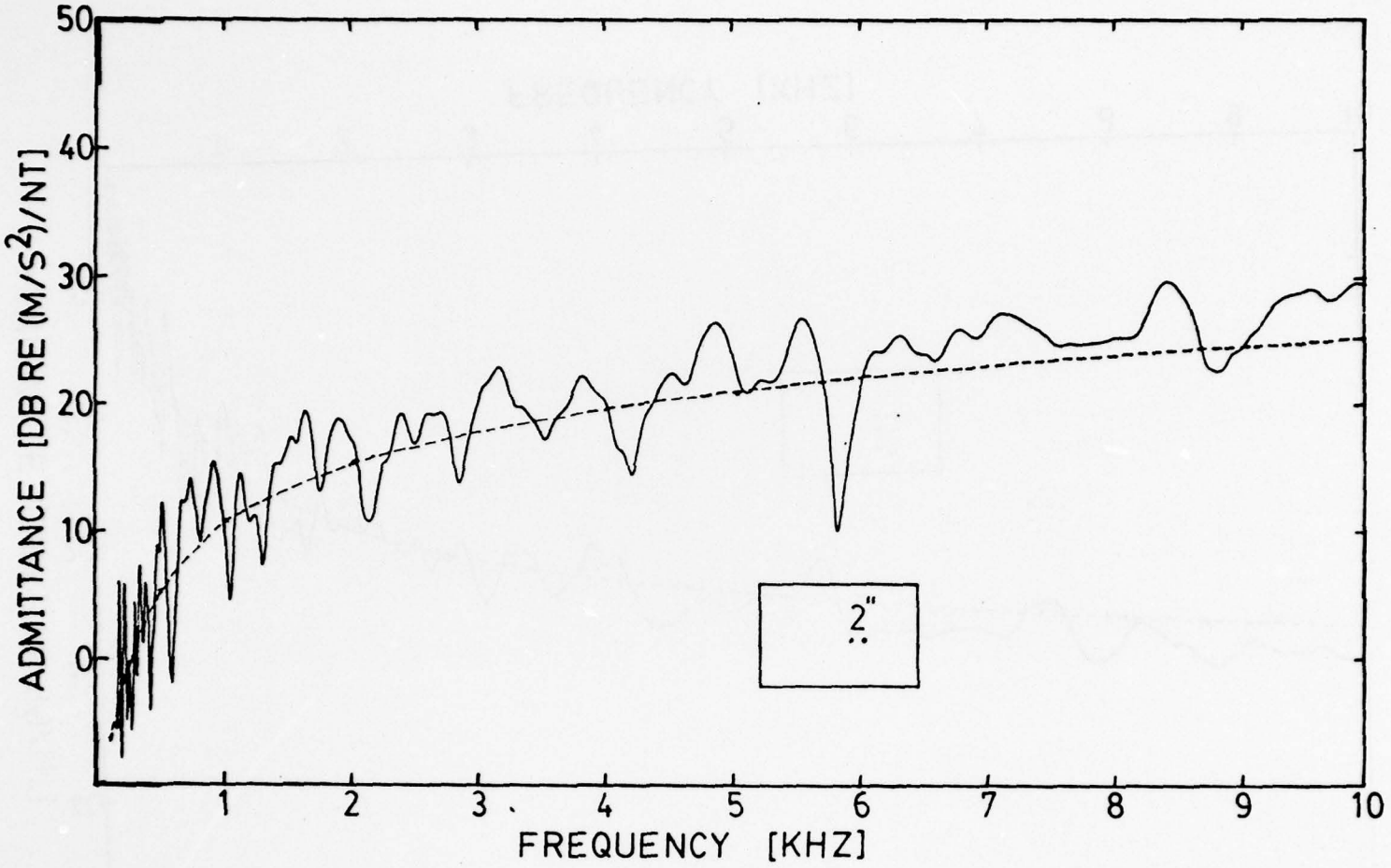

Figure 4.22 Transfer Admittance - Damped Plate

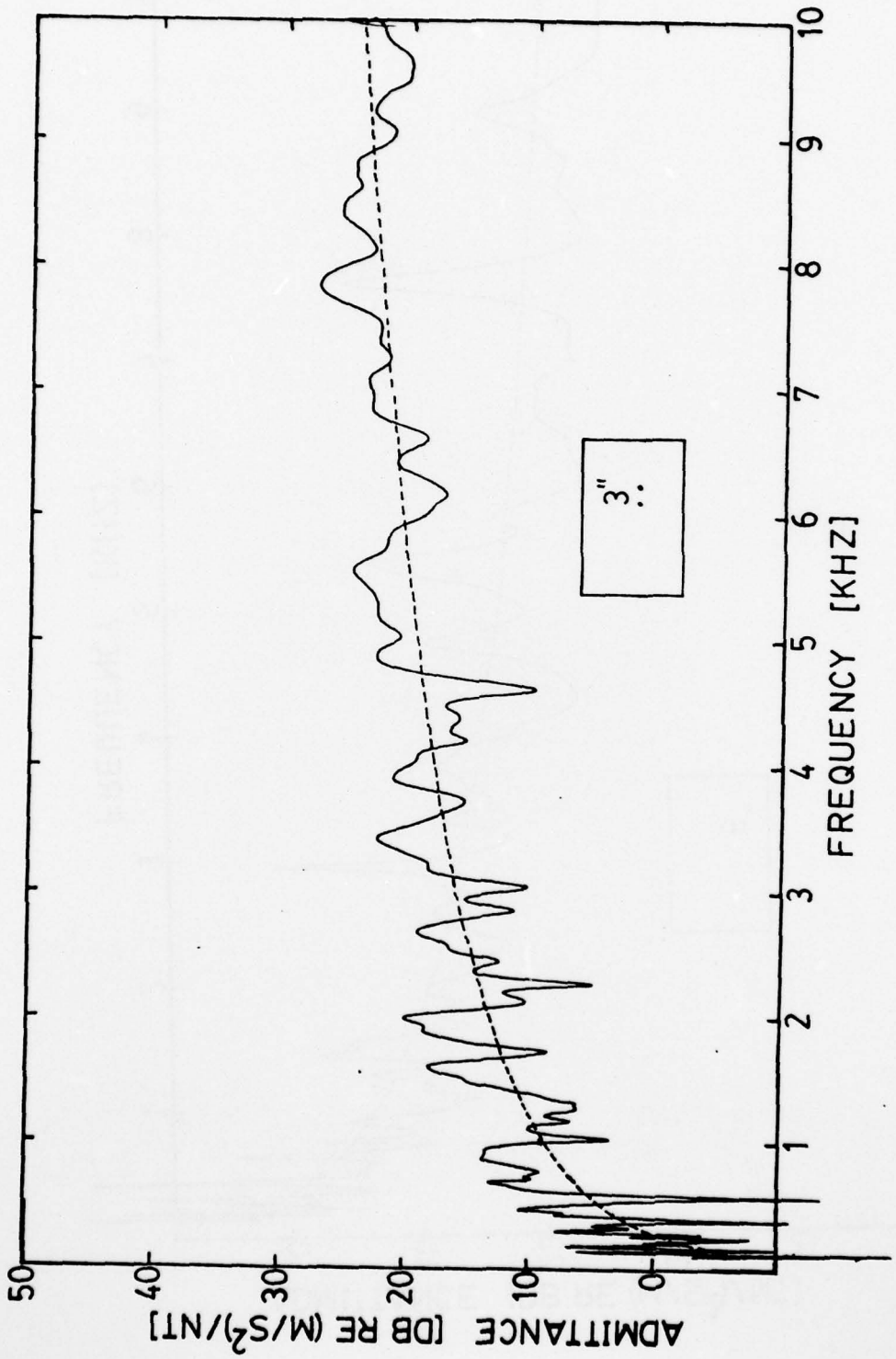

Figure 4.23 Transfer Admittance - Damped Plate

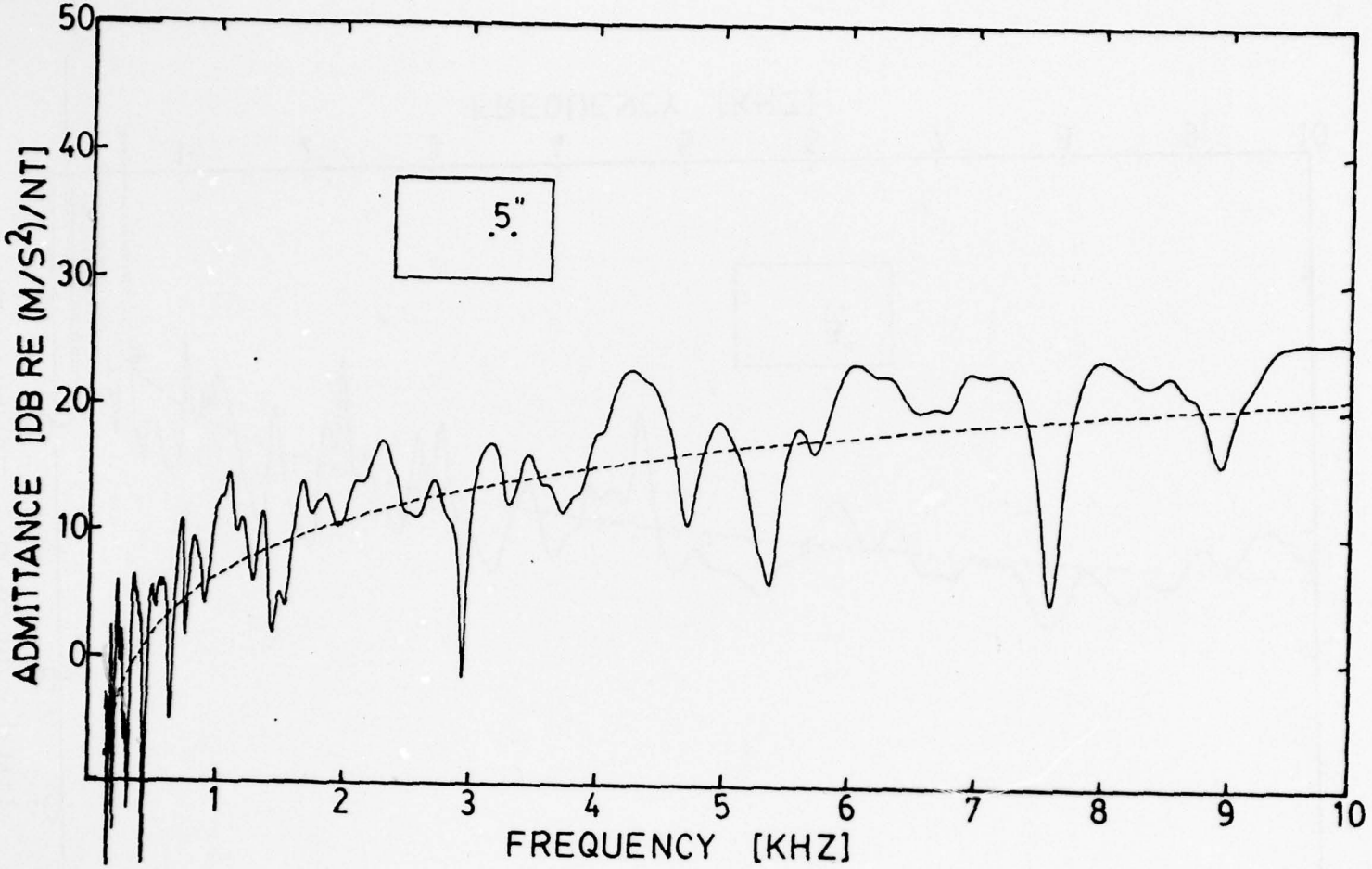

Figure 4.24 Transfer Admittance - Damped Plate

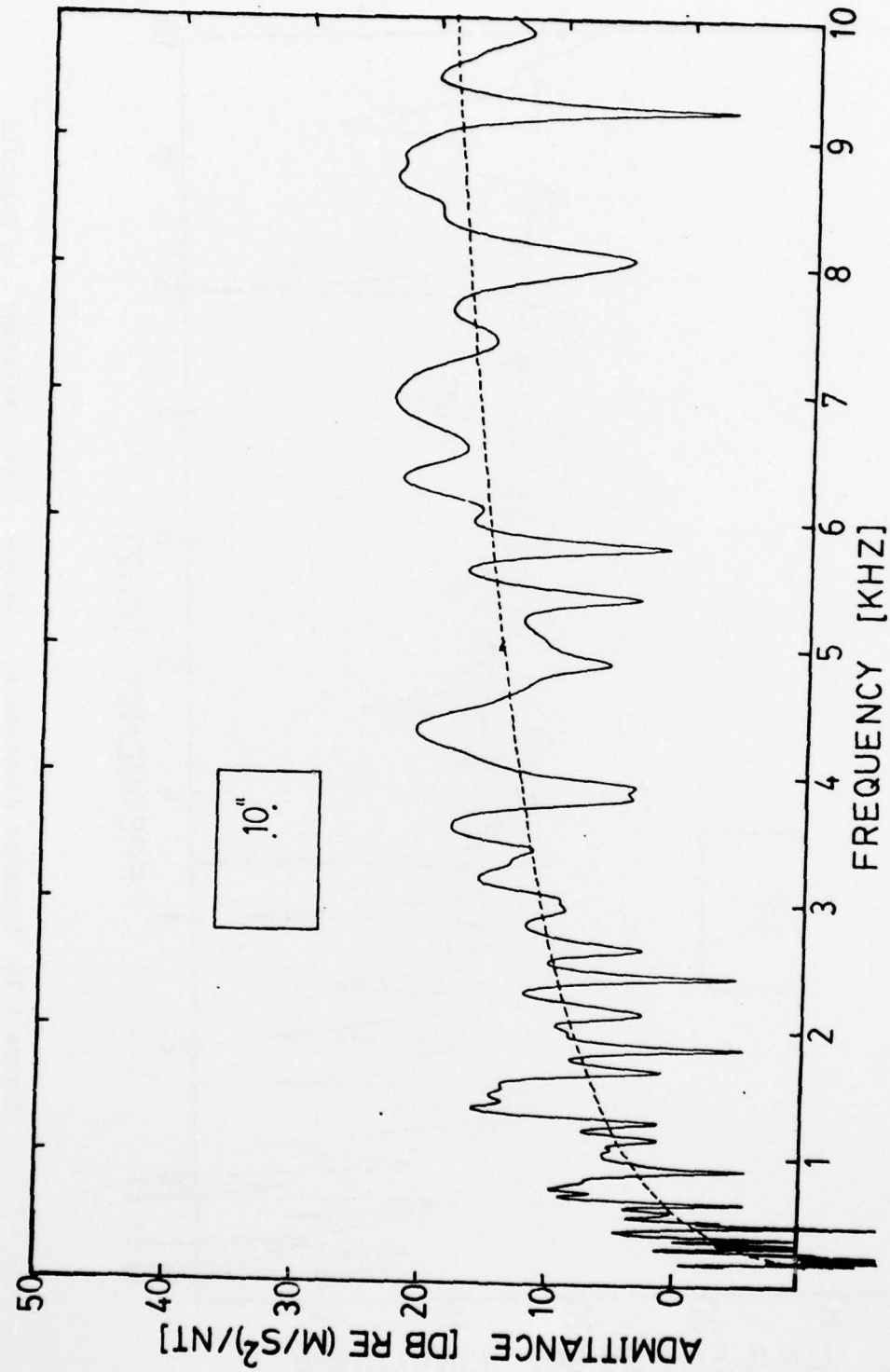

Figure 4.25 Transfer Admittance - Damped Plate

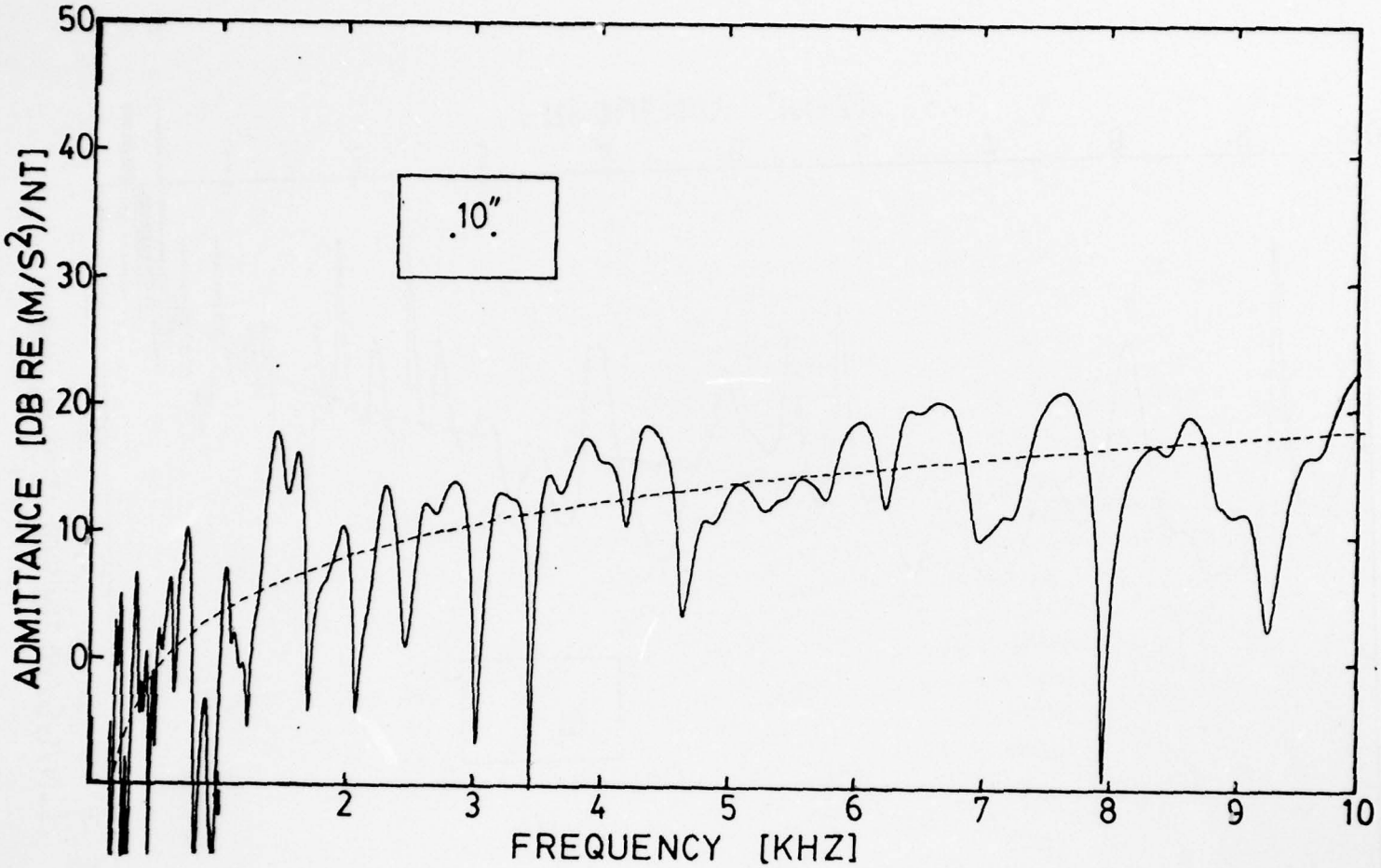

Figure 4.26 Transfer Admittance - Damped Plate, Receiver on Opposite Side of the Driver

AD-A076 185 PENNSYLVANIA STATE UNIV UNIVERSITY PARK APPLIED RESE--ETC F/G 11/6
VIBRATION OF PLATES OF VARIOUS GEOMETRIES.(U)
JUN 79 E G WILLIAMS N00024-79-C-6043
UNCLASSIFIED ARL/PSU/TM-79-130 NL

2 OF 2
AD
AD78185

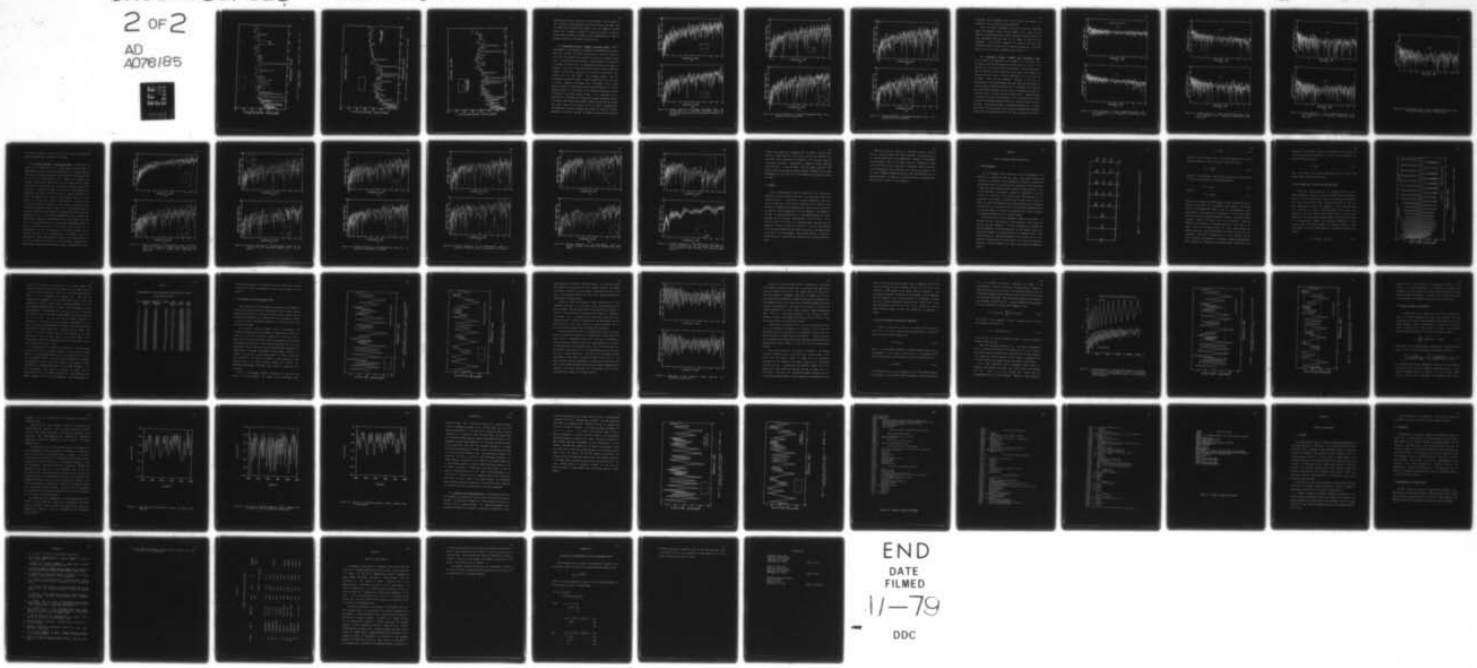

END
DATE
FILMED
11-79
DDC

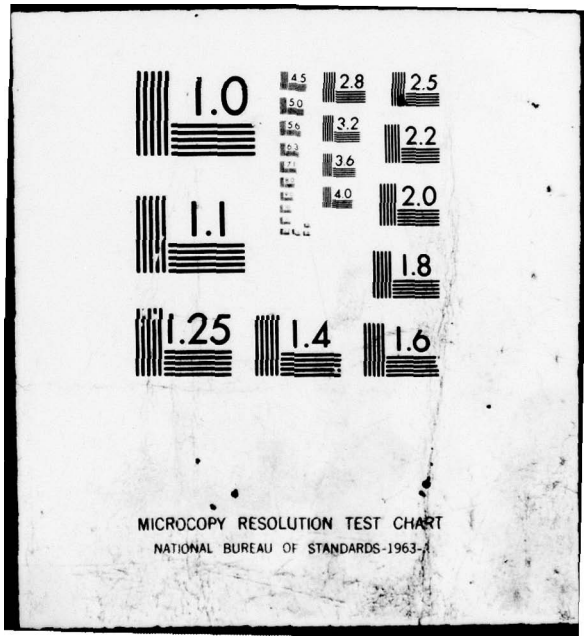
1.0
1.1
1.25
1.4
1.6
1.8
2.0
2.2
2.5
2.8
3.2
3.6
4.0
4.5
5.0
5.6
MICROCOPY RESOLUTION TEST CHART
NATIONAL BUREAU OF STANDARDS-1963-A

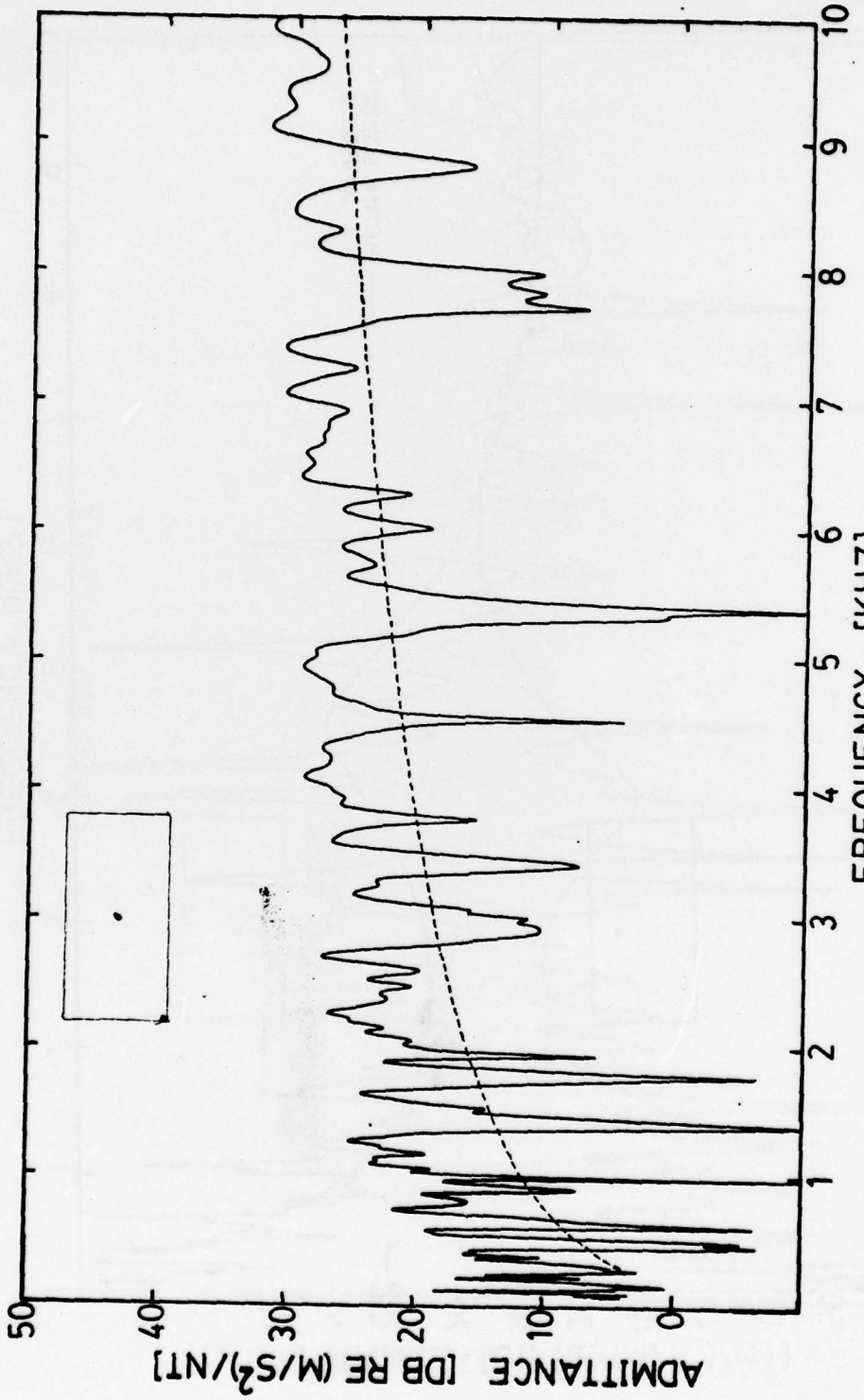

Figure 4.27 Transfer Admittance - Damped Plate, Driver Center and Receiver at Corner

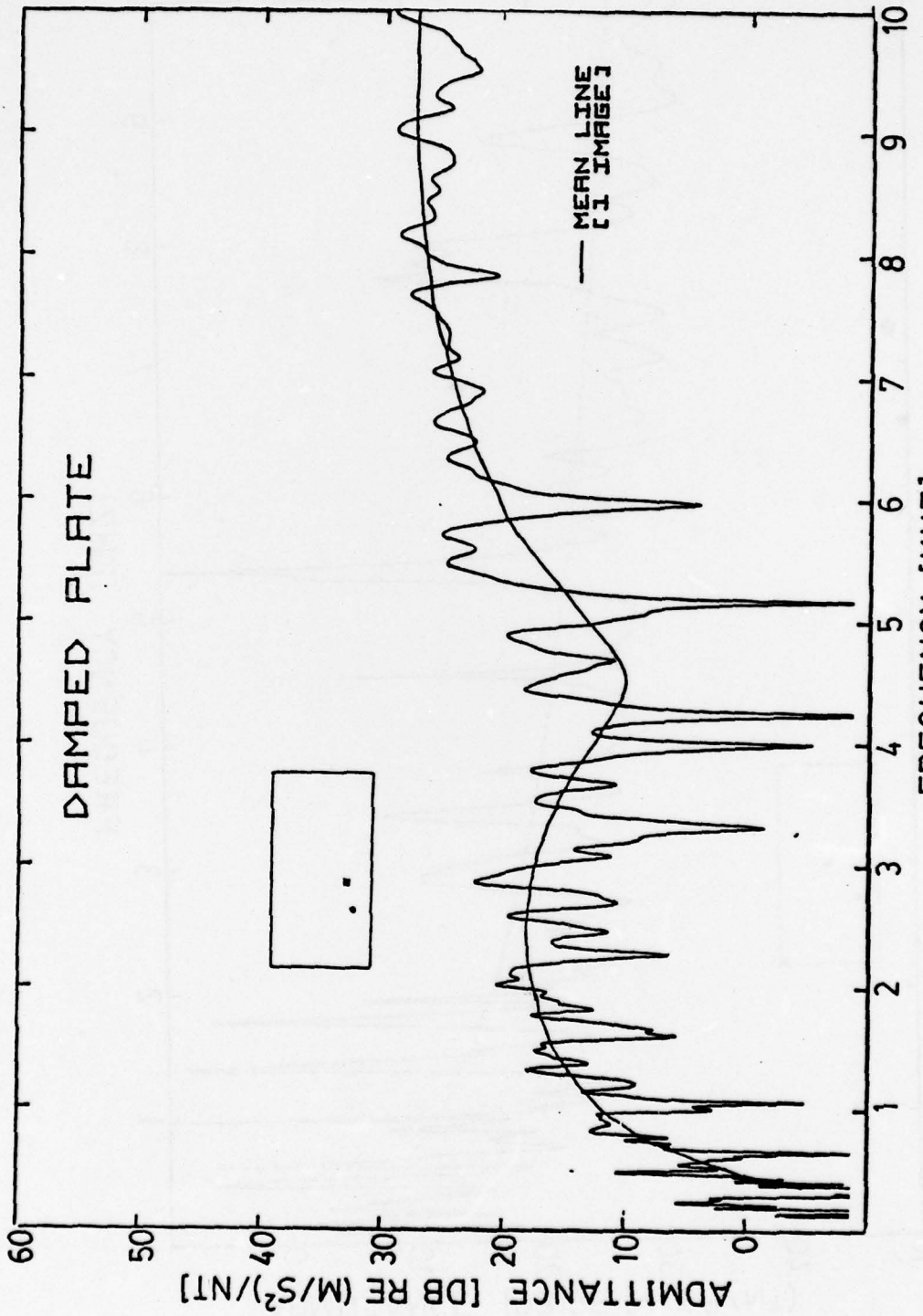

Figure 4.28 Transfer Admittance - Damped Plate, Source 5" from Edge

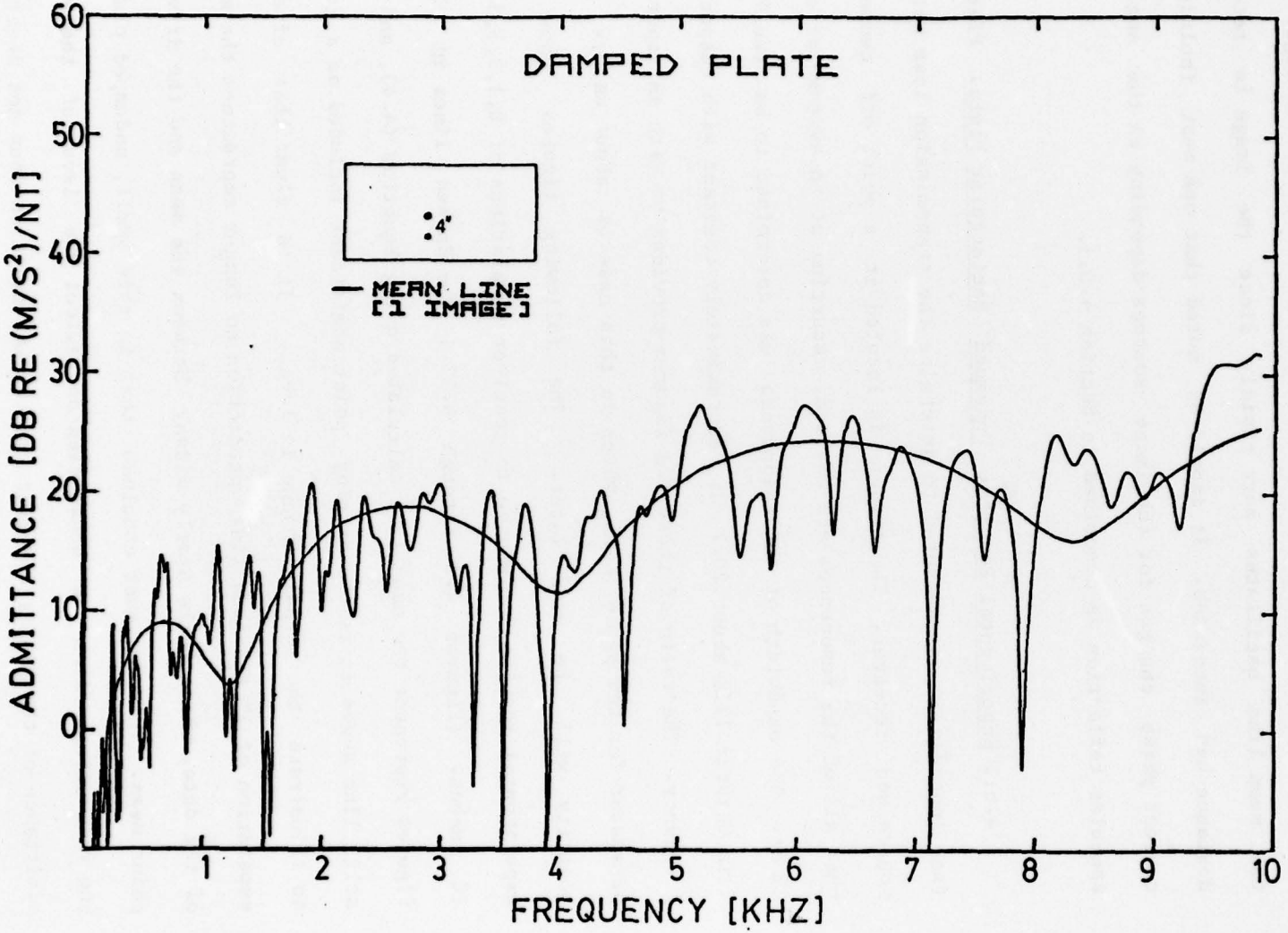

Figure 4.29 Transfer Admittance - Damped Plate, Source 5" from Edge

the latter figure the receiver is 4" from the source and is aligned so that it shares a mutual perpendicular with the source to the edge. Here the mean line oscillates more rapidly since the image to receiver distance has increased. It should be noted that one must include the correct phase changes for the image sources depending on the angle of specular reflection as described in Section 4.5.1.

4.6.2 Experimental Results: Undamped Rectangular Plate. Plate II (see Appendix I) was measured to determine the transmission loss between source and receiver. The driver is located at a point off center so that all of the resonances are excited, occurring at an average of every 23 Hz. The bandwidth of the resonances was determined to be (see Table I in Chapter III) about 20.7 Hz, approximately constant with respect to frequency. The ratio of these two figures provides us with an important parameter for the plate ϵ_v/ω_b which in this case is about unity. This quantity will be used later. The following figures show the experimental results for source to receiver separations of 0,1,2,3,5 and 10 inches. (Figures 4.30 through 4.32.) The dashed lines in these figures represent the mean line calculated using Equation (4.4), and the solid line above it is the driving point admittance included as a guide to illustrate the actual change in level. It is clear that after a separation of 1" the mean line prediction no longer represents the mean of the data, which falls nearly midway between the mean and the driving point mean. Thus, we must conclude that in this small, undamped plate, the reflections from the boundaries do affect the level of the mean admittance of the plate, and that the Hankel function does not describe

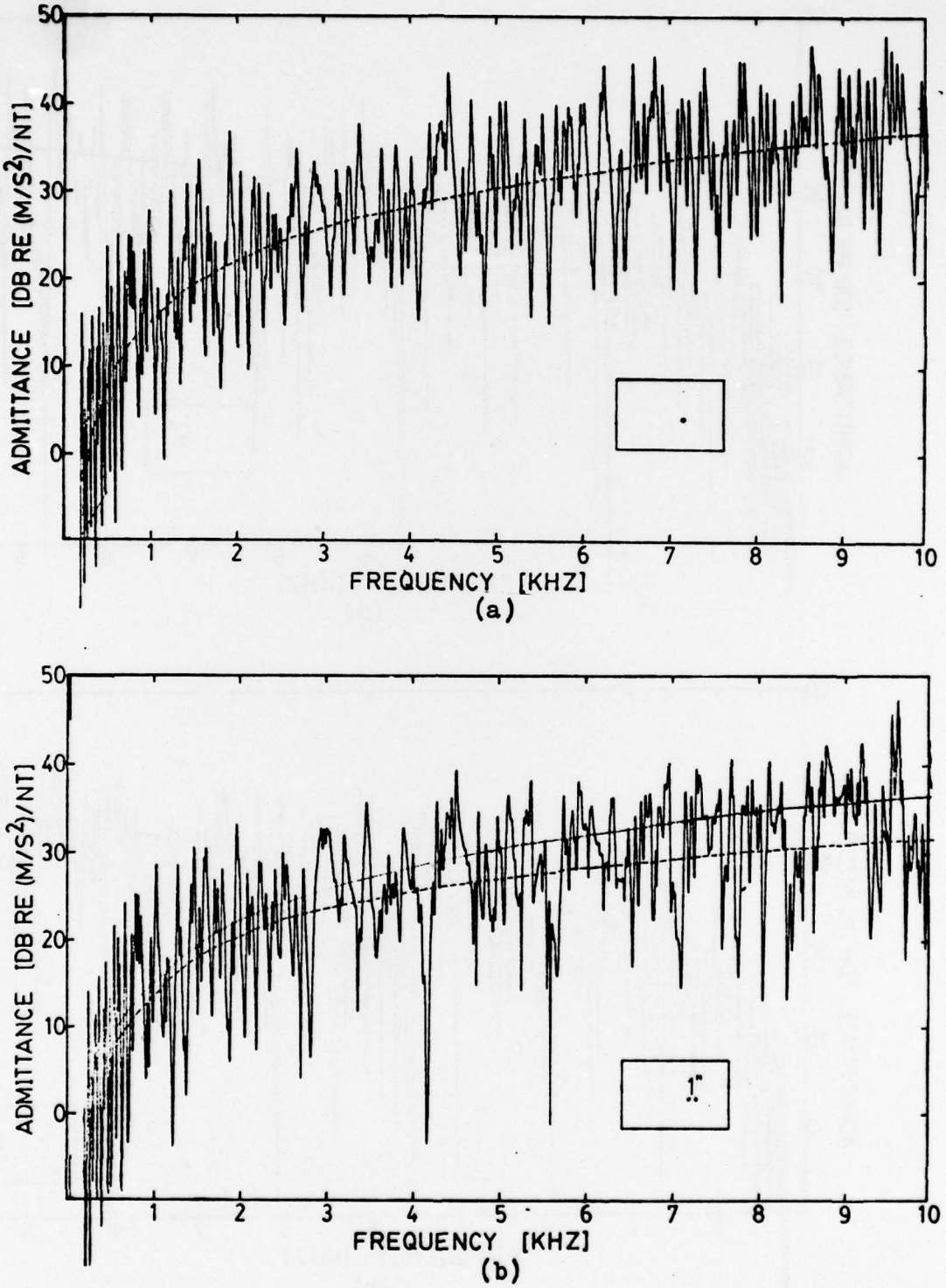

Figure 4.30 Transfer Admittance of Undamped Rectangular Plate: (a) Driving Point; (b) 1" Separation (The dashed line is the mean and the line above is the driving point admittance for reference.)

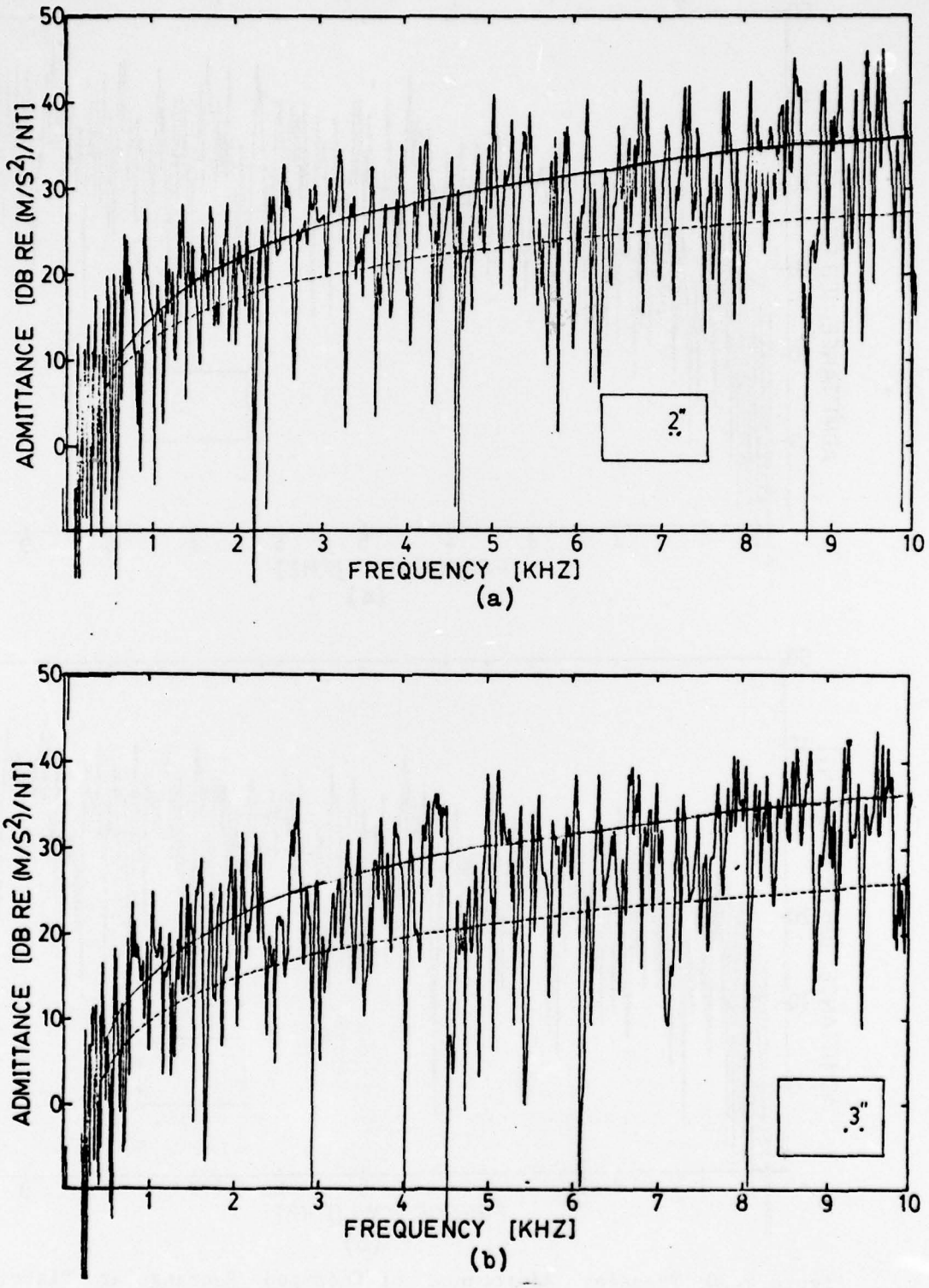

Figure 4.31 Transfer Admittance of Undamped Rectangular Plate: (a) 2" Separation; (b) 3" Separation

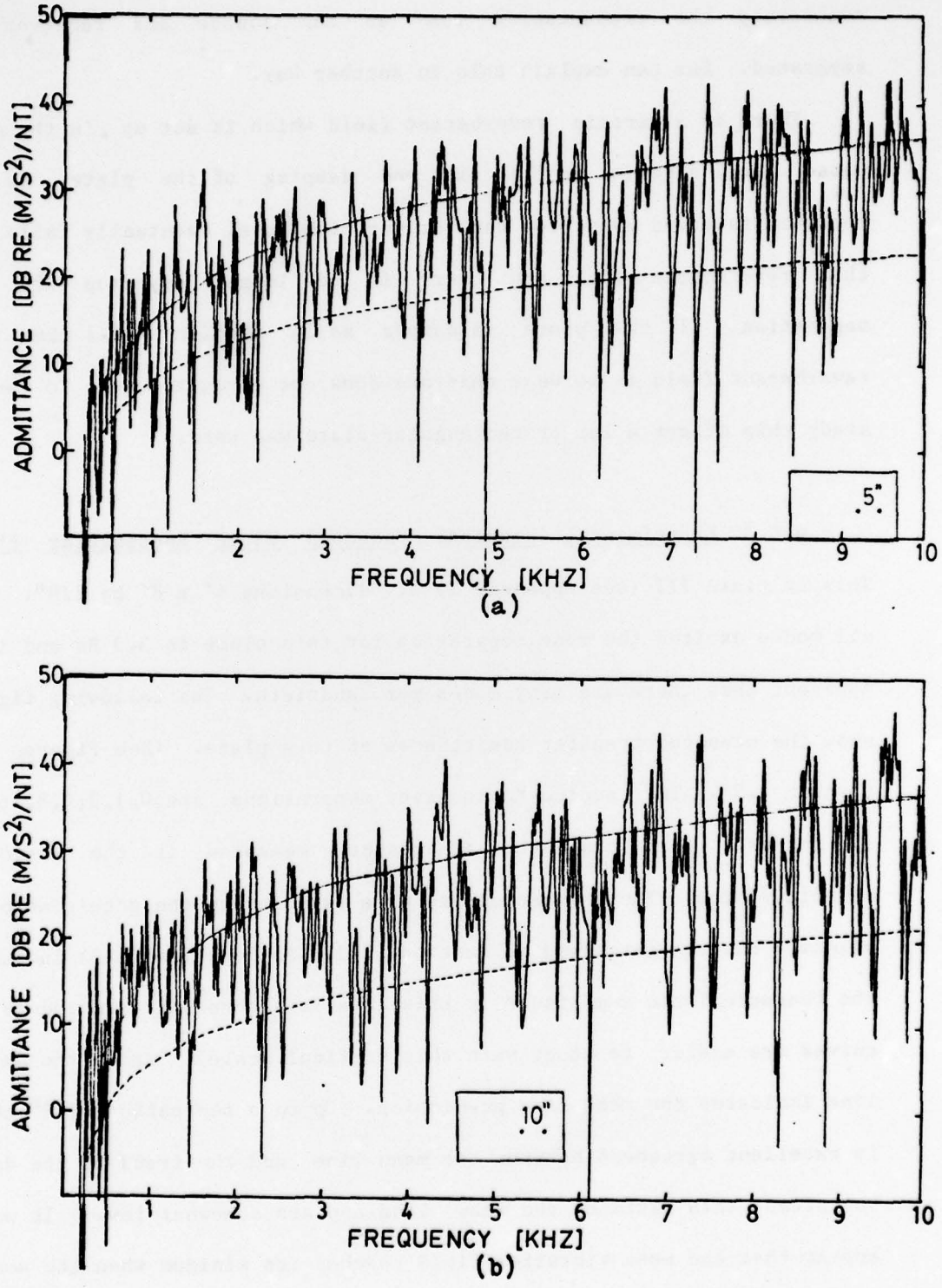

Figure 4.32 Transfer Admittance of Undamped Rectangular Plate: (a) 5" Separation; (b) 10" Separation

accurately the transmission loss as the source and receiver are separated. One can explain this in another way.

There is a certain reverberant field which is set up in the plate whose level depends on the size and damping of the plate. As the receiver is moved away from the driver, its level eventually falls into this reverberant field and there is no longer any drop off with separation. If the plate is damped as in Section 4.6.1 then this reverberant field is so weak that one does not encounter it. To further study this effect a larger rectangular plate was used.

4.6.3 Experimental Results: Undamped Large Rectangular Plate. This is plate III (see Appendix I) of dimensions 4′ x 8′ by 1/8". With all modes excited the mode separation for this plate is 3.3 Hz and it is apparent that there are many modes per bandwidth. The following figures show the measured transfer admittances of this plate. (See Figures 4.33 through 4.36.) The source to receiver separations are 0,1,2,4,8,16 and 32 inches. Note that the admittance measured is the ratio of velocity/force. These measurements were taken using the acceleration to velocity convert described in Section 2.3. As Equation (4.3) indicates the characteristic admittance in this case is a constant, and indeed the curves are easier to study with this vertical scale. Again the dashed line indicates the mean line prediction. Up to a separation of 8" there is excellent agreement between the mean line and the trend of the data, but after this distance the mean line appears somewhat low. It would appear that the mean vibration field reaches its minimum when the source and receiver are separated beyond 8", and after this there is little if

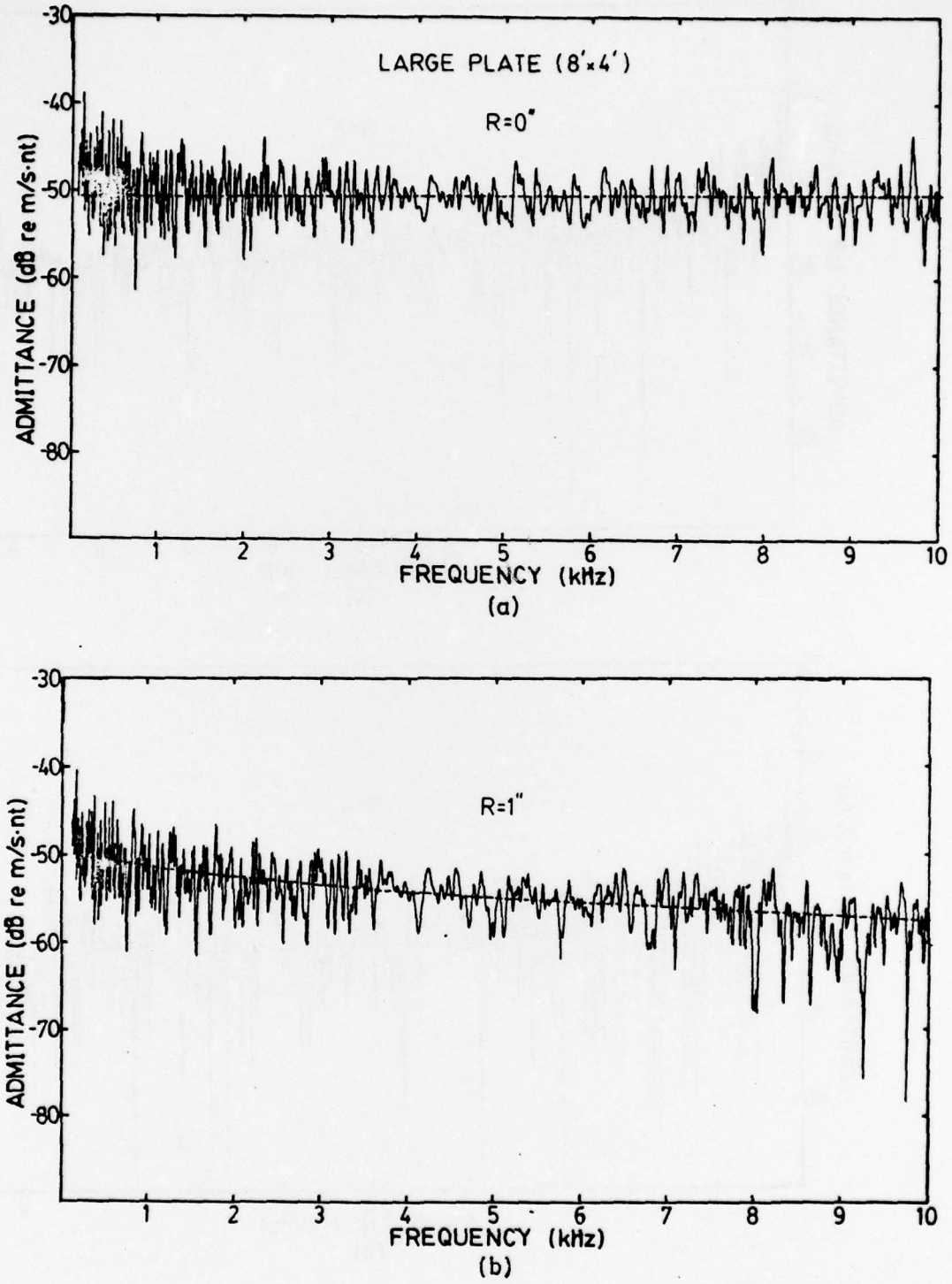

Figure 4.33 Transfer Admittance of Large Undamped Rectangular Plate: (a) Driving Point; (b) 1" Separation (Dashed curve is the mean line.)

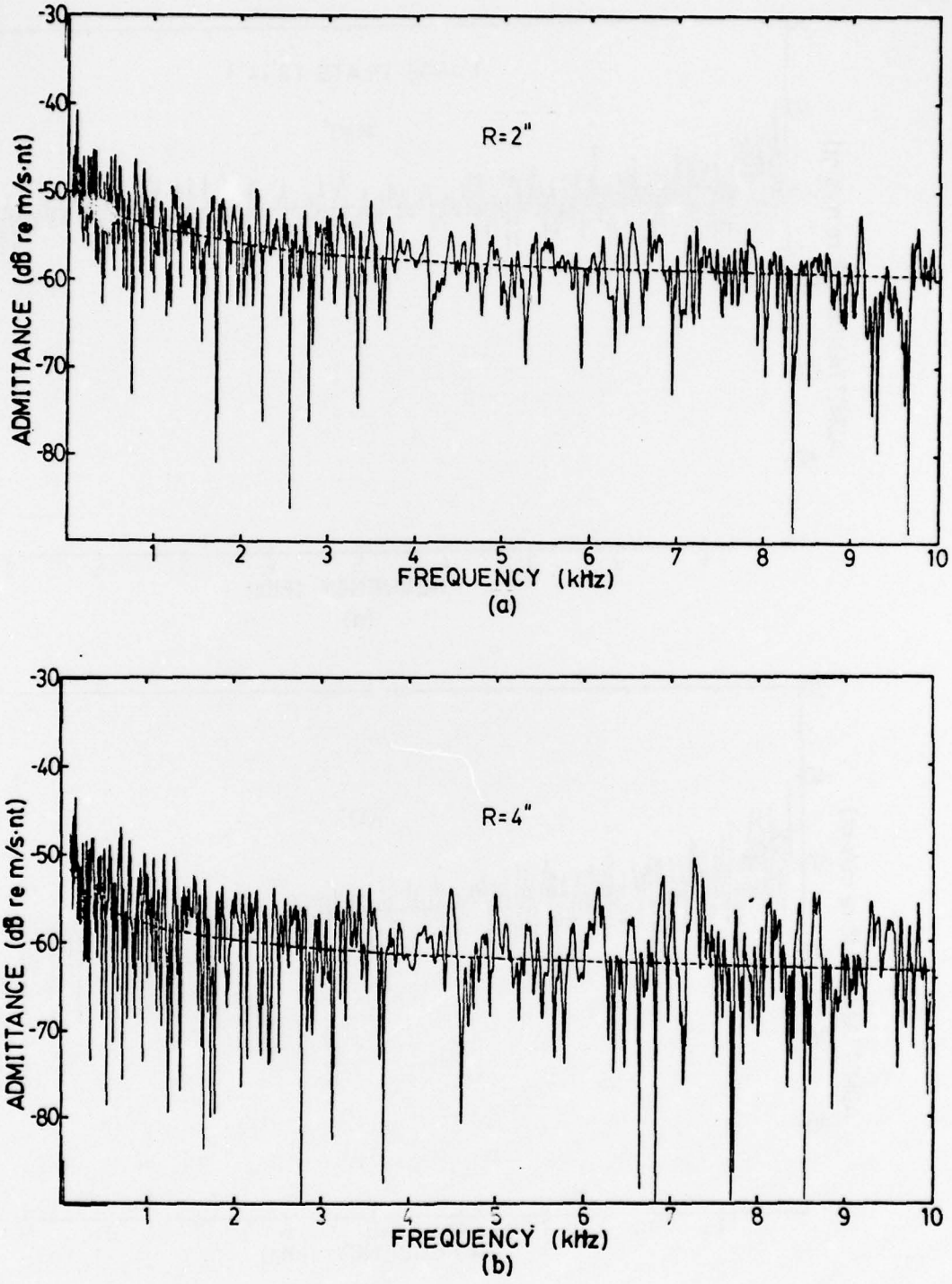

Figure 4.34 Transfer Admittance of Large Undamped Rectangular Plate: (a) 2" Separation; (b) 4" Separation (Dashed curve is the mean line.)

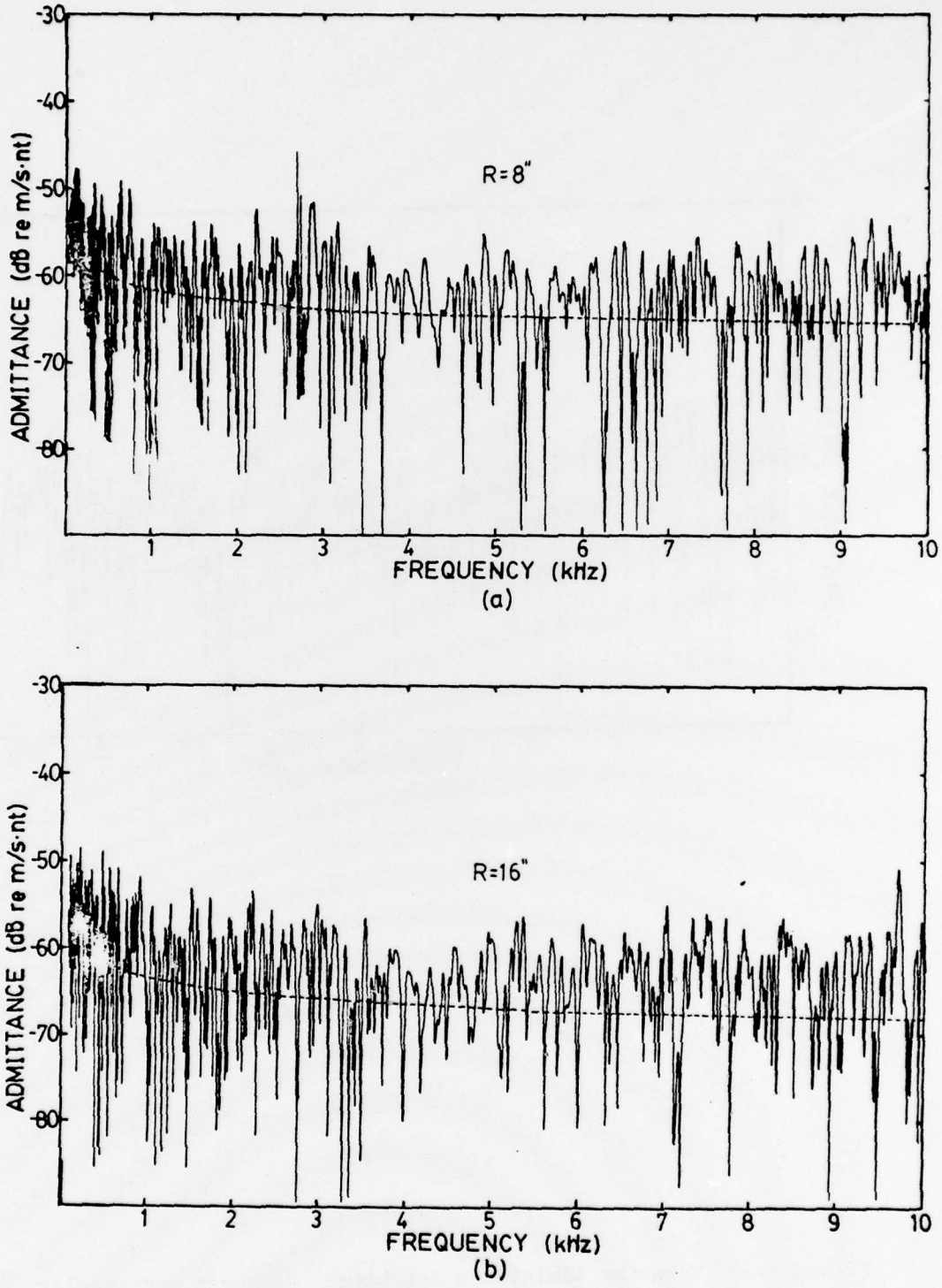

Figure 4.35 Transfer Admittance of Large Undamped Rectangular Plate: (a) 8" Separation; (b) 16" Separation (Dashed curve is the mean line.)

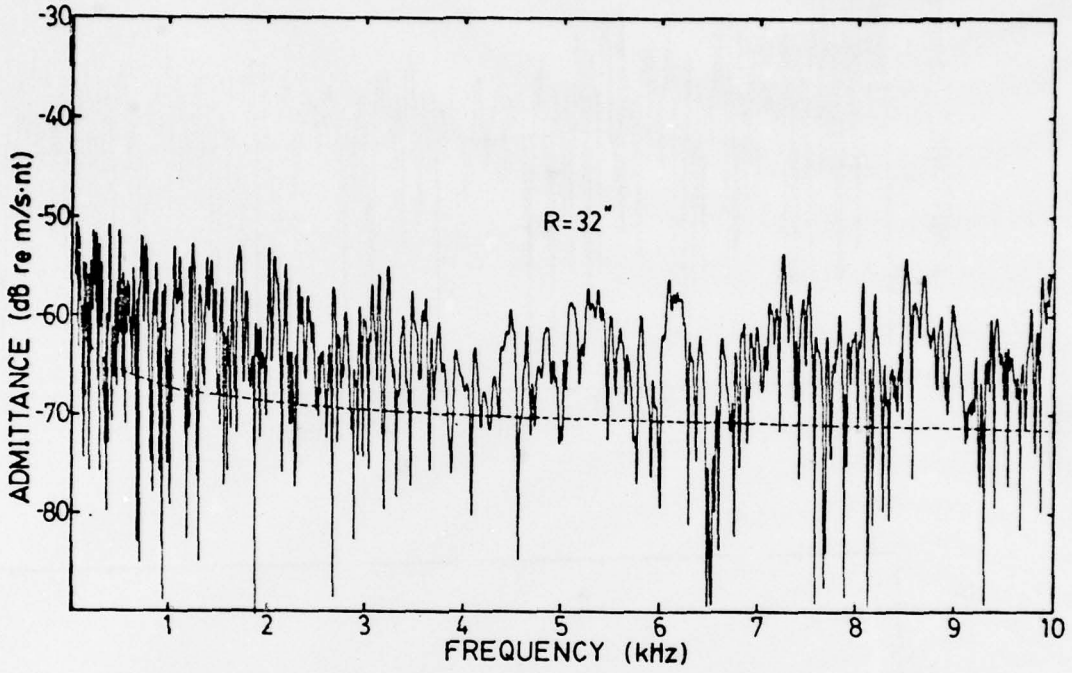

Figure 4.36 Transfer Admittance of Large Undamped Rectangular Plate, 32" Separation (Dashed curve is the mean line.)

any further decrease in the mean of the data. Thus the reverberant field is reached after a separation of 8 inches.

4.6.4 Transfer Admittance: Quadrilateral Plate. The area of this plate is 14.7 square feet or 1.4 square meters and its shape is indicated in the inserts in the following figures. It is about one half of the area of the large rectangular plate described in the last section but is of the same thickness (1/8"). Figures 4.37 through 4.42 represent driving point admittances for this plate with the driver placed at the center of mass and the receiver at various positions on the plate. By reference to Figure 4.37 one can see that the mean line prediction is already a bit low for a source to receiver separation of 8 inches. At separations of 16 and 26 inches (Figure 4.38) it is below most of the recorded data. Figure 4.40 indicates the increase in mean level when the receiver is placed on a free boundary, and parts (a) and (b) show a difference in levels of about 8 dB. It would appear that the distortion field near the free edge is increasing the level as with the rectangular plate. As the receiver approaches the sharp corner of the quadrilateral, however, an interesting effect is seen. (Figures 4.41 and 4.42.) A large undulation occurs in the transfer admittance, especially when the receiver is placed in the corner, in which case it is surprising to note that the admittance of the plate around 8 kHz is actually less than at the low frequencies. This effect is only so pronounced in a sharp corner and does not occur in the other corners of the plate. (Figures 4.40 and 4.41.) No other frequency response curves measured have demonstrated this type of effect. Figure 4.42 (b) is a

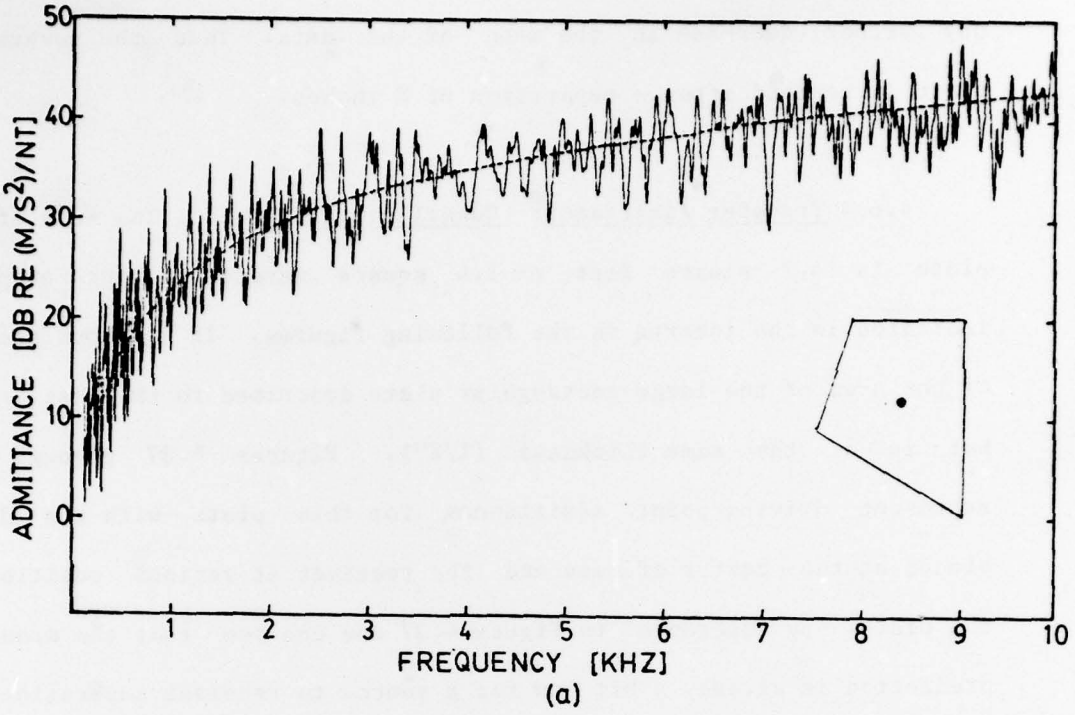

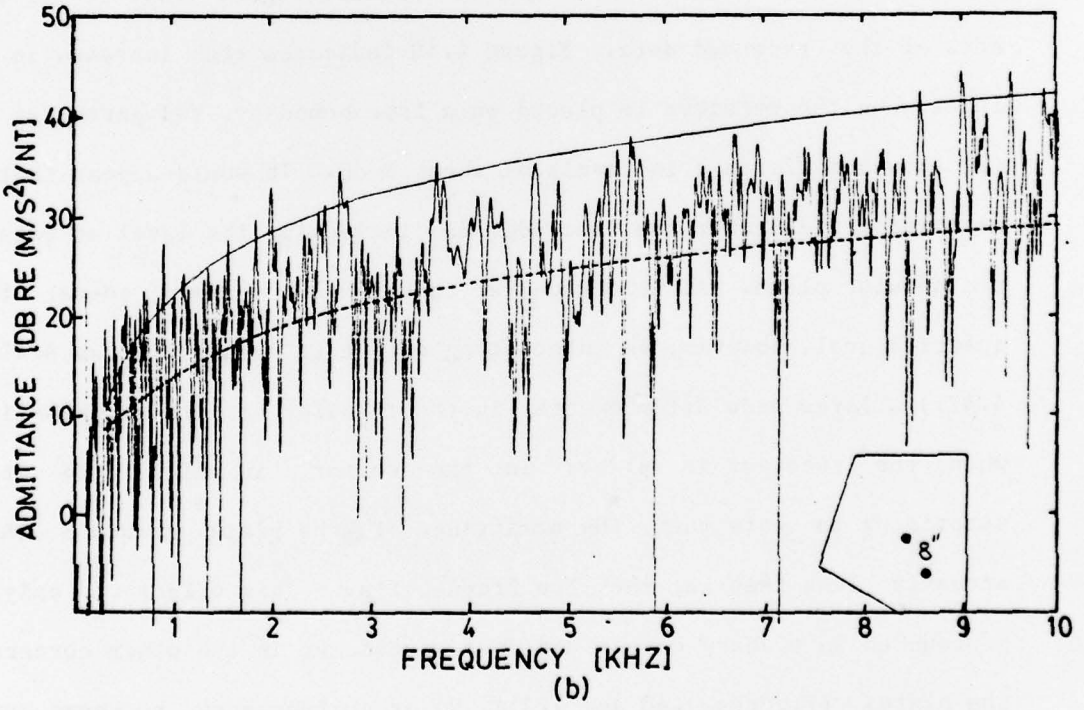

Figure 4.37 Transfer Admittance of the Quadrilateral plate: (a) Driving Point; (b) 8" Separation (Dashed curve is mean line and solid curve above is driving point admittance for reference.)

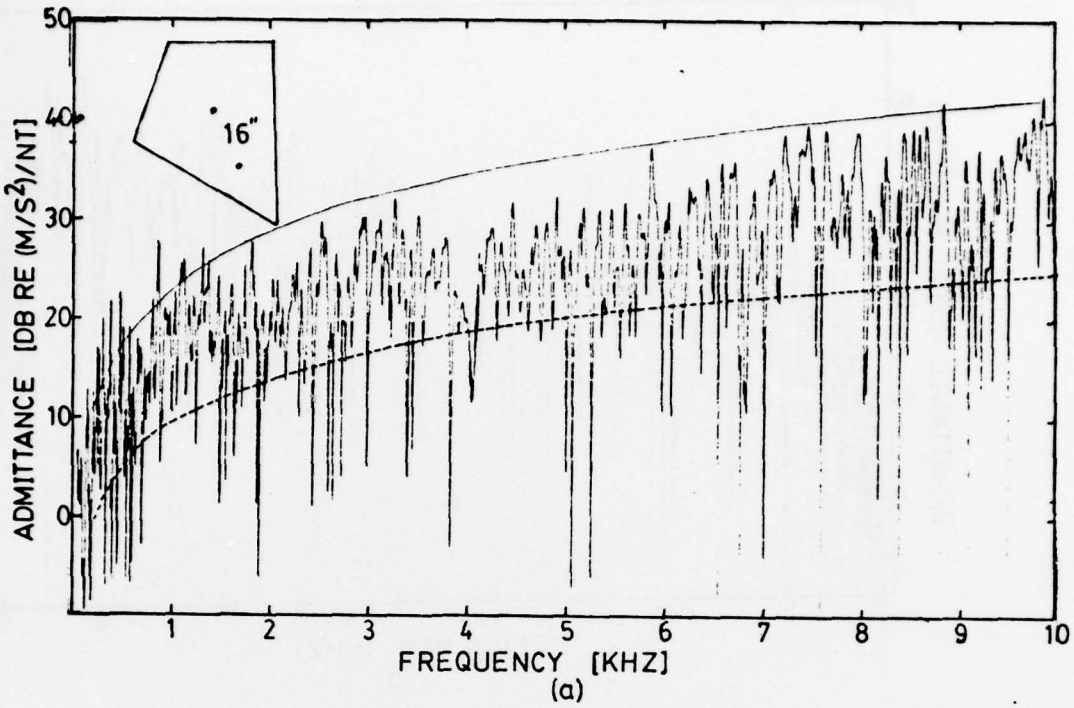

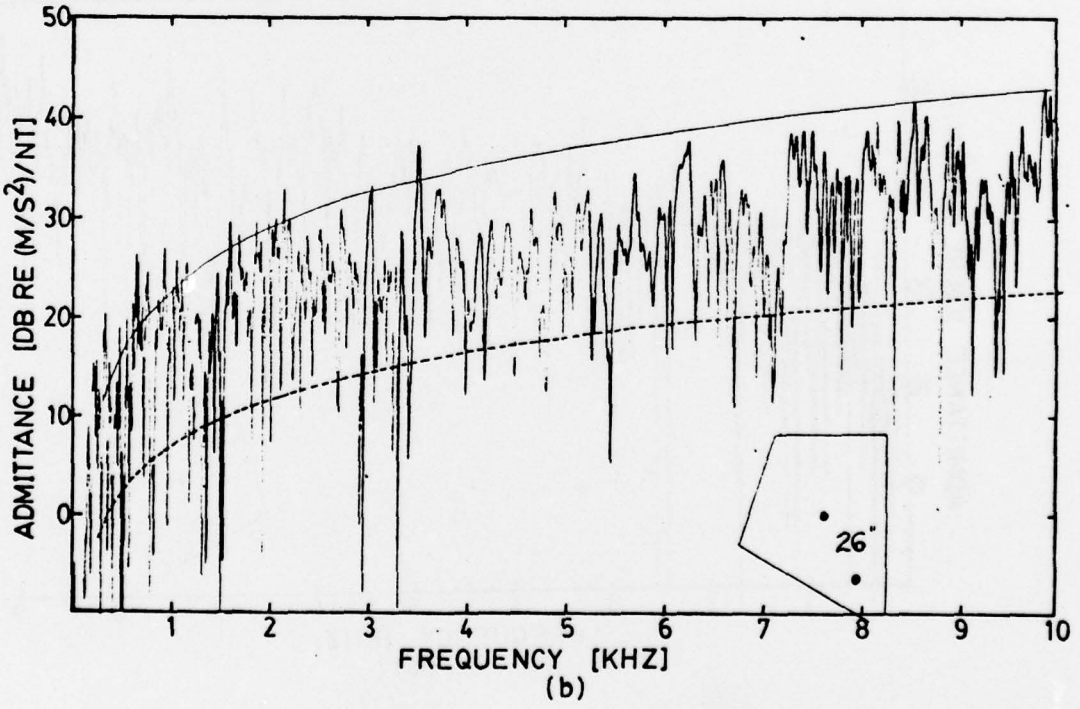

Figure 4.38 Transfer Admittance of the Quadrilateral Plate: (a) 16" Separation; (b) 26" Separation (Dashed curve is the mean line.)

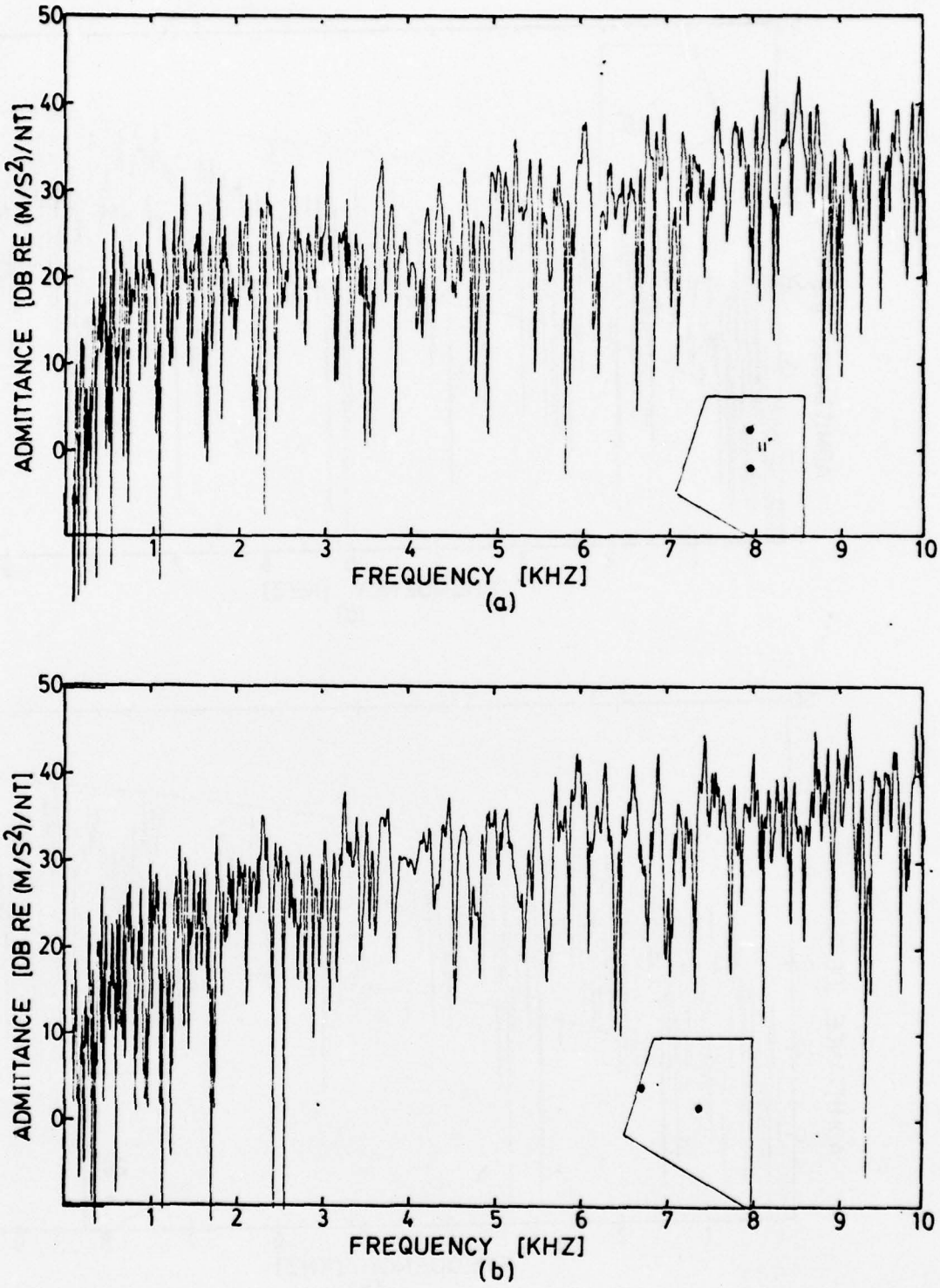

Figure 4.39 Transfer Admittance of the Quadrilateral Plate: (a) 11" Separation; (b) Receiver at an Edge

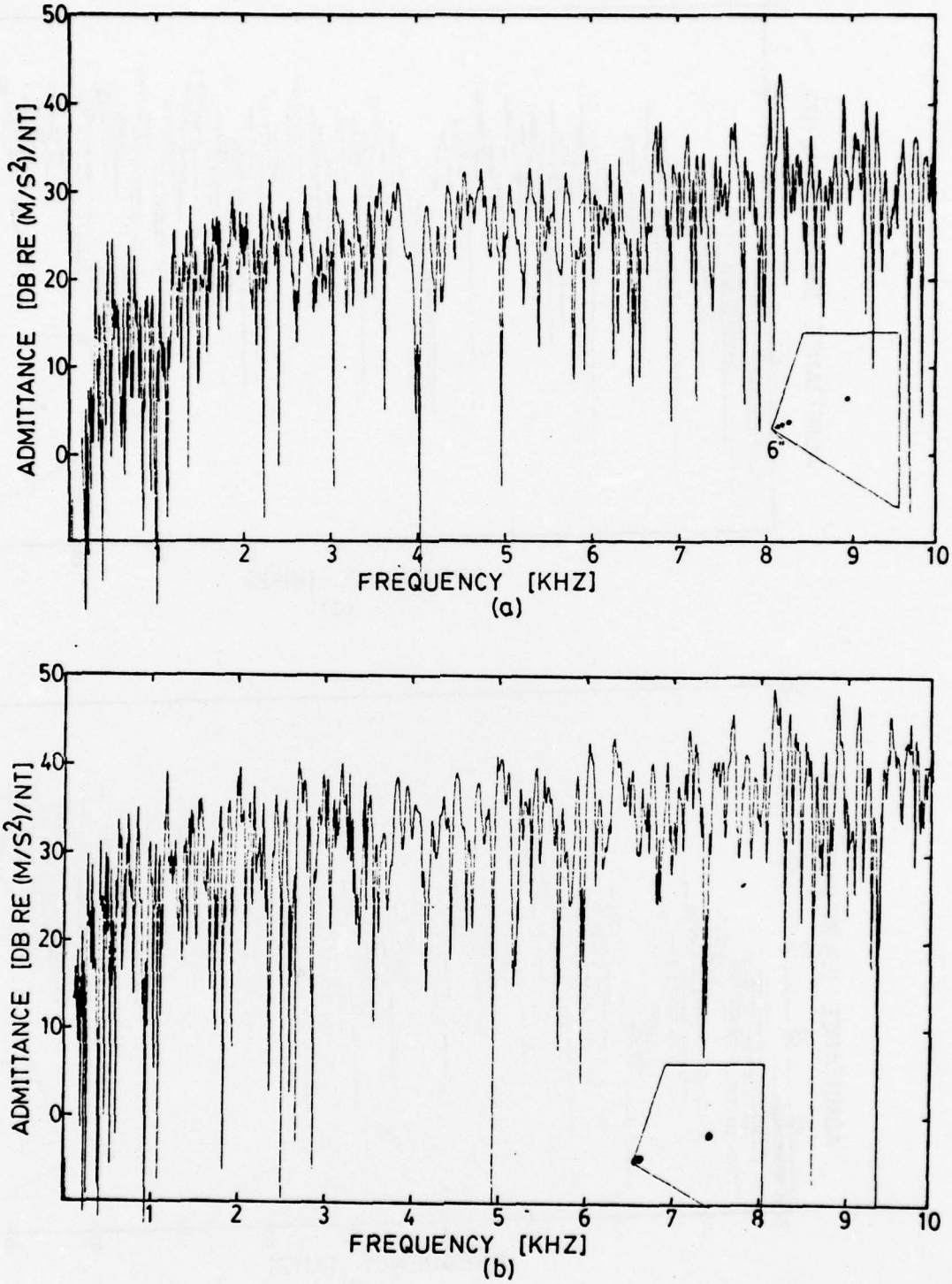

Figure 4.40 Transfer Admittance of the Quadrilateral Plate: (a) Receiver 6" from Left Corner; (b) Receiver at Left Corner

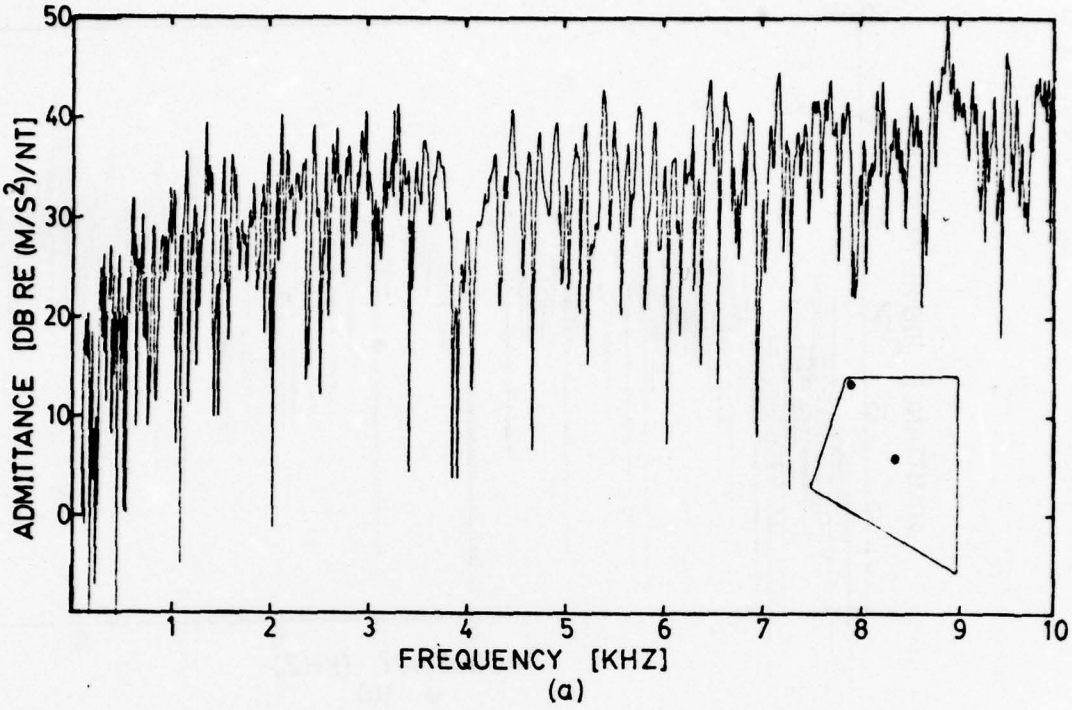

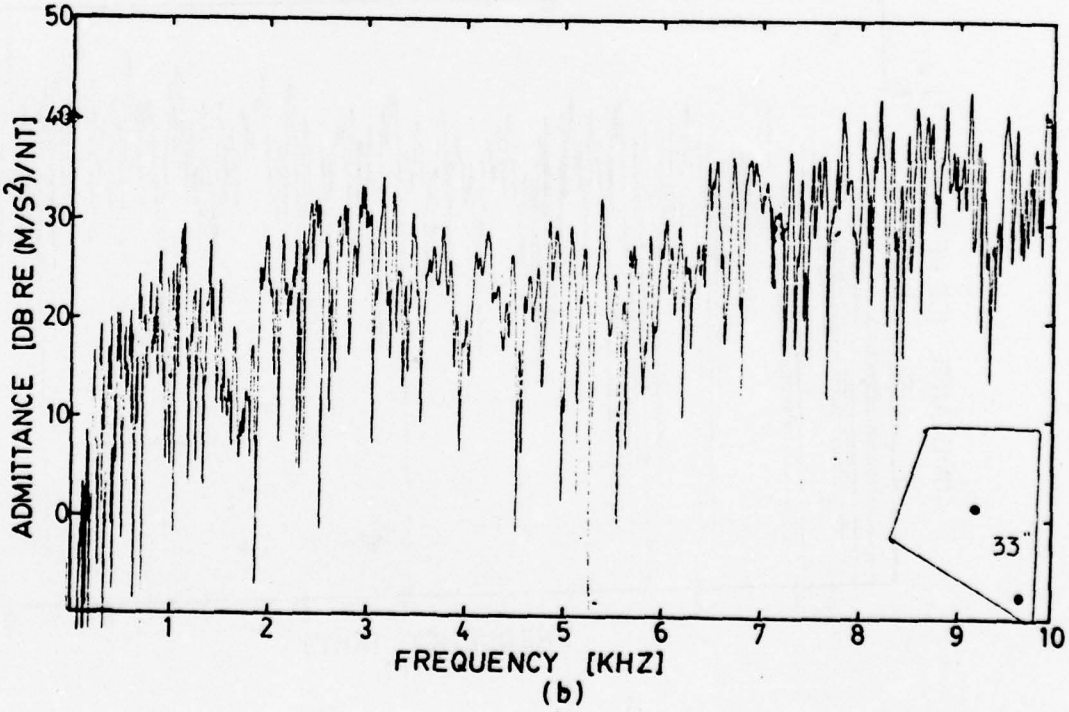

Figure 4.41 Transfer Admittance of the Quadrilateral Plate: (a) Receiver in Upper Left Corner; (b) Receiver near Sharp Corner

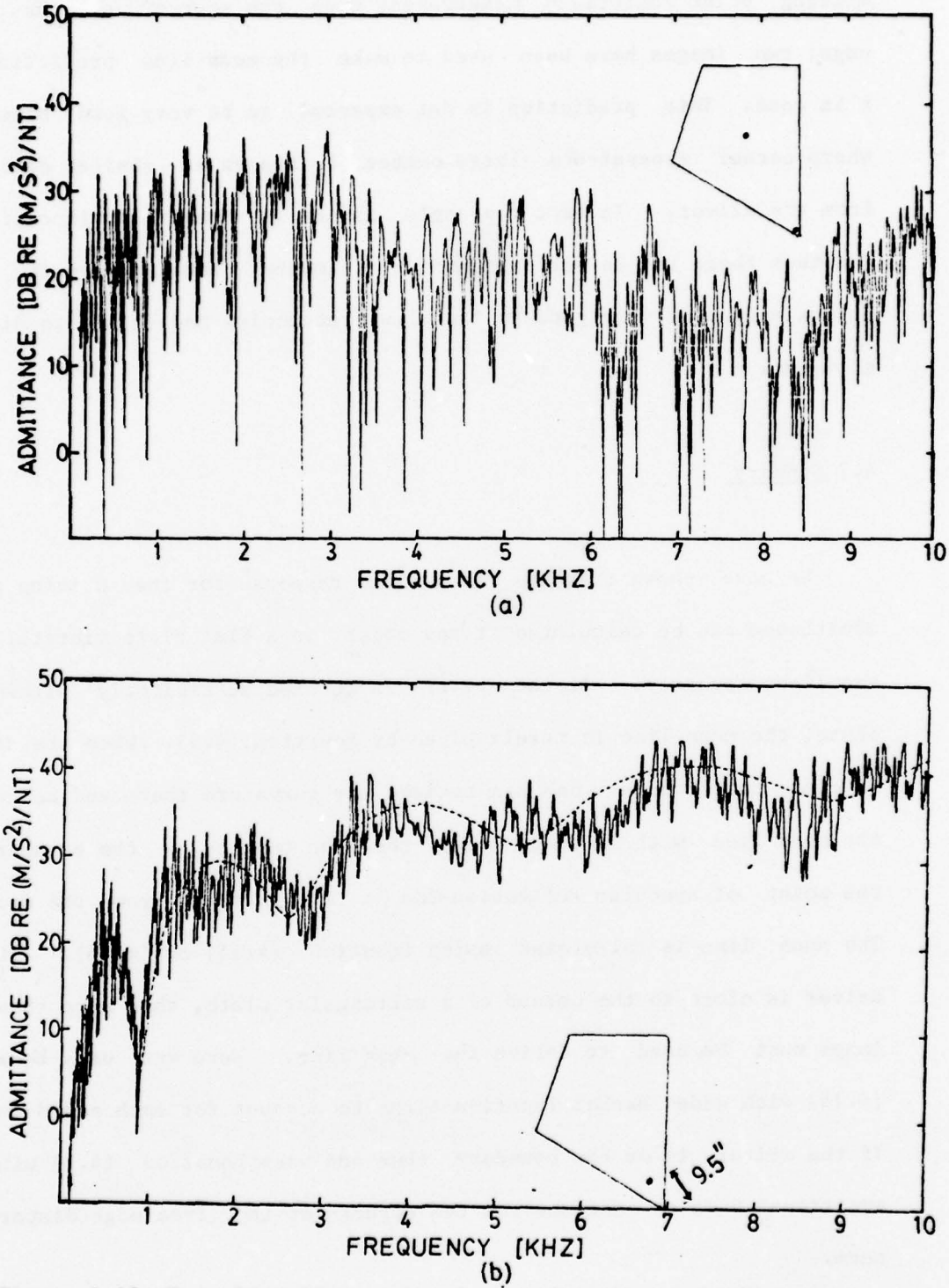

Figure 4.42 Transfer Admittance of the Quadrilateral Plate with (a) Receiver in Sharp Corner, and (b) Driving Point Admittance 9.5" from Sharp Corner with Mean Line Using Two Image Sources

driving point admittance measurement with the source near the sharp edge; two images have been used to make the mean line prediction for this case. This prediction is not expected to be very good since the sharp corner generates a large number of images at similar distances from the driver. In fact the angle is not an integer divisor of 180^{o} and thus there are an infinite number of images. However, the two image approximation is very good at the low frequencies and begins to diverge at 4 kHz.

4.7 Summary

We have shown that the mean line response for the driving point admittance can be calculated at any point in a flat plate vibrator with excellent accuracy. If the driver is located sufficiently within the plate, the mean line is merely given by Equation (4.3). When the driver is close to a boundary one can neglect any curvature there and calculate the mean line with an image about the line tangent to the boundary at the point of specular reflection for a ray generated from the driver. The mean line is calculated using Equation (4.15) or (4.16). If the driver is close to the corner of a rectangular plate, then more than one image must be used to derive the mean line. Here one uses Equation (4.15) with added Hankel function terms to account for each added image. If the driver is on the boundary then one uses Equation (4.3) with an additional 6 dB to account for the effects of the free edge distortion term.

When the source and receiver are separated we can use Equation (4.4) to predict the mean line trend of the data (velocity/force) and the technique works well for the damped plate. However, in the undamped small rectangular plate we have shown that this technique no longer works and that the data is limited by a reverberant field in the plate that is measurable at small separations of the source and receiver. For the larger undamped rectangular plate the mean line works well out to farther distances, but again the reverberant field is encountered and the mean line no longer is a good predictor.

CHAPTER V

LEVEL OF VARIATION ABOUT THE MEAN LINE

5.1 Mode Parameters

In the following we will make use of the mode parameters (see Reference 4, Chapter IX) for the plate. This system defines the vibrator as an electric circuit consisting of parallel branches each representing a mode of the plate and each containing a mass (mode mass), a compliance (mode compliance) and a resistance (mode resistance). This circuit description is described in detail in Reference 5. We will confine our attention to the driving point admittance and to the prediction of the levels of variation about the mean line for this case. Figure 5.1 shows this canonical circuit representation and is reproduced from Reference 5. The accuracy of the circuit method is demonstrated in the mode sum program in Section 5.5, which uses the circuit to predict the frequency response curve for a plate vibrator.

Each branch of this circuit represents a mode of the vibrator. At resonance the mass and compliance of that particular branch cancel and the mode resistance dominates. If these resonances are separated by several bandwidths, the mode resistances for the resonant branch will determine the height of the resonant peak in the admittance curve. Thus $Y_\nu = 1/R_\nu$ where R_ν is the mode resistance of the ν'th mode and Y_ν is the admittance (velocity/force) for this mode of the plate at the resonance frequency. R_ν can be related to the loss in the plate by the important relation

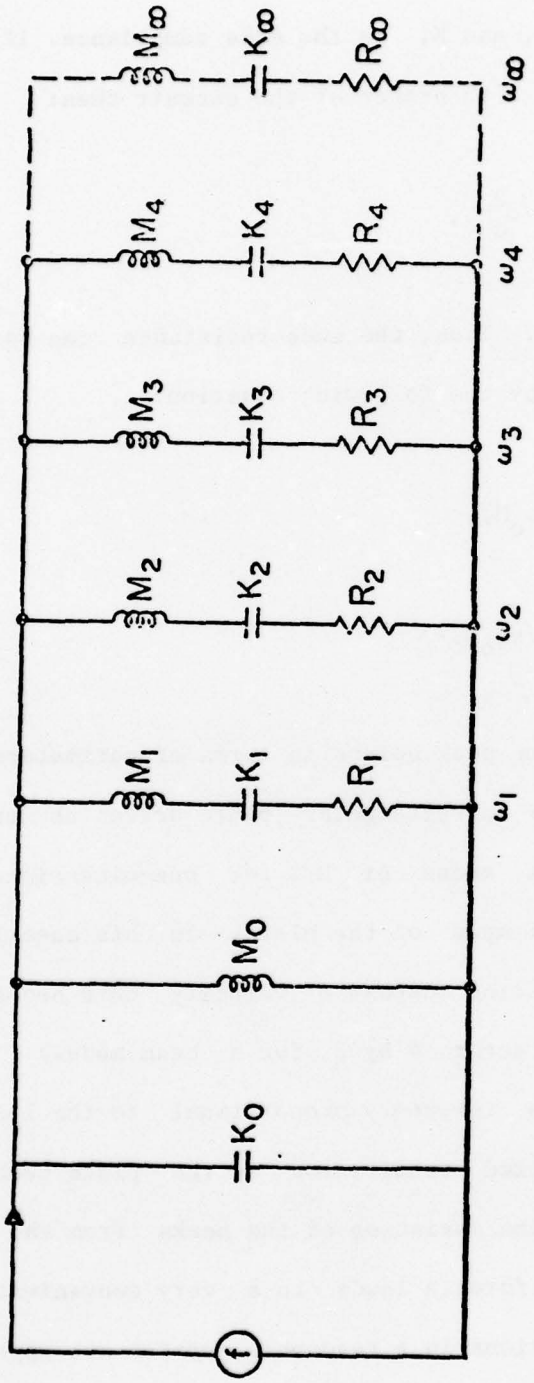

Figure 5.1 Cannonical Circuit Representation for a Vibrating System

$$\eta = \omega K_\nu R_\nu, \tag{5.1}$$

where η is the loss factor, and K_ν is the mode compliance. If ω_o is the resonance frequency of the ν'th branch of the circuit then:

$$K_\nu = 1/\omega_o^2 M_\nu, \tag{5.2}$$

where M_ν is the mode mass. Thus, the mode resistance can be expressed in terms of the mode mass by the following equation:

$$R_\nu = \eta \omega_o M_\nu, \tag{5.3}$$

and thus:

$$Y_\nu = 1/\eta \omega_o M_\nu. \tag{5.4}$$

Equation (5.4) expresses the peak height in terms of parameters that are known for the system. For a rectangular plate driven at the center, $M_\nu = M/4$ for two-dimensional modes or $M/2$ for one-dimensional (beam) modes, where M is the total mass of the plate. In this case $Y = 4/\eta \omega_o M$ and if we measure acceleration instead of velocity this becomes merely $Y_a = 4j/\eta M$. (Replace the factor 4 by 2 for a beam mode.) Thus, the height of the resonance is inversely proportional to the loss in the plate. This is the expected result, for as the plate becomes more damped we have seen that the deviation of the peaks from the mean line is reduced. This latter formula leads to a very convenient rule of thumb: The peak accelerations in a resonance system are approximately given by FxQ/M. The dynamic mass is reduced by the quality factor Q of

the system. Since we have found that the bandwidth of the resonances of plates on foam is nearly constant, it is better to write Equation (5.4) using the relation $\omega_b = \eta\omega_o$ as:

$$Y = 1/\omega_b M \ . \tag{5.5}$$

Thus, if we measure the velocity admittance of the plate the peak heights should also be nearly constant.

5.2 Peak Heights for a Center Driven Circular Plate

In this case the mode masses are not constant as with the center driven rectangular plate but are given by $M_\nu = 2M/\nu\pi^2$ (see Reference 4, page 272). The following figure, Figure 5.2, represents the admittance of a center driven circular plate (velocity/force) with its mean line from a measurement on plate VI (see Appendix I). Only a one dimensional set of resonances is excited representing modes with circular nodal rings only. Since the plate was not a perfect circle, one can see the appearance of the modes with one nodal diameter by the peaks which occur in the antiresonance minima. The resonance frequencies of these nonradial modes occur midway between the resonance frequencies of the radial modes. The actual frequencies of the resonances are given by the formula:

$$f = \nu^2\pi a^2/2R^2 \ , \ \nu = 1,2,3,\ldots \tag{5.6}$$

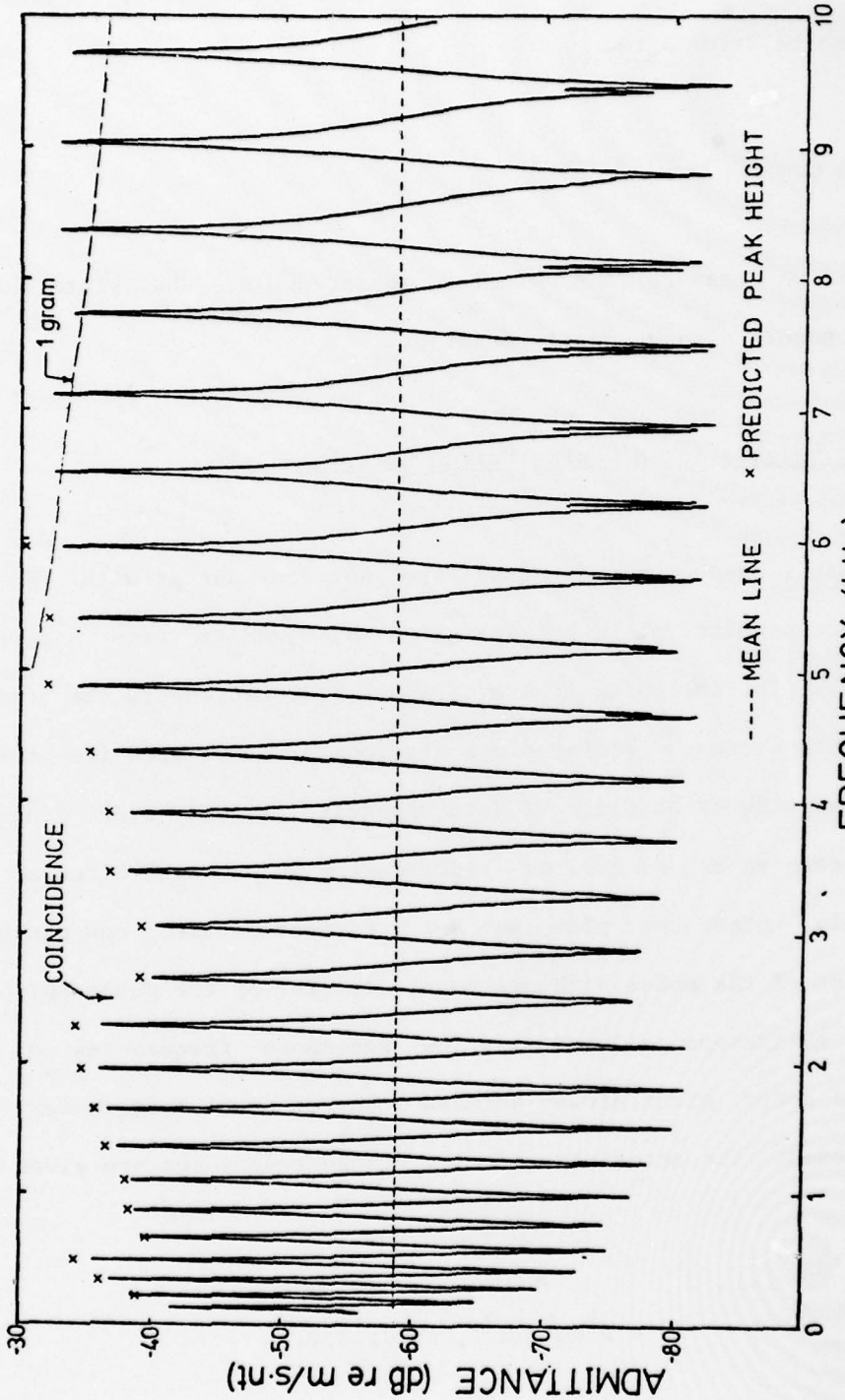

Figure 5.2 Driving Point Admittance and Mean for a Center Driven Circular Plate

where R is the radius of the plate and ν is the mode number. This formula is valid above the first few resonances of the plate. Table 5.1 lists the necessary quantities so that the actual peak heights shown in Figure 5.1 can be predicted via Equation (5.4). Note that the bandwidths are measured at the 6 dB down points instead of the 3 dB points since this will provide a more accurate measurement for these well separated resonance peaks. To derive the 3 dB bandwidths one need only divide the 6 dB measurements by the square root of 3. Comparing with Figure 5.2 one can see that the peak heights have been plotted with x's up to 6 kHz. The line with the long dashes represents an admittance of the equivalent of one gram mass. Admittances less than this are subject to high experimental error due to the mass cancellation process which cannot be expected to be accurate in this range. (Note that it is the peak heights that are most affected by the mass cancellation.) Thus, the peak heights are not plotted beyond 6 kHz. The agreement between the predicted and actual values is good and the worst deviation at 5.3 kHz is 2 dB.

It is interesting to note that the second dip in the peak heights occurs exactly at the coincidence frequency for this plate, although there is no corresponding explanation for the occurrence of the first dip in the peaks at 500 Hz. Note that the antiresonances and resonances are equidistant from the mean line, the dip in the peaks is always reflected by a corresponding increase in the valleys, although at the lower frequencies noise begins to increase the height of the antiresonances, and at the higher frequencies the first nonradial mode begins to appear out of the antiresonances. (The system noise is

TABLE 5.1

EIGENFREQUENCIES, LOSS FACTORS AND PEAK HEIGHTS FOR A CENTER DRIVEN CIRCULAR PLATE

MODE	FREQUENCY (THEORY) Hz	FREQUENCY (MEASURED) Hz	% ERROR	6 DB BANDWIDTH Hz	LOSS FACTOR	PEAK HEIGHT dB
4	218	215	1.40	13	.0349	-38.2
5	340	337	.89	11.5	.0197	-35.2
6	490	487	.62	11	.0130	-33.2
7	667	664	.45	24	.0209	-38.6
8	872	871	.11	24	.0159	-37.5
9	1103	1102	.09	26	.0136	-37.1
10	1362	1364	.15	24	.0102	-35.5
11	1648	1650	.12	24	.0084	-34.7
12	1961	1962	.00	23.5	.00692	-33.8
13	2301	2301	.00	25	.00627	-33.6
14	2669	2666	.11	46.5	.00585	-38.4
15	3064	3064	.00	52	.00980	-38.7
16	3486	3483	.09	41	.00680	-36.1
17	3936	3927	.23	43	.00632	-36.0
18	4412	4401	.25	39	.00512	-34.6
19	4916	4894	.45	29	.00342	-31.6
20	5447	5407	.74	31	.00331	-31.7
21	6007	5959	.77	26	.00252	-29.8
22	6591	6528	.97	25	.00221	-29.0
23	7204	7118	1.2	19	.00154	-26.3
24	7844	7737	1.4	37	.00276	-31.7
25	8511	8374	1.6	26	.00119	-28.3
26	9206	9041	1.8	36	.00230	-30.8

essentially proportional to acceleration and thus drops off at 6 dB per octave in our velocity measurement, as can be seen in Figure 5.2 up to 500 Hz.)

5.3 Peak Heights for the Rectangular Plate

These results are for a rectangular plate (plate II of Appendix I) driven at the center so that the mode density is not too high. Similar measurements were made on this plate so that the peak heights could be predicted using Equation (5.4), where M_r=M/4 or M/2 depending on whether the mode is a plate or beam mode respectively. For this plate the total mass M was 8.36 kgms.

The results are shown in Figures 5.3 and 5.4 representing the frequency response curves with an expanded frequency scale, from 100 to 2,500 Hz in the first and 2,500 to 5,000 Hz in the second figure. Unlike the results for the center driven circular plate the predicted peak heights seem to vary at random about the measured ones. Note that predictions have been made only for well separated peaks consisting of a single mode. The average discrepancy in peak heights amounts to an average 3 dB variation. Similar measurements of a thicker plate show this deviation to be worse even though the mode peaks are better separated due to the thicker plate's smaller mode density. The following investigations were made in an effort to account for this discrepancy.

First, we investigated radiation loading on the plate and its effect on the peak heights. We thought that the different modal

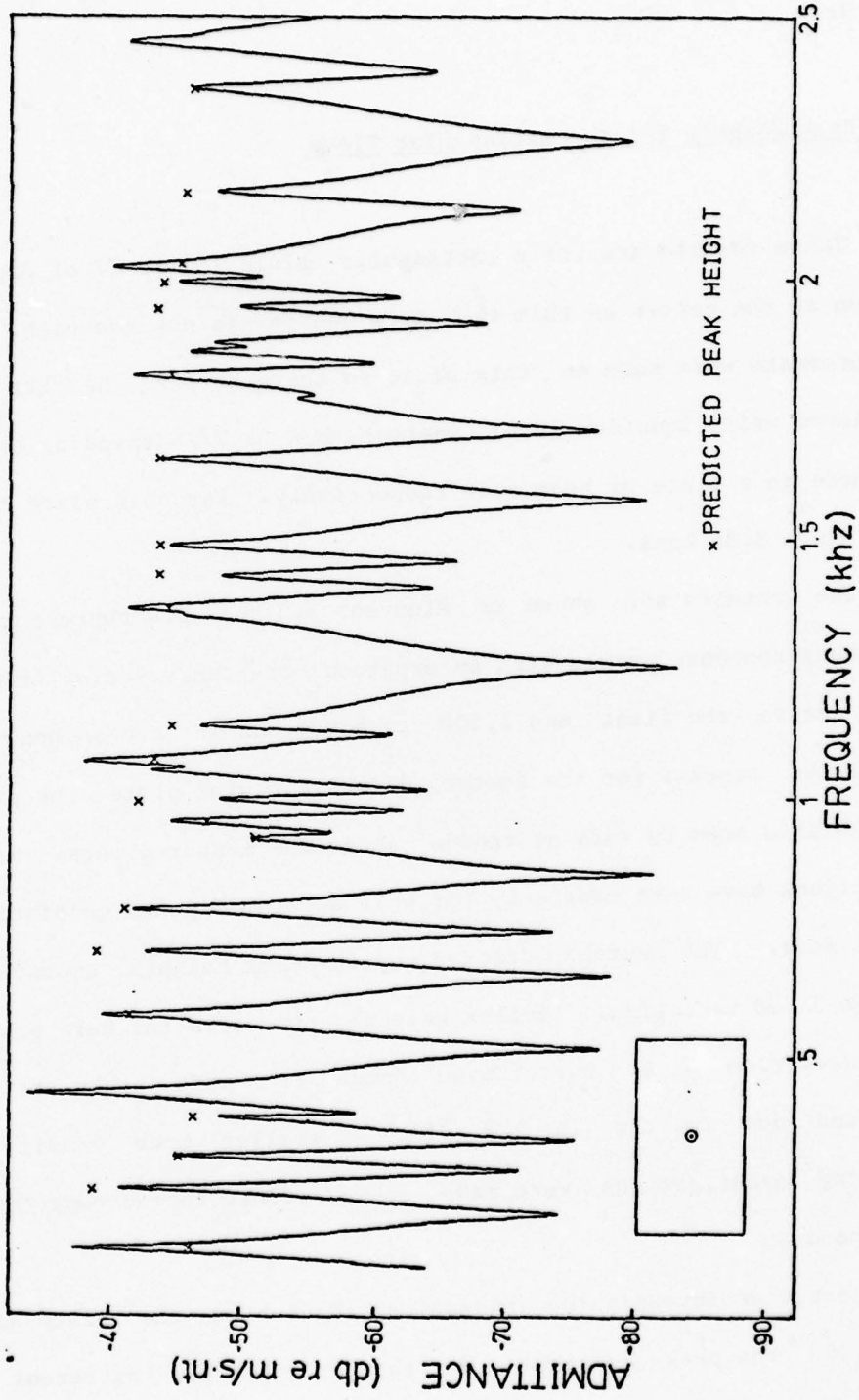

Figure 5.3 Frequency Response Curve for a Center Driven Rectangular Plate with the Predicted Peak Heights Indicated by x's

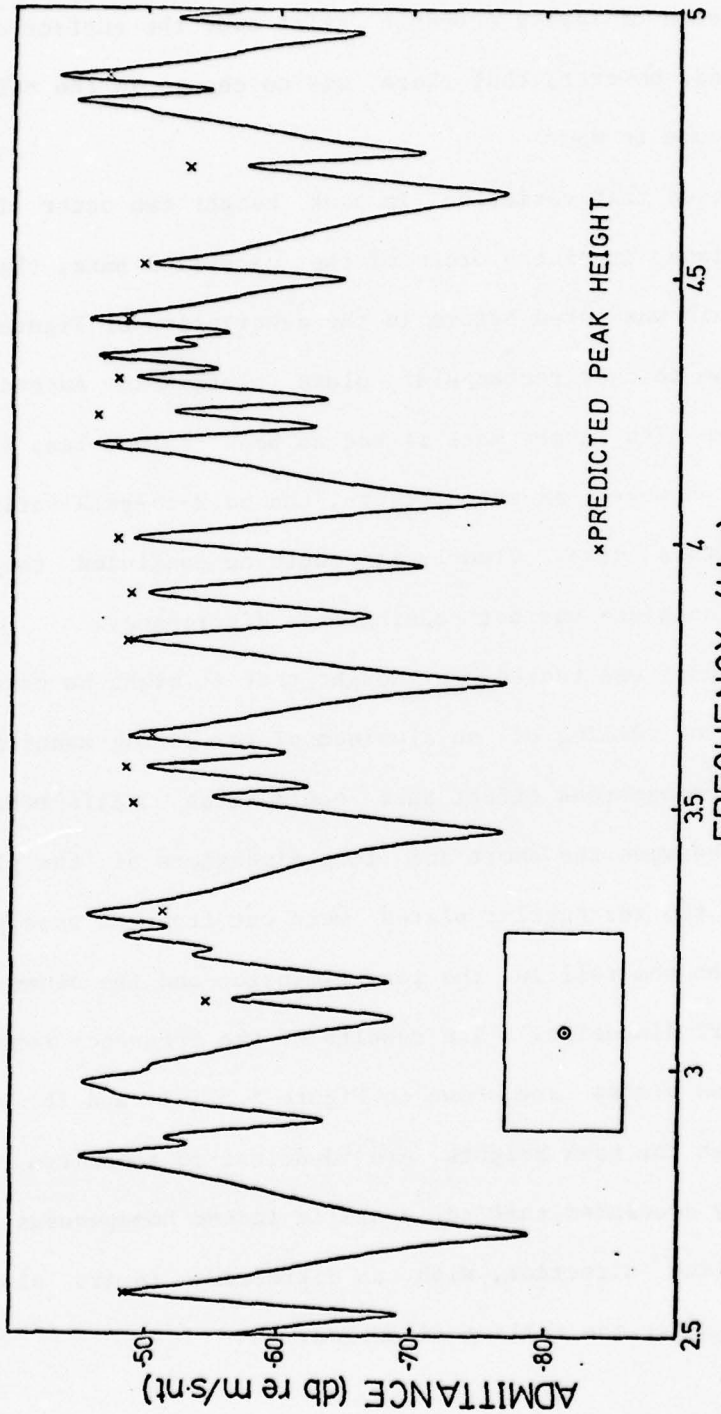

Figure 5.4 Frequency Response Curve for a Center Driven Rectangular Plate with Predicted Peak Heights

patterns might be loaded by different amounts. The radiation loading was changed to see its effect by several different methods. One method, for example, consisted of laying acoustic tiles over the surface of the plate. It was found, however, that there was no change in the relative peak heights from mode to mode.

Second, we noted that variation in peak height can occur if the impedance of the plate is of the order of the cancelled mass, that is, about one gram. This was noted before in the description of Figure 5.2. For this reason the thicker rectangular plate (plate X in Appendix I) was studied. Due to its larger mass it had no peak values less than a 5-gram equivalent. However, as noted before, the peak-to-peak variation was even worse in this case. Clearly it could be concluded that the mass cancellation technique was not causing this discrepancy.

A third hypothesis was tested. We thought that it might be possible that the direction of rolling of an aluminum plate during manufacture might create an inhomogeneous effect that could cause a difference in elastic character between the short and long dimensions of the plate. To investigate this two rectangular plates were cut from the same piece of aluminum, one with the roll in the long dimension and the other with the roll in the short dimension. The results of the frequency response measurements on these plates are shown in Figure 5.5 (a) and (b). The figure indicates that the peak heights are identical in these two cases and it can be safely concluded that the plate is indeed homogeneous with respect to the rolling direction, with no difference in its elastic character with or against the rolling direction.

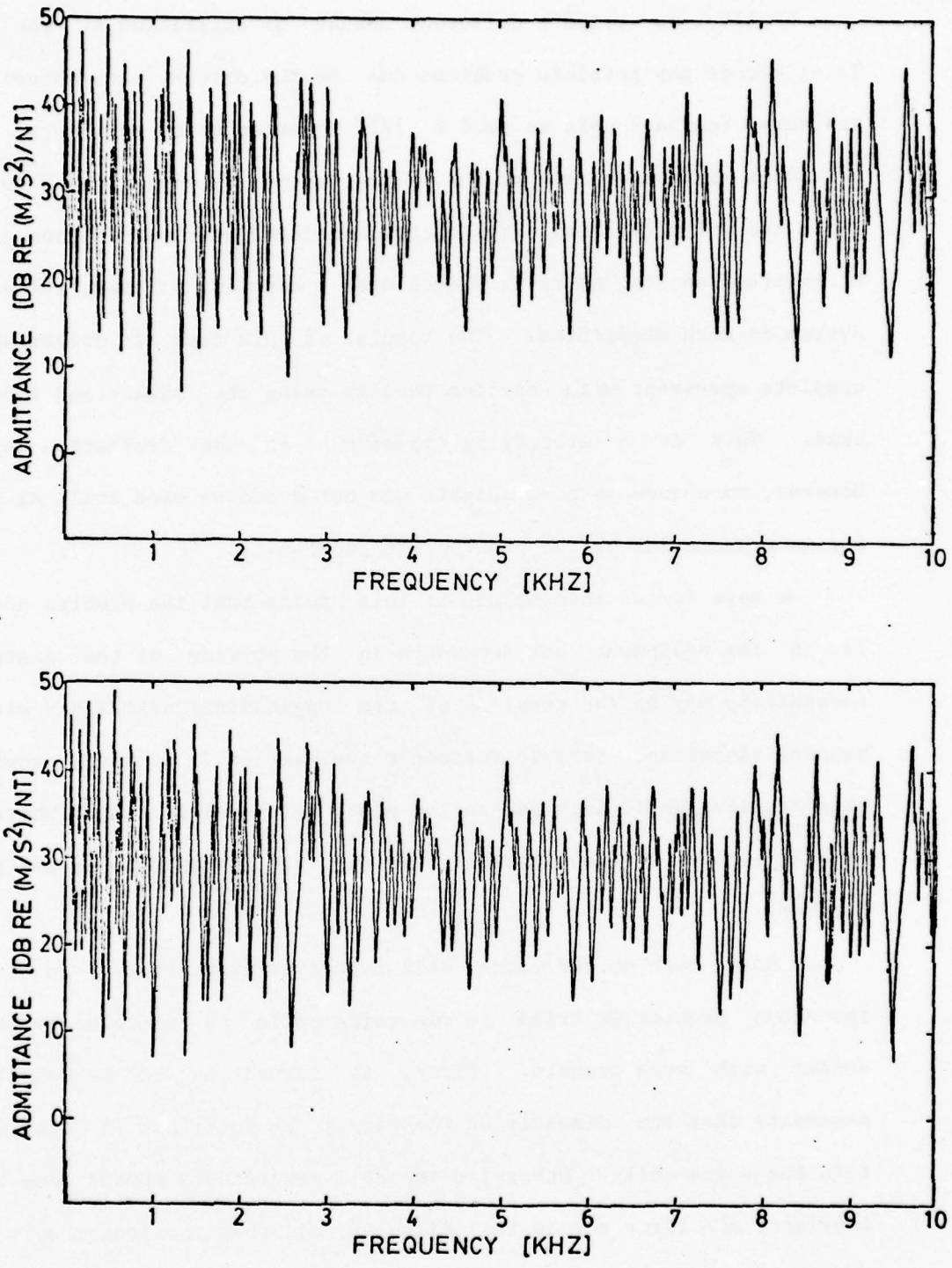

Figure 5.5 Admittance of Two Identical Plates with Roll in Perpendicular Directions

Finally, we tried a different method of excitation of the plate. To eliminate any possible problems due to the driver, mass cancellation and servo feedback unit we used a 1/2" diameter voice coil taken from a 0.3 watt miniature loudspeaker, along with its magnet as a driver. Since the voice coil maintains a constant force over the frequency range of interest as long as it is driven with a constant voltage, the driving system is much simplified. The results of this type of driver were in complete agreement with earlier results using the shaker and impedance head. This is a gratifying crosscheck on the excitation system. However, no change in peak heights was noted and we were still at a loss for an explanation of the peak height problem.

We were forced to conclude at this point that the problem does not lie in the equipment but somewhere in the physics of the plate. One possibility may be the coupling of the longitudinal vibrations with the bending vibrations through Poisson's contraction. It would seem that this coupling would increase as the plate thickness increases where this problem becomes worse. However, we did not carry this investigation further.

A note here on the voice coil method of excitation. In studying the above problem we tried to use voice coils to excite beams at the center with much trouble. First, it turned out to be absolutely necessary that the diameter of the magnet be such that it fits snugly into the voice coil. Otherwise the coil generates a moment due to the imbalance of force across its diameter, and thus no longer acts as a point source. Even with a coil and matching magnet combination one can still easily generate moments if these components are detached from each

other. We had the best success when we used a loudspeaker with its cone and metal bracing around it removed but with the voice coil still connected to the housing by the inside compliant suspension. This provided good alignment between the coil and magnet and the compliance was small enough so that it did not affect the measurements. We found also that the moment generation problem was not nearly as bad in the plate measurements with the voice coil. Since the plate is stiff in both directions, unlike the beam, the moments are not generated so easily.

5.4 Minimum and Maximum Predictions of Admittance

Skudrzyk has outlined the theory in his paper[5] and the results are quoted here. The average height of the resonance maxima is given by β times the characteristic admittance and

$$\beta = 2\epsilon_\nu / \pi\omega_b \ , \tag{5.7}$$

where ϵ_ν is the frequency difference between successive modes, and ω_b the bandwidth. If the driver is at the center of a rectangular plate, then the mode density can be related to the area σ and stiffness a by:

$$\epsilon_\nu = 16\pi a^2/\sigma \ . \tag{5.8}$$

For the driver not on a line of symmetry, the 16 in this equation should be replaced by 4 since the mode density quadruples. Note that the units

of ϵ_ν are radians per second. Similarly, the height of the antiresonances is given by $1/\beta$ times the characteristic admittance. Thus once the mean line is plotted on the frequency response curve, the minimum and maximum excursions below and above this mean line are found by calculating $20 \times LOG_{10}(\beta)$. When the modes are spaced close together so that more than one mode occurs in a single bandwidth ($\epsilon_\nu < 5\ \omega_b$), Equation (5.7) must be modified. Skudrzyk has[5] [Equation (4.7)]:

$$\beta = (2\epsilon_\nu/\pi\omega_b)\left(1 + \sum_{\nu=0}^{\infty} 2/[1+(2\nu\epsilon_\nu/\omega_b)^2]\right) . \qquad (5.9)$$

From Jolley's book on summation of series (Formula 124) one can show that Equation (5.9) reduces to:

$$\beta = \text{cotanh}\ (\pi\omega_b/2\epsilon_\nu) . \qquad (5.10)$$

It can be seen that when the argument of cotanh is small this equation reduces to Equation (5.7).

Figure 5.6 illustrates Equation (5.7). Here plate V (see Appendix I) is a circular plate driven at the center and at 4" off the center. Only radial modes are excited at the center and thus the mode separation ϵ_ν is larger than when the driver is 4" off center. As Equation (5.7) or (5.10) indicates β decreases due to the increase in mode density.

For a more quantitative look a rectangular plate (plate II, Appendix I) was driven at the center with $\sigma = 25.6\ m^2$ and $\epsilon_\nu = 570$ rad/sec (90.7 Hz). Values for ω_b were averaged over several kHz and corresponding values for β were obtained. Figures 5.7 and 5.8 show the

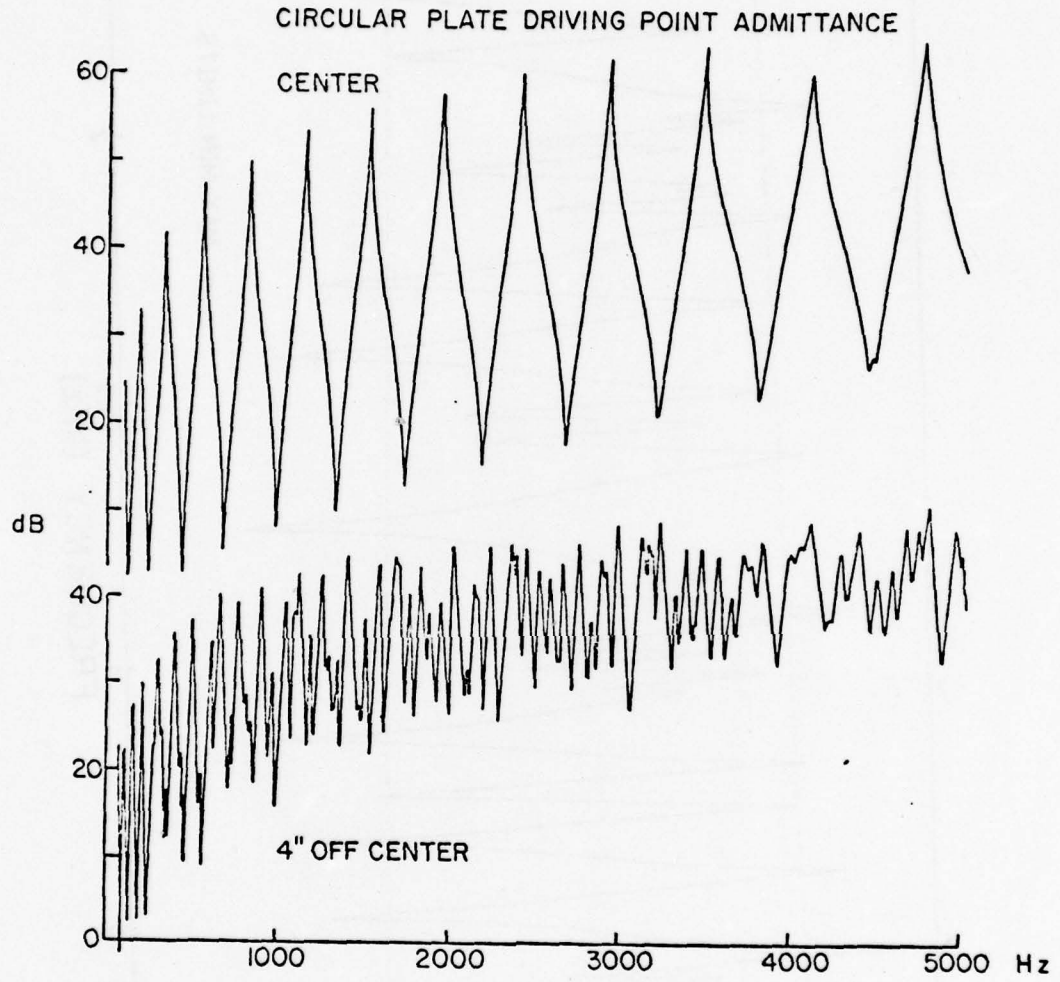

Figure 5.6 Response Curves for a Circular Plate Driven at the Center and 4" Off-Center, Illustrating the Effect of the Increase in Mode Density on the Height and Depth of the Resonances and Antiresonances

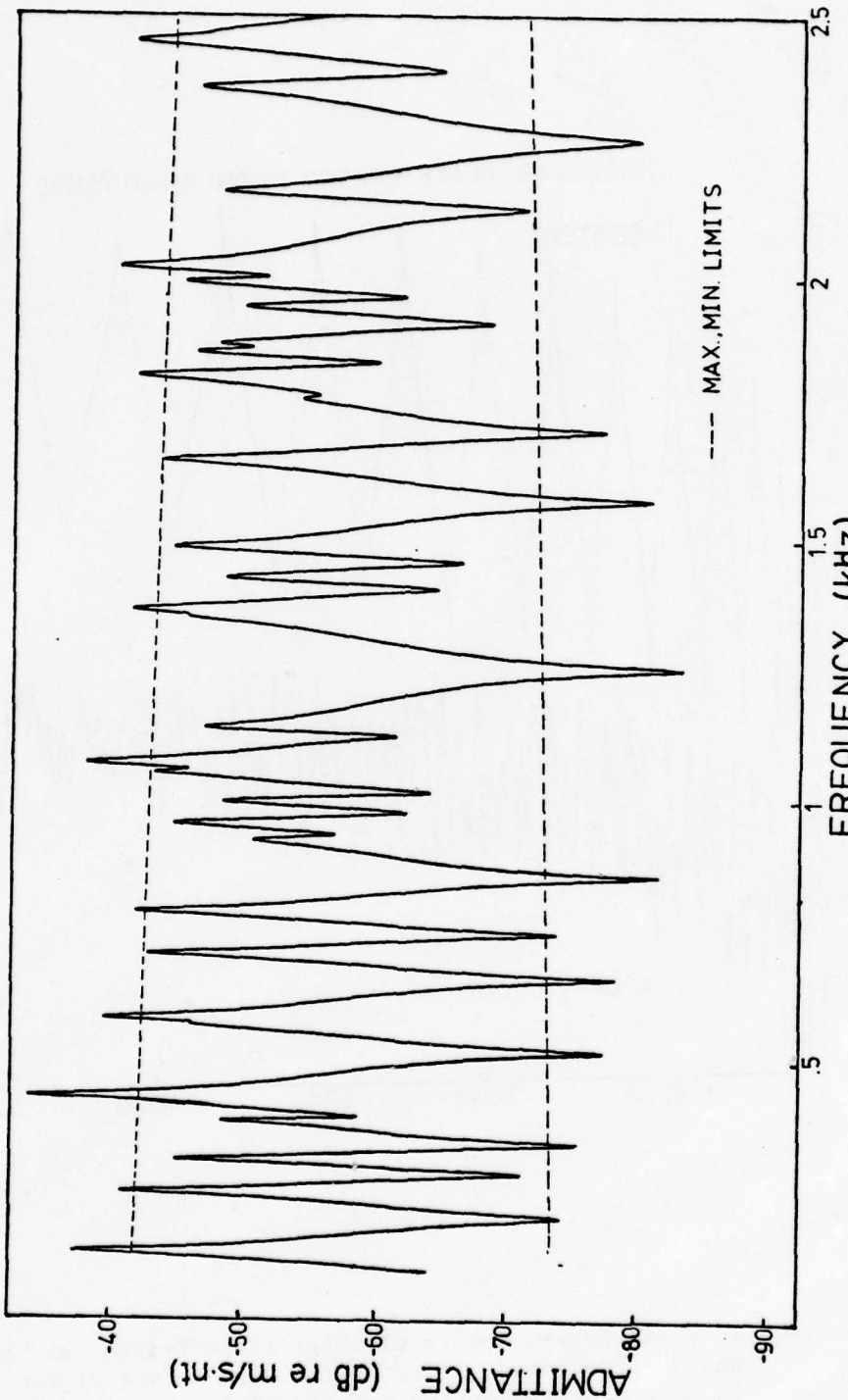

Figure 5.7 Center Driven Rectangular Plate - Minimum and Maximum Mean Level Predictions (0.1 to 2.5 kHz)

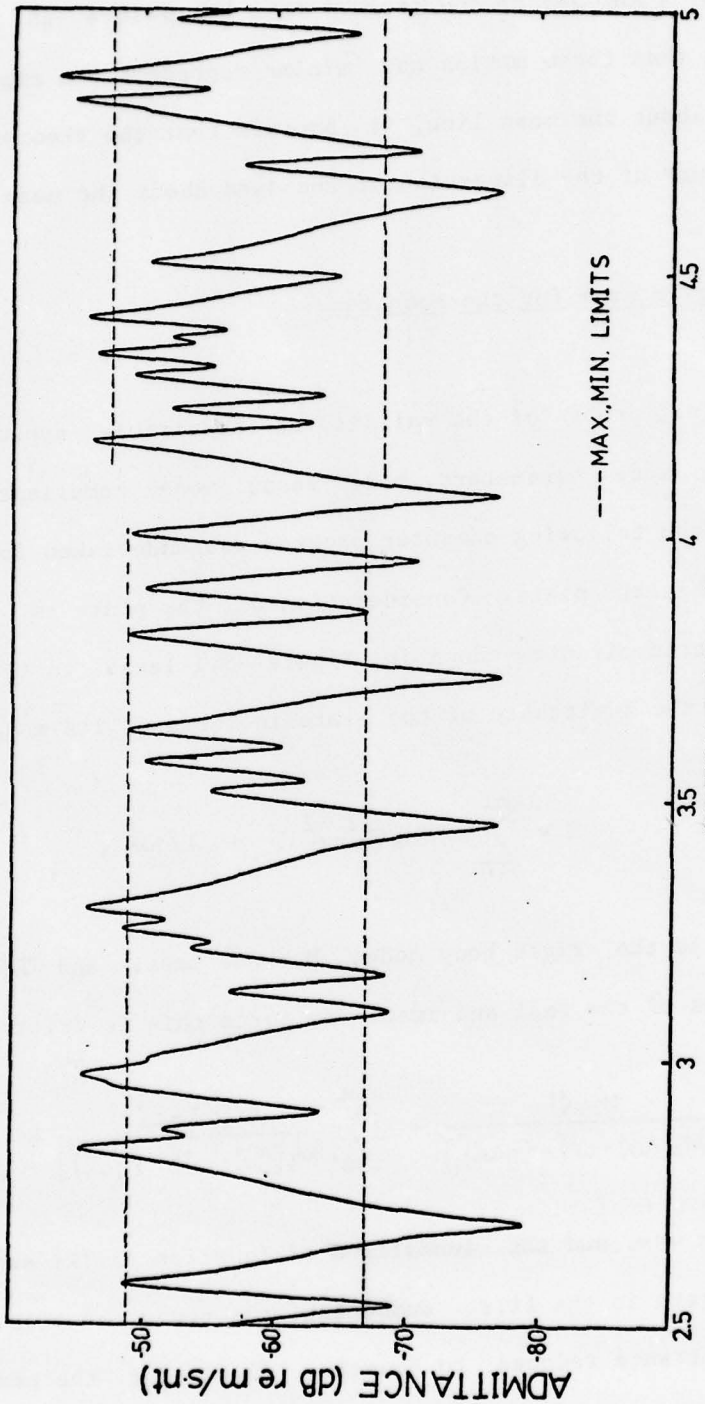

Figure 5.8 Center Driven Rectangular Plate - Minimum and Maximum Mean Level Predictions (2.5 to 5 kHz)

results. Up to 2.5 kHz (Figure 5.7) β decreases from 16 dB to 14 dB. From 2.5 to 4 kHz β=9 dB and from 4 to 5 kHz β=10.4 dB (Figure 5.8). Remembering that these maxima and minima represent the expected average deviations about the mean line, it appears that the theory is providing a good measure of the dispersion of the data about the mean line.

5.5 Computer Program for the Mode Sum

As a final proof of the validity of the circuit approach with its use of the mode parameters, mode mass, mode compliance and mode resistance, the following computer program was undertaken for the center driven rectangular plate. Consideration of the plate as the parallel branch electric circuit shown in Figure 5.1 leads to the following equation for the admittance of the plate in terms of its modes:

$$Y = \sum_{\nu=1}^{\infty} j\omega/[M_\nu(\bar{\omega}_\nu^2 - \omega^2)] + 1/j\omega M , \qquad (5.11)$$

where $1/j\omega M$ is the rigid body mode, M_ν=mode mass, and $\bar{\omega}_\nu^2 = \omega_\nu^2(1+j\eta)$. Thus, in terms of the real and imaginary parts this is written as:

$$Y = \sum_{\nu=1}^{\infty} \frac{(\eta\omega_\nu^2)}{M_\nu[(\omega_\nu^2-\omega^2)^2 + (\eta\omega_\nu^2)^2]} + j\sum_{\nu=1}^{\infty} \frac{\omega(\omega_\nu^2-\omega^2)}{M_\nu[(\omega_\nu^2-\omega^2)^2 + (\eta\omega_\nu^2)^2]} + \frac{1}{j\omega M} \qquad (5.12)$$

At a resonance $\omega=\omega_\nu$ and the summations of Equation (5.12) are dominated by just one term in the first summation, the resonance term. In this case the admittance reduces to Equation (5.4) for the peak height. This is true as long as the modes are separated by more than a

bandwidth. Also it can be seen that at a resonance the admittance is essentially real.

Although only one term is needed to find Y at a resonance, at an antiresonance this is not the case. It turns out that the number of terms one must consider increases to over double the frequency of the excitation. The eigenfrequencies are determined by Warburton's equations as explained in Chapter III, and the losses are average measured values.

The comparison of the real and imaginary parts and the magnitude of their combination are shown in Figures 5.9 through 5.11, respectively, using this mode sum on a hypothetical plate. In Figure 5.11 an effort was made to plot the magnitude of the admittance with a dotted curve (a reproduction of Figure 5.9) on top of the imaginary component to show the relationship. The results show that the regions of resonance are determined by the real part of the admittance, that is, the mode resistance of that particular resonance excited; and that the depth of the antiresonance is also determined by the real part. However, close examination indicates that as soon as we pass out of the tip of the valley the imaginary part immediately takes over. For example, compare the antiresonance sections of Figures 5.9 and 5.10. Thus the imaginary part determines the antiresonance frequency but the real part determines the actual level of this antiresonance.

The significance of the imaginary part is interesting and if it is pursued a little further some insight can be gained into the general nature of vibrators. Since η is small the second term in each of the denominators of Equation (5.12) can be neglected and the admittance reduces simply to:

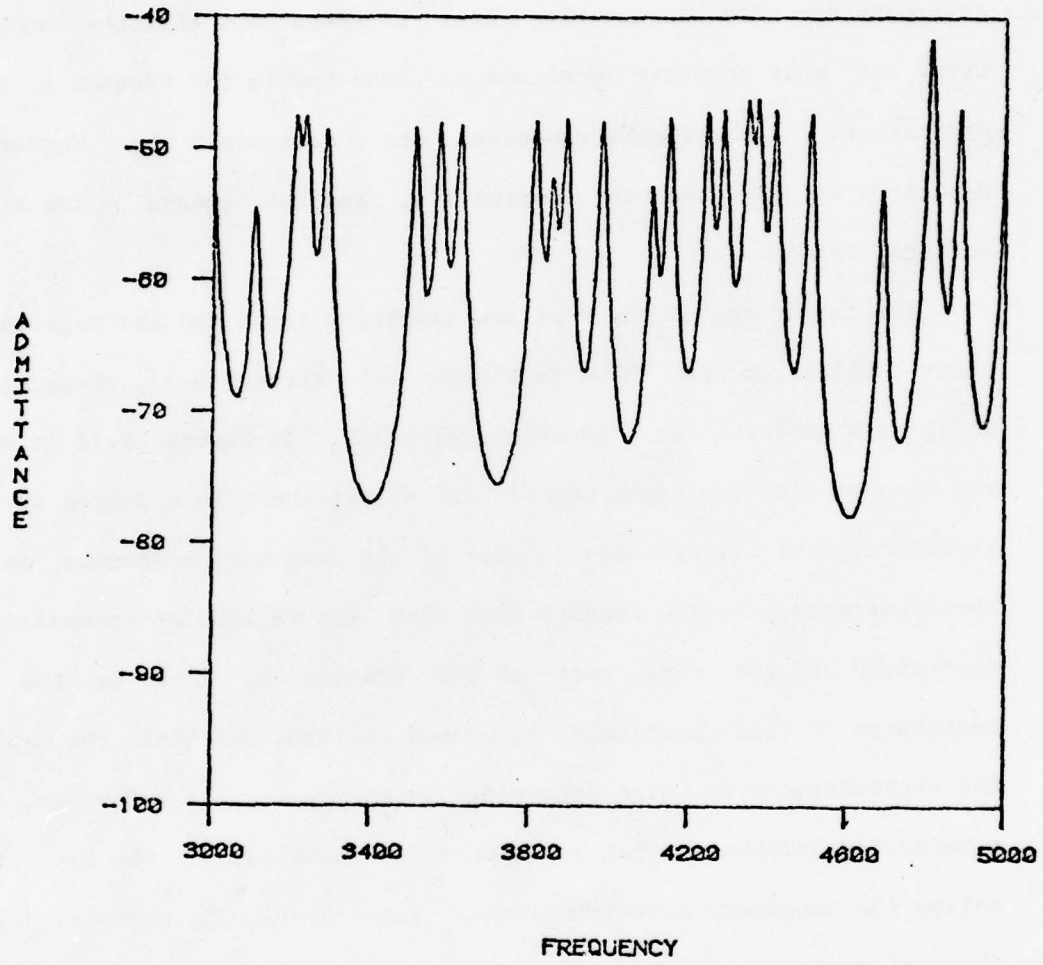

Figure 5.9 42" x 24" x 3/16" Plate Driven at Center. Real Part of the Admittance

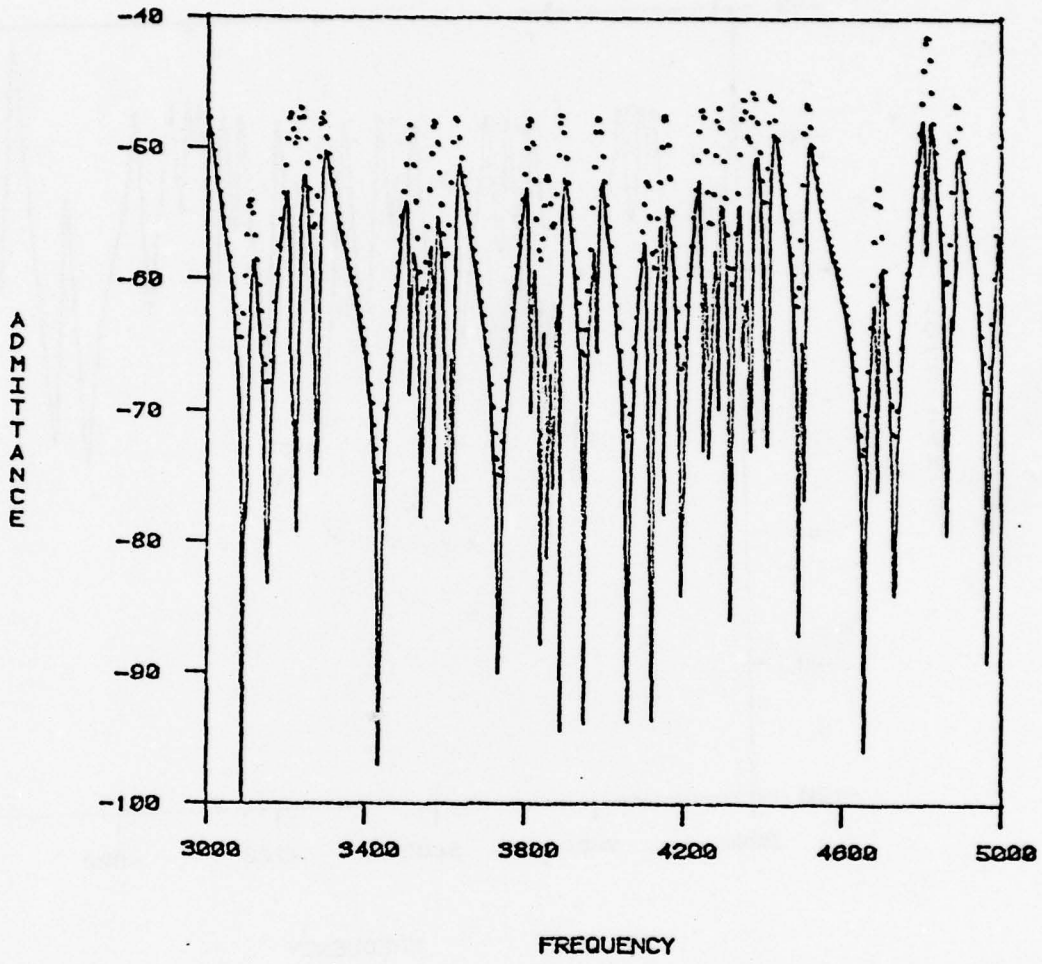

Figure 5.10 42" x 24" x 3/16" Plate Driven at Center. Imaginary Part of Admittance (Dots are magnitude of admittance.)

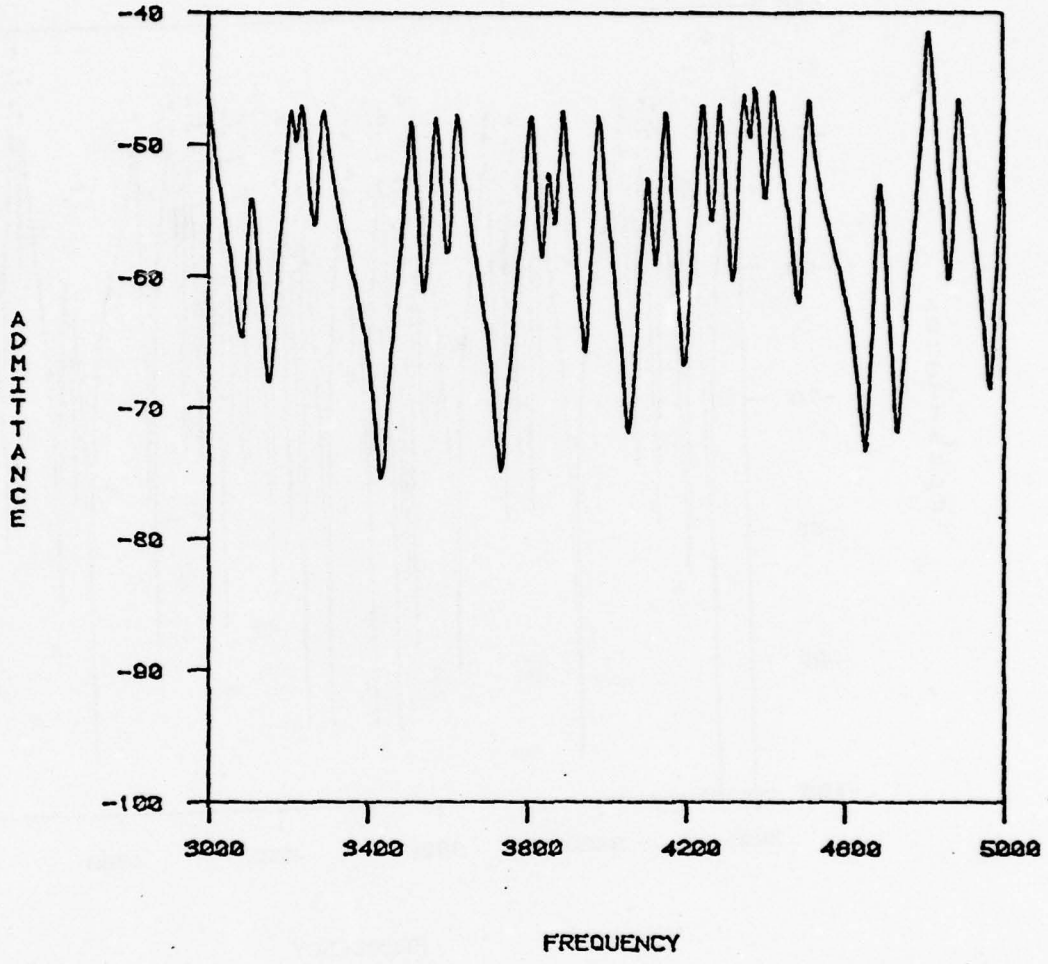

Figure 5.11 42" x 24" x 3/16" Plate Driven at Center. Absolute Value of the Admittance

$$j\omega/M_\nu(\overline{\omega_\nu}^2-\omega^2)\ , \qquad (5.13)$$

except when $\omega_\nu \approx \omega$. Thus, when $\omega_\nu > \omega$ the terms in the sum with ν greater than the resonance mode number act as positive terms, and since they behave proportionally to $+j\omega$ they act as compliances. (Note that the admittance of a compliance is $j\omega K$.) The modes which are excited below the resonance frequency provide a negative denominator and thus a $1/j\omega M$ dependency acting as mass impedances. At some point the mass reactance of the modes below just cancel the compliant reactance of the modes above and the antiresonance is formed. As more and more terms are added to the reactive sum in Equation (5.12), more compliance is added to the system and the result is a shift in the antiresonance frequency to a lower frequency. In practice it was found in a particular example that an antiresonance frequency occurred at 7360 Hz when this sum was cut off at 10 kHz. It dropped to 7320 Hz when the sum was taken to 15 kHz and finally to 7318 when taken to 20 kHz. This is exactly analogous to the effect noted in Chapter II of the compliance added by the mounting of the driver to a plate system. In our mode sum model this compliance adds a significant positive component to the reactive sum and, indeed as we have seen, shifts the antiresonances to the lower frequencies.

5.5.1 Comparison with Experimental Data A rectangular plate (plate II of Appendix I) was driven at the center and the losses were carefully measured. The losses were averaged over 500 Hz frequency intervals and inserted into the computer program. The resonance frequencies were calculated by Warburton's formulas[13] as described in Chapter III. Since

the plate was center driven the mode mass was M/4 for a two-dimensional resonance or M/2 for a one-dimensional resonance. The mode compliances could then be calculated by the formula $K = 1/M\ \omega_o^2$. An average value for a of 2.70 $m/sec^{1/2}$ was used. The results are shown in Figures 5.12 and 5.13. The agreement is excellent in the frequency range 100 to 2.5 kHz and remarkable in the fact that the levels of the antiresonance minima are predicted so well by this model. As would be expected the peak heights show some discrepancy, as was noted earlier in this chapter. (The modes were summed up to 20 kHz for this example.) There is no doubt that the mode sum program provides a very accurate and quick (about 10 sec CPU time on the IBM 370) method for predicting the response curves of rectangularly shaped plates. This method should work for any shape plate, although the work was not carried any further. The actual computer program is included in Figures 5.14 and 5.15; the principal program is named MODESUM, and the plotting program is named PLTSUM.

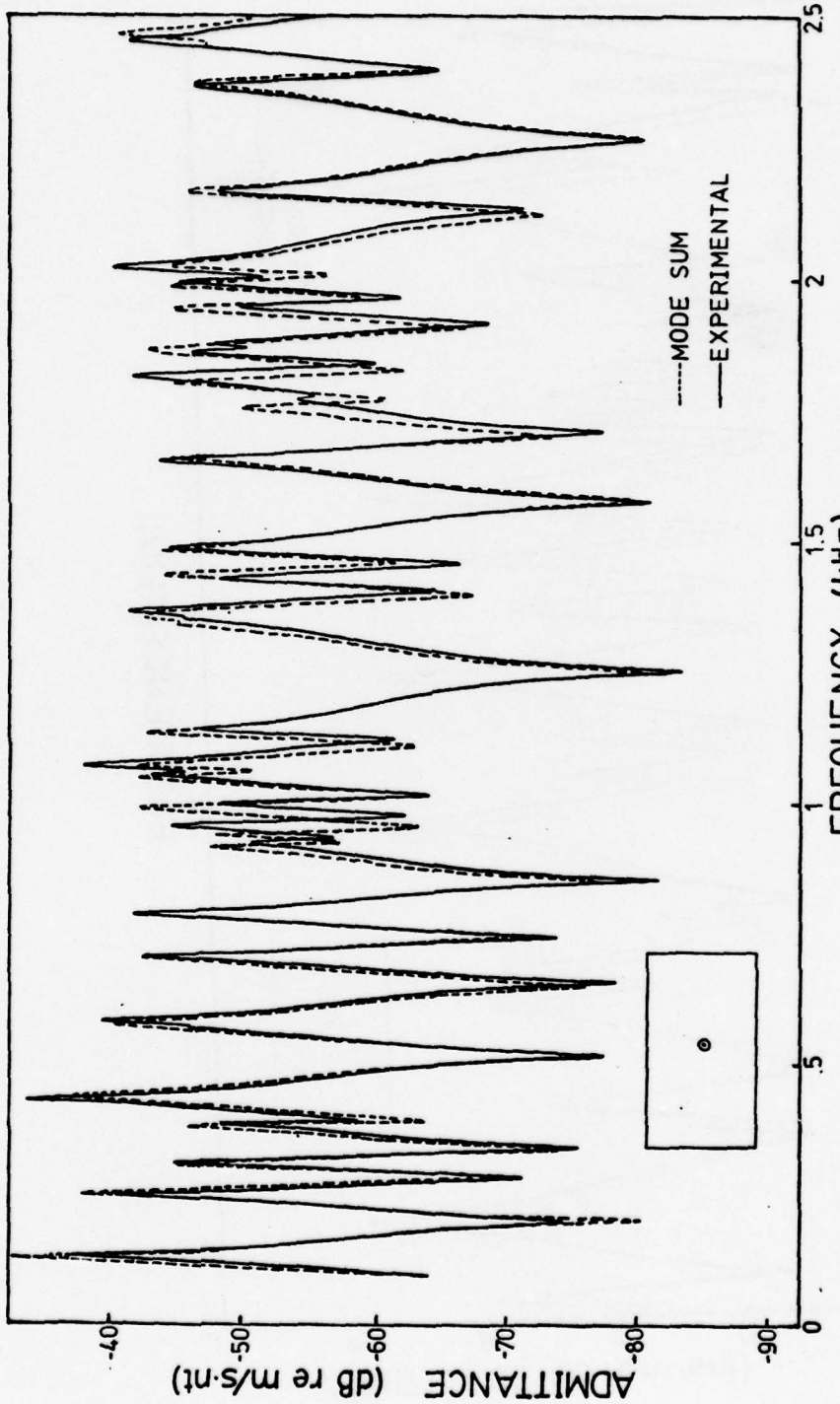

Figure 5.12 Driving Point Admittance Predicted from MODESUM versus Experimental Data (0.1 to 2.5 kHz)

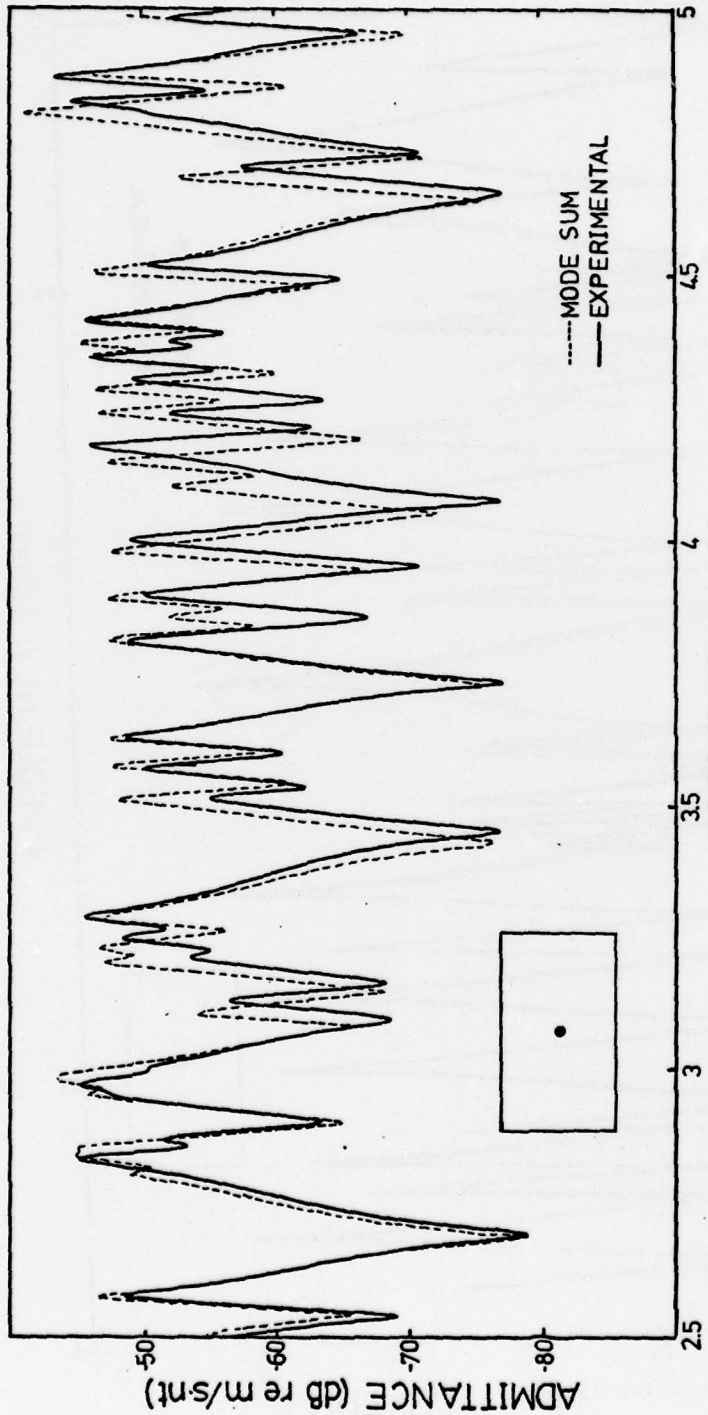

Figure 5.13 Driving Point Admittance Predicted from MODESUM versus Experimental Data (2.5 to 5 kHz)

```
00050 /*USERID EGW02
00100 // EXEC FWCG
00150 //SYSIN DD *
00200       DIMENSION FF(2000),FREQ(4000),FV(2000),YR(4000),YI(4000)
00250       DIMENSION ORDER(3000),ETA(40),ETAF(3000),MASS(2000),MMASS(2000)
00300       DIMENSION FVS(2000),YA(3000),NV1(2000),MV1(2000)
00350       DIMENSION NV(2000),MV(2000)
00400       REAL J,MASS,MMASS
00450       INTEGER ORDER
00500 C
00550 C              INPUT LENGTH,WIDTH,STIFFNESS PARAMETER,THICKNESS
00600 C
00620 C
00630 C           INPUT UPPER FREQUENCY CUTOFF
00640 C
00650       DATA A,B,ALPHA,HT/42.,24.,2.711,.1875/
00700       DATA FVMAX/10000./
00720 C
00730             INPUT PLOTTING FREQUENCY RANGE
00740 C
00750       DATA FMIN,DF,FMAX/3000.,5.,5000./
00770 C
00780 C           INPUT LOSS FACTORS IN 500 HZ INTERVALS
00790 C
00800       DATA (ETA(I),I=1,11)/.0315,.018,.0105,.008,.0067,.0068,.0076,
00850      A.006,.0049,.00405, 0035/
00900       A=A*.0254
00950       B=B*.0254
01000       HT=HT*.0254
01050       PI=3.14159265
01100       TPI=2*PI
01150       CON=PI*ALPHA*ALPHA/(2.*A*A)
01200       RAT1=A*A/(B*B)
01250       RAT2=RAT1*RAT1
01300       RHO=2700.
01350       AMTOT=RHO*A*B*HT
01400 C
01450 C              CALCULATION OF RESONANCE FREQUENCIES
01500 C
01550       NFQ=0
01600       DO 105 N=0,100,2
01650       DO 100 M=0,100,2
01700       IF (N+M.EQ.0.OR.N+M.EQ.1) GO TO 100
01750       E=CON*SQRT(G(M)**4+RAT2*G(N)**4+2.*RAT1*(.325*H(M)*H(N)+
01800      1 .675*J(M)*J(N)))
01850       IF (E.GE.FVMAX  .AND.M.EQ.0) GO TO 200
01900       IF (E.GE.FVMAX) GO TO 105
01950       NFQ=NFQ+1
02000       IF (N.EQ.0.OR.M.EQ.0) GO TO 80
02050       MMASS(NFQ)=AMTOT/4.
02100       GO TO 90
02150    80 MMASS(NFQ)=AMTOT/2.
02200    90 FF(NFQ)=E
02250       MV1(NFQ)=M
02300       NV1(NFQ)=N
02350       GO TO 100
02400   100 CONTINUE
02450   105 CONTINUE
```

Figure 5.14 Computer Program for MODESUM

```
02 500 C
02 550 C                        SORTING OF MODE FREQUENCIES
02 600 C
02 650    200  IT=NFQ
02 700         IDUMM=14
02 750         CALL QSORT(FF(1),FF(2),ORDER,IT,3,IDUMM)
02 800         WRITE (6,890)
02 850    890  FORMAT (' ',9HFREQUENCY,18H N   M   MODE MASS//)
02 900         DO 300 I=1,NFQ
02 950         IS=ORDER(I)
03000          FV(I)=FF(IS)
03050          FVS(I)=FV(I)*FV(I)
03100          MV(I)=MV1(IS)
03150          NV(I)=NV1(IS)
03200          WRITE (06,992) FV(I),NV(I),MV(I),MMASS(IS)
03250    992   FORMAT (' ',F8.2,2I4  ,F15.4)
03300    300   MASS(I)=MMASS(IS)
03350          NFV=NFQ
03400 C
03450 C                        MERGE MODE AND PLOTTING FREQUENCIES
03500 C
03550          F=FMIN
03600    310   IF (F.GT.FMAX)  GO TO 320
03650          NFQ=NFQ+1
03700          FF(NFQ)=F
03750          F=F+DF
03800          GO TO 310
03850    320   IDUMM=14
03900          IT=NFQ
03950          CALL QSORT(FF(1),FF(2),ORDER,IT,3,IDUMM)
04000          DO 400 I=1,NFQ
04050          IS=ORDER(I)
04100    400   FREQ(I)=FF(IS)
04150 C
04200 C                        CALCULATE ADMITTANCE
04250 C
04300          DO 600 N=1,NFQ
04350          YR(N)=0.
04400          YI(N)=(-1./(FREQ(N)*FREQ(N)*AMTOT))
04450          FS=FREQ(N)*FREQ(N)
04500          IF (FREQ(N).LT.FMIN.OR.FREQ(N).GT.FMAX) GO TO 600
04550          INF=INT(FREQ(N)/500.)+1
04600          ETAF(N)=(ETA(INF+1)-ETA(INF))*(FREQ(N)/500.-INF+1)+ETA(INF)
04650          DO 500 I=1,NFV
04700          EFVS=ETAF(N)*FVS(I)
04750          DIF=FVS(I)-FS
04800          DIFS=DIF*DIF
04850          DEN=(DIFS+EFVS*EFVS)*MASS(I)
04900   9999   FORMAT (' ',2F6.0,4E16.8)
04950          YR(N)=YR(N)+EFVS/DEN
05000          YI(N)=YI(N)+DIF/DEN
05050    500   CONTINUE
05100          YR(N)=YR(N)*FS/(TPI*FREQ(N))
05150          YI(N)=YI(N)*FS/(TPI*FREQ(N))
05200          YA(N)=10.*ALOG10(YR(N)*YR(N)+YI(N)*YI(N))
05250          YR(N)=20.*ALOG10(ABS(YR(N)))
```

```
05300       YI(N)=20.*ALOG10(ABS(YI(N)))
05350   600 CONTINUE
05400       NN=NFQ/5
05450       DO 991 K=1,NN
05500       WRITE (06,990) (FREQ(I),YA(I),YR(I),YI(I),I=K,NFQ,NN)
05550   990 FORMAT (' ',6(F6.0,3F5.1))
05600   991 CONTINUE
05650       WRITE (7,995)
05700   995 FORMAT (14HXXXXXXXXYYYYYYY)
05750       NFIRST=0
05800       DO 996 K1=1,NFQ
05850       IF (FREQ(K1).LT.FMIN.OR.FREQ(K1).GT.FMAX) GO TO 996
05900       IF (NFIRST.NE.0) GO TO 700
05950       NFIRST=1
06000       KSAV2=K1
06050       YAMAX=YAMIN=YA(K1)
06100   700 IF (YA(K1).GT.YAMAX) YAMAX=YA(K1)
06150       IF (YA(K1).LT.YAMIN) YAMIN=YA(K1)
06200       WRITE (7,998) FREQ(K1),YA(K1),YR(K1),YI(K1)
06250   998 FORMAT (F7.1,3F7.2)
06300       KSAV=K1
06350   996 CONTINUE
06400        ADD10=10.
06450        IF (YAMAX.LE.0.0) ADD10=0.0
06500       YDUM2=(INT(YAMAX)/10)*10.+ADD10
06550       YDUM1=YDUM2-60.
06600       WRITE (7,998) FREQ(KSAV),YDUM1,YDUM1,YDUM1
06650       WRITE (7,998) FREQ(KSAV),YDUM2,YDUM2,YDUM2
06700       WRITE (7,998) FREQ(KSAV2),YDUM2,YDUM2,YDUM2
06750       STOP
06800       END
06850             FUNCTION H(I)
06900       IF (I-2) 1200,1100,1000
06950  1000 H=(I-.5)**2*(1.-.6366/(I-.5))
07000       RETURN
07050  1100 H=1.248
07100       RETURN
07150  1200 H=0.
07200       RETURN
07250       END
07300             FUNCTION G(I)
07350       IF (I-2) 1200,1100,1000
07400  1000 G=I-.5
07450       RETURN
07500  1100 G=1.506
07550       RETURN
07600  1200 G=0.
07650       RETURN
07700       END
07750             FUNCTION J(I)
07800       REAL J
07850       IF (I-2) 120,110,100
07900   100 J=(I-.5)*(I-.5)*(1.+1.910/(I-.5))
07950       RETURN
08000   110 J=5.017
08050       RETURN
08100   120 J=1.216*I
08150       RETURN
08200       END
08250 //DATA.FT07F001 DD UNIT=BAT,FILES=($MSUM1,$MSUM2,$MSUM3)
```

```
00001 C                    LISTING FOR PLTSUM
00002 C
00003 C
00004 C    THIS PROGRAM PROVIDES :  PLOT OF THE RESULTS OF MODESUM.
00005 C
00050 /*USERID EGW02
00100 // EXEC RUN,PROG=GRAPHTK
00150 //SYSIN DD *
00200 //DATA.FT17F001 DD UNIT=BAT,FILES=$PLOT1
00250 //DATA.INPUT DD *
00260 CP OVERSIZE
00310
00320 FREQUENCY
00330 ADMITTANCE
00340 FIGURE       42 X 24 X 3/16 INCH PLATE DRIVEN AT CENTER.
00341 THEORETICAL PREDICTION FROM THE MODE SUM WITH MODES SUMMED
00342 UP TO 20000 HZ. RIGID BODY MODE ADDED.
00350 CP TI X 6 Y 7
01340 CP CURVE
01400 CP
01500 /*INCLUDE EGW02.$MSUM1
01510 /*INCLUDE EGW02.$MSUM2
01550 CD
01600 /*INCLUDE EGW02.$MSUM1
01610 /*INCLUDE EGW02.$MSUM2
```

Figure 5.15 Computer Program for PLTSUM

CHAPTER VI

SUMMARY AND CONCLUSIONS

6.1 Summary

This work provides a method in which the average characteristics of the point admittance of a vibrator, in this case flat plates of various geometries, can be predicted. These predictions include the mean line through the response curve (admittance versus frequency) over the frequency range of 100 Hz to 10 kHz, and the average height of the resonances and depth of the antiresonances on the response curve for the vibrator. In other words, given a point source exciting a flat plate vibrator, the resultant average velocity and expected maximum and minimum variations about this average at the driving point can be predicted. Also the average velocity at other points on the plate surface has been predicted.

The mean line is easily calculated when the point source is in the interior of the vibrator. When the source is close to a boundary an image method is used for the calculation of the mean line.

A computer program was developed modeling the vibrator as an electric circuit representing the sum of the modes of the vibrator. The program predicted the actual driving point admittance (not the average value) for a center driven rectangular plate over the frequency range of 0.1 to 5 kHz.

Also, predictions of the eigenvalues of the free-free square and rectangular plates were made using a simple algebraic equation.

6.2 Conclusions

The predictions of the mean admittance are generally accurate to within 1 dB. The predictions of the excursions about the mean provide a good measure of the expected minimum and maximum response of the vibrator to the driving force. The calculations used are quick and numerically simple. The only measured data used in the predictions were the the loss factors for the vibrator. We have also been able to deal very accurately with the coupling between the vibrator and the point driver attached. The accuracy of the circuit theory approach in the prediction of the actual admittance of a vibrating plate has been demonstrated. Further, the predictions of the eigenvalues for the square and rectangular free plates were found to be generally within 1% of the actual measured values.

6.3 Recommendations for Further Study

The next logical step would be to apply these techniques to more complicated structures such as ribbed plates and ribbed shells, making use of the mean line theory and also the circuit theory approach. The MODESUM program should be extended to deal with transfer admittance.

REFERENCES

1. A. W. Leissa, "Vibration of Plates",NASA,SP-160 (1969).

2. M. D. Waller, Chladni Figures - A Study in Symmetry (G. Bell and Sons, London, 1961).

3. L. Cremer and M. Heckl, Structure - Borne Sound (Springer-Verlag,New York, Heidelberg, Berlin, 1973).

4. E. Skudrzyk, Simple and Complex Vibratory Systems (The Pennsylvania State University Press, University Park, Penna., London, 1968).

5. E. Skudrzyk, "The Mean-Value Method of Predicting the Dynamic Response of Complex Vibrators" (1979) (unpublished)

6. J. C. Snowdon, "Forced Vibration of Internally Damped Circular Plates with Supported and Free Boundaries," J.A.S.A. 47, 882-891 (1970)

7. J. C. Snowdon, "Forced Vibration of Internally Damped Circular and Annular Plates with Clamped Boundaries," J.A.S.A. 50, 846-858 (1971)

8. J. C. Snowdon, "Forced Vibration of Internally Damped Rectangular and Square Plates with Simply Supported Boundaries," J.A.S.A. 56, 1177-1184 (1974)

9. J. C. Snowdon and J. B. Ochs, "Transmissibility Across Simply Supported Thin Plates. I. Rectangular and Square Plates with and without Damping Layers," J.A.S.A. 58, 832-840 (1975)

10. J.C. Snowdon and J. B. Ochs, "Transmissibility Across Simply Supported Thin Plates, II. Rectangular Plates with Loading Masses and Straight Ribs," J.A.S.A. 59, 350-363 (1976)

11. R. Hannon, "Vibration and Sound Radiation of a Plate," (Ph.D. Thesis, The Pennsylvania State University, 1975).

12. Wilcoxon Research, "Choosing an Impedance Head," Bulletin No. 2 (Wilcoxon Research).

13. Warburton, "Vibration of Rectangular Plates," Proc. Inst. Mech. Eng.; Sec. A 168, (1954)

14. J. C. Snowdon, Vibration and Shock in Damped Mechanical Systems (Wiley, New York, 1968)

15. Brekhovskikh, Waves in Layered Media (Academic Press, New York, 1960)

16. M. D. Waller, "Vibration of Free Elliptical Plates," Proc. Roy. Soc. Lond. B 63, 451-458 (1950)

APPENDIX I

PHYSICAL DESCRIPTION OF PLATES STUDIED

PLATE	SHAPE	DIMENSIONS	THICK-NESS	ALPHA $m/sec^{1/2}$	Y_c dB re sec/kg	ALUMINUM ALLOY
I	Rectangular	24" x 48"	3/16"	2.716	-57.7	
II	Rectangular	24" x 42"	3/16"	2.708	-57.6	
III	Rectangular	4′ x 8′	1/8"	2.22	-50.6	6061-T6
IV	Quadrilateral	1.374 m^2	1/8"	2.23	-50.8	
V	Circular	45" diam.	1/8"	2.22	-50.6	
VI	Circuar	72.125" diam.	.190"	2.70	-57.6	6061-T6
VII	Square	24" x 24"	.190"	2.68	-57.5	6061-T6
VIII	Elliptical	36.6" x 23.9"	1/8"	2.23	-50.8	2024-T3
IX	Figure 8		1/8"	2.23	-50.8	2024-T3
X	Rectangular	24" x 53.7"	3/8"	3.81	-69.5	6061-T6

APPENDIX II

DAMPING OF PLATE SURFACE

A rectangular plate (plate I of Appendix I) was coated with two coats of GP-1 damping compound which, when it dries, has the constancy of a cement. The mass of the undamped plate was 9.80 kilograms and after damping this weight increased to 12.92 kilograms. This was equivalent to a 32% increase in weight. Certainly some of the effectiveness of this damping material is in this mass loading. By virtue of Equation (4.3) it is evident that this increase in mass will lower the mean line, decreasing the characteristic admittance of the plate. In this case the loading is equivalent to a 2.4 dB drop, as did indeed occur. Also the thickness of the plate was increased from 0.188" to 0.304" due to the damping layer.

An important consequence of the damping on the response curves for the rectangular plate is a stretching of the frequency response curve. For example, a sharp antiresonance which occured at 8350 Hz shifted to 8925 Hz when the plate was damped. In Figure 4.1 of Chapter IV, page 43, the damped plate response is plotted along with the undamped response. For this comparison the shift in mean line due to the mass loading and the stretching of the frequency response curve were removed so that the curves could be compared properly. The stretching of the frequency spectrum is equivalent to an increase in the stiffness parameter [see Equation (4.2)] of the plate from 2.73 to 2.84 $m/sec^{1/2}$. It is apparent that the effect of the damping compound on the plate is

to stiffen the top surface of the plate by increasing the resistance to bending. Note, however, that the increase in mass in the plate has the opposite effect. Since the mode mass must also increase it is apparent that this effect alone will reduce the resonance frequencies of the system. [see Equation (4.2) for example.]

The frequency response curves using this damped plate in Section 4.6.1 had their mean line predictions decreased by 2.4 dB to account for the added mass due to the damping compound.

APPENDIX III

CALCULATION OF EIGENFREQUENCIES FOR THE RECTANGULAR PLATE

The following results are taken from Warburton.[13] Equation (15) of his paper is recast in terms of the stiffness parameter alpha so that

$$f_{m,n} = \lambda \pi a^2 / 2a^2 ,$$

where a is the long dimension in meters, a is the stiffness parameter, f the frequency in Hz, and λ is given below:

$$\lambda^2 = G_x^4 + G_y^4 \, a^4/b^4 + 2a^2/b^2 [H_x H_y + (1-\sigma) J_x J_y]$$

where
$$G_x = m - .5 \quad m>2$$
$$= 1.506 \quad m=2$$
$$= 0 \quad m<2$$

$$H_x = (m - .5)^2 [1 - 2/(m-.5)] \quad m>2$$
$$= 1.248 \quad m=2$$
$$= 0 \quad m<2$$

and
$$J_x = (m - .5)^2 [1 + 6/(m-.5)] \quad m>2$$
$$= 5.017 \quad m=2$$
$$= 12/\pi^2 \quad m=1$$
$$= 0 \quad m=0.$$

To evaluate G_y, H_y and J_y replace m with n in the above equations. Here σ is Poisson's ratio, m and n represent the mode numbers and b is the shorter dimension of the plate in meters.

DISTRIBUTION

Commander (NSEA 09G32)
Naval Sea Systems Command
Department of the Navy
Washington, DC 20362 — Copies 1 and 2

Commander (NSEA 0342)
Naval Sea Systems Command
Department of the Navy
Washington, DC 20362 — Copies 3 and 4

Defense Documentation Center
5010 Duke Street
Cameron Station
Alexandria, VA 22314 — Copies 5 through 16